



PONTIFICIA  
**UNIVERSIDAD  
CATÓLICA**  
DEL PERÚ

  
TECHNISCHE UNIVERSITÄT  
**ILMENAU**

# Pontificia Universidad Católica del Perú

Escuela de Posgrado

## Tesis de Maestría

Experimental setup for measuring the mechanical behavior  
of loaded thin compliant joints with highest precision

Para obtener el grado de:

Master of Science (M. Sc.)

en Ingeniería Mecatrónica

Presentado por: Braulio Jesús  
García Ayala

Fecha y Lugar de Nacimiento: 20/09/1988 Lima, Perú

Tutor Responsable (TU Ilmenau): MSc. Maximilian Darnieder  
Professor Responsable (TU Ilmenau): Prof. Dr.-Ing. René Theska  
Professor Responsable (PUCP): Prof. Julio Cesar Tafur Sotelo

Fecha y Lugar: 06/06/2018, Lima

# Declaration of originality

I confirm that the content of this thesis is my own work and that I have not sought or used inadmissible help of third parties for the elaboration of this document and that I have clearly referenced all sources used in the work. This work has not yet been published or submitted to another examination institution-neither in Germany nor outside of Germany.

Ilmenau, den 02.05.2018

Braulio Jesús García Ayala



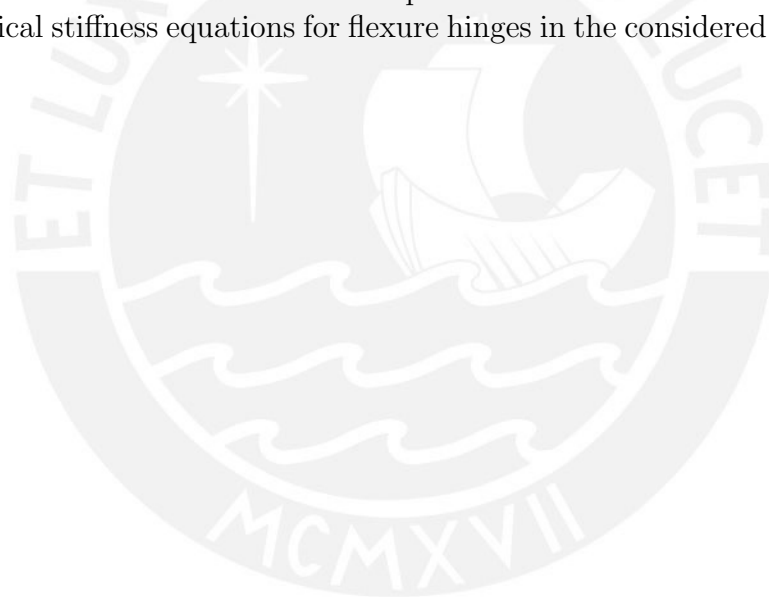
# Acknowledgements

I am grateful to all those who contributed on the realization of this work. First, I give thanks to my parents for the unconditional support and for the constant encouragement from so far away. Second, I am also deeply thankful to the Professors who helped me with their advices until the completion of this work. Third, I express my thanks to Mr. Döll from Zentrum für Mikro und Nanotechnologien (ZMN) of the TU Ilmenau, who provided the facilities to get the microscope pictures. Last but not least, I express my special and sincere gratitude to my supervisor Maximilian Darnieder who supported me academically from the beginning to the end of this research. Finally, I dedicate this Master thesis to my parents.



# Abstract

Compliant mechanisms with flexure hinges represent a defining element of many precision devices in various fields of science and technology. Due to their importance, the ability of modeling their behavior with high precision represents the key for a further enhancement of their performance. The present scientific work contributes to the experimental verification of distinct mechanical models for thin semi-circular flexure hinges. For this purpose an experimental setup for the load application on the hinge has been developed, designed and set up. The device is designed to precisely determine the rotational stiffness of thin flexure hinges in their elastic range with a minimal notch height of 50, 75 and 100  $\mu\text{m}$ , but can be applied in a wider context in other applications as well. Two sets of hinges were analyzed, both manufactured by wire EDM in different companies. Although both sets were made with the same geometric dimensions, pronounced differences in their stiffness were measured. It is demonstrated that manufacturing has a large impact on the stiffness of the hinges because it affects the resulting geometry in the microscopic scale. The experimental results for one of the hinge sets are in good agreement with the calculations using the finite element method. Further research is required to confirm this trend. This would provide solid evidence for the invalidity of existing analytical stiffness equations for flexure hinges in the considered thickness range.



# Kurzzusammenfassung

Nachgiebige Mechanismen mit Festkörpergelenken bestimmen die Leistungsfähigkeit von vielen Präzisionsgeräten in verschiedenen Bereichen der Wissenschaft und Technik. Die präzise Modellierung der mechanischen Eigenschaften ist dabei eine entscheidende Grundlage für die Verbesserung deren Leistungsfähigkeit. Die vorliegende wissenschaftliche Arbeit trägt zur experimentellen Verifikation verschiedener mechanischer Modelle dünner Festkörpergelenke mit Halbkreis Kontur bei. Zu diesem Zweck wurde ein experimenteller Aufbau für die präzise Lasteinleitung auf das Festkörpergelenk entworfen und eingerichtet. Das Gerät ist zur präzisen Bestimmung der Drehsteifigkeit dünner Festkörpergelenke in ihrem elastischen Bereich mit einer minimalen Kerbenhöhe von 50, 75 und 100  $\mu\text{m}$  bestimmt, kann aber darüber hinaus auch zur hochgenauen Lastaufbringung für weitere Anwendungen eingesetzt werden. Es wurden zwei Sätze von Gelenken analysiert, die in verschiedenen Firmen durch Drahterodieren hergestellt wurden. Obwohl beide Gruppen mit den gleichen geometrischen Abmessungen gefertigt wurden ergaben sich große Steifigkeitsabweichungen. Es zeigte sich, dass die Herstellung einen großen Einfluss auf die Steifigkeit der Gelenke hat, da sie die resultierende Geometrie im mikroskopischen Maßstab beeinflusst. Die zu erwartende thermische Beeinflussung und Gefügeänderung des Werkstoffes bleiben zunächst unberücksichtigt. Die experimentellen Ergebnisse sind für einen Festkörpergelenksatz in guter Übereinstimmung mit den Berechnungen unter Nutzung der Finite Elemente Methode. Weitere Untersuchungen sind notwendig, um diese Tendenz zu bestätigen. Damit wäre ein solider Nachweis gegeben, dass die existierenden analytischen Ansätze zur Berechnung der Steifigkeit für den betrachteten Dickenbereich der Gelenke nicht mehr zutreffend sind.

# Contents

<b>1. Introduction</b>	<b>1</b>
<b>2. State of the Art</b>	<b>3</b>
2.1. Flexure Hinges . . . . .	3
2.1.1. Types of Flexure Hinges . . . . .	4
2.1.2. Applications . . . . .	6
2.2. Experimental setups . . . . .	6
<b>3. Design of the setup</b>	<b>10</b>
3.1. Requirements definition . . . . .	10
3.2. Conceptual design and operation . . . . .	11
3.3. Setup design and dimensioning . . . . .	13
3.4. Components and assembly . . . . .	24
3.5. Motion setup system . . . . .	27
3.5.1. Schematic overview . . . . .	27
3.5.2. Physical connections . . . . .	28
3.5.3. Operation modes . . . . .	30
<b>4. Experiment and results</b>	<b>33</b>
4.1. Rotational system behavior . . . . .	33
4.2. Experimental tests . . . . .	39
4.2.1. Tests of flexure hinges manufactured by manufacturer A . . . . .	39
4.2.2. Tests of Flexure Hinges manufactured by manufacturer B . . . . .	51
4.2.3. Results Evaluation and Discussion . . . . .	61
<b>5. Conclusions and Future work</b>	<b>67</b>
<b>Bibliography</b>	<b>68</b>
<b>A. Tables</b>	<b>72</b>
<b>B. Flow Diagrams</b>	<b>73</b>

# 1. Introduction

Compliant mechanisms have become an essential part in various fields of science and technology and continue to be of great importance for the field of precision engineering. They are composed of rigid parts linked by compliant joints and constitute the mechanical centerpiece of many precision devices.

At present, for high precision applications, compliant mechanisms are being used due to their advantages over conventional mechanisms. Among the main advantages is the fact that they are almost free of frictional losses, eliminate the use of lubricants and do not require maintenance. All these advantages come from the fact that in compliant mechanisms, conventional hinge joints are replaced by thin flexure hinges. Although compliant mechanisms offer important advantages, their disadvantages are related to the mechanical properties of all the structure like the limited range of motion that is dependent on the material properties and the geometry of both: hinges and the overall mechanism.

According to the way compliance is distributed in compliant mechanisms, they are classified as concentrated and distributed compliance. They are known as distributed compliance when the deformations are distributed throughout its topology and shape. However, mechanisms of concentrated compliance are those whose deformations are concentrated mainly in few regions of their parts. Compliant mechanisms with concentrated compliance are characterized by low load bearing capacity and low flexibility. In contrast, distributed compliance mechanisms are characterized by greater load capacity and greater flexibility.

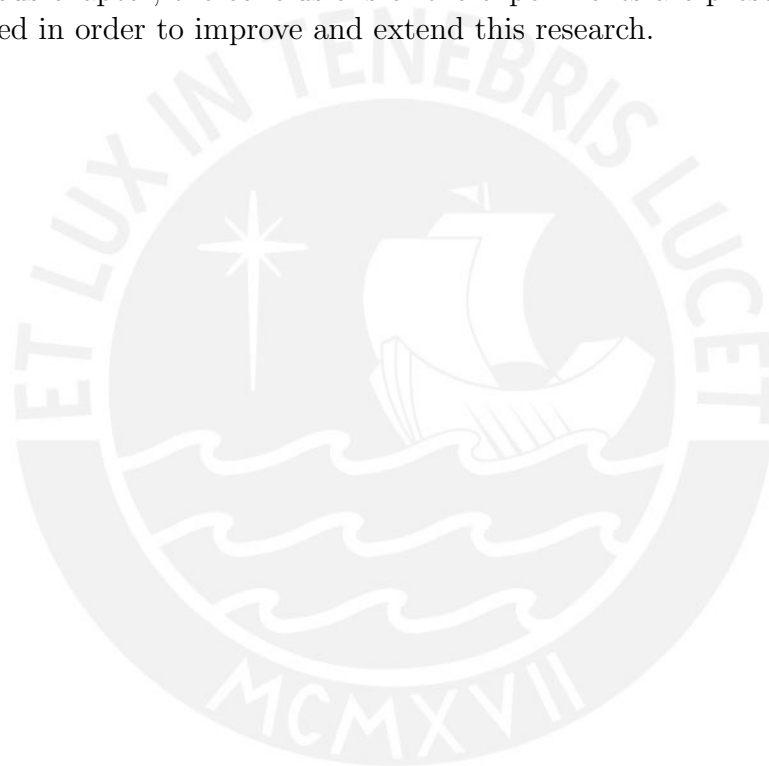
Flexure hinges are increasingly used in precision engineering, micromechanical systems and nanotechnology (e.g. EMFC-weighing cells, precision tiltmeters). They are made from a rigid single block which is mechanized in its middle part to create a mostly symmetric slender region that concentrates the biggest part of the overall compliance and contains the rotational axis.

Previous research has mostly contributed to identify relevant parameters and their correlation with the most important mechanical properties. There are some that focus on analyzing the behavior of the flexure hinge according to the applied load; others investigate the influence of hinge geometry on their stiffness. Further, there are some that compare hinges of different material; and even some research that study the behavior of compliant mechanisms. In most of the cases, the elaborated models of other researchers are predominantly based on finite element analysis (FEA). However, the revised literature is lacking a relevant scientific approach to identify the mechanical properties of thin

flexure hinges experimentally with the required precision.

The purpose of this thesis is to design and implement an experimental setup that allows the testing of thin flexure hinges. The test consists of a pure torque application on a thin flexure hinge and a measurement of the deflection response. Further, applied torque and flexed angle is arranged in a two-dimensional graph and compared with data obtained by analytical procedure and FEA. Thereby, the stiffness and mechanical behavior of the hinge can be determined in a the range of measurement.

The content of this thesis is organized in five chapters. Chapter 2 shows a brief overview about flexure hinges and the state of the art of experimental setups for similar applications. In Chapter 3, requirements of measuring are established according to chosen flexure hinge geometries and the design of the system is completely detailed. In Chapter 4, the setup operation is specified and results of the measurements are shown and compared to results of analytical formulas and FEA. Finally, in Chapter 5, using the results from the previous chapter, the conclusions of the experiments are presented and future work is proposed in order to improve and extend this research.





## 2. State of the Art

In this chapter, the topic of this thesis is contextualized, the the flexure hinge to be analyzed is defined and some previous approaches with similar objectives in measurements are presented.

### 2.1. Flexure Hinges

Flexure hinges are defined in [Lob03] as mechanical elements made from a monolithic piece which consists of two rigid parts linked by a slender section in the middle. The slender section results from a machining process of the monolithic piece and is mainly defining the mechanical properties of the flexure hinge. A generic flexure hinge configuration is shown in Fig. 2.1.

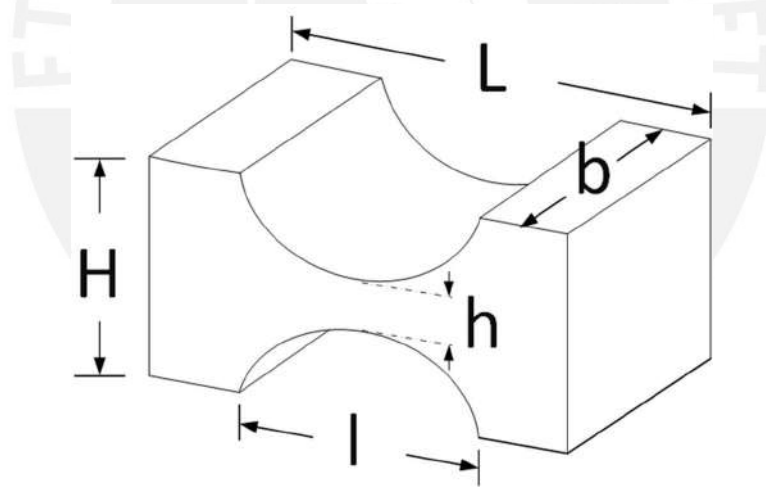


Figure 2.1.: Geometry of the semi-circular flexure hinge

One of the main reasons for using flexure hinges instead of conventional joints is that, when conventional joints are deflected, its center of rotation is modified. In contrast, when flexure hinges are deformed, the center of rotation is not greatly modified, by which the effect of the load is better applied [Du16; Par14]. Flexure hinges do have advantages and disadvantages that are listed as follows, according to [Lob03] in Table 2.1.

Table 2.1.: Advantages and disadvantages of flexure hinges

Advantages	Disadvantages
Small friction losses	Low angle of rotation
No need for lubrication	Not pure rotation
Small hysteresis	Sensitivity to temperature variations
Compactness	
Capacity to be utilized in small-scale applications	
virtually no maintenance needed	

Since the middle of the last century, research about flexible mechanisms has been introduced [Lob03]. In the mid-1960s, Paros and Weisbord [PW65] presented the compliance equations for flexure hinges with circular shape in their middle section. In this way, they set the basis for numerous analytical investigations for flexure hinges of different geometries and shapes.

Based on Paros and Weisbord research, there was an investigation made for elliptical flexure hinges in which there were determined analytically compliance equations for this kind of hinges, the analysis was developed for specific range of ratio between the major and minor radius of the elliptical section. In addition, the results obtained analytically and by finite element analysis were supported experimentally [Smi97]. As well as these, other investigations with particular objectives were made for a variety of cross section profiles of flexure hinges. Some focused on determine the equation compliance according to the shape of the hinge. Others comparing behavior of these with FEA and even some that analyze joints to improve fatigue life [ZH09; Sch05; IC14].

### 2.1.1. Types of Flexure Hinges

Flexure hinges may be classified by their geometry and by their applications, as is shown in Fig. 2.2 and Fig. 2.3 respectively. Based on their geometry, they can be grouped principally in circular, elliptical, polynomial, leaf-spring, 'V' profile, conic and miscellaneous notch shapes. Based on the applications, they can be grouped according to the degrees of freedom they can be used for, it may be single-axis, two-axis and multiple-axis [Lob03; Zhu15; IC14].

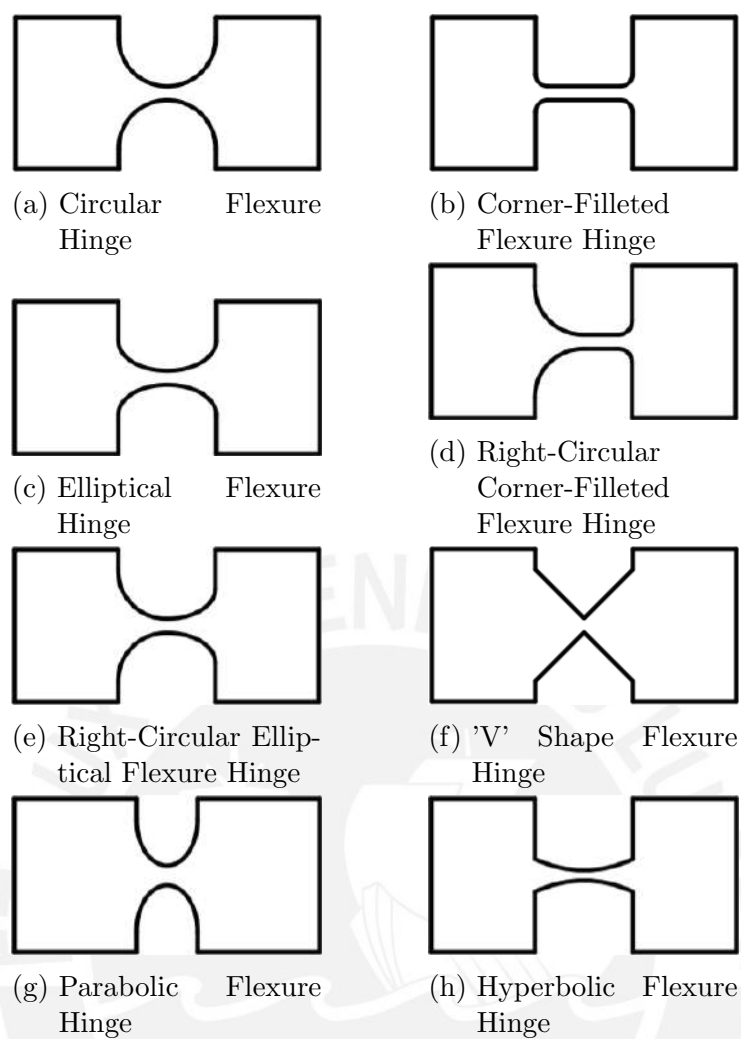


Figure 2.2.: Geometric shapes for Flexure Hinges Notches [Men12].

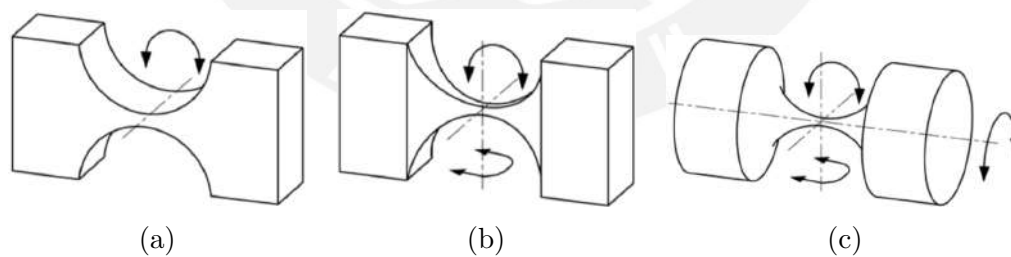


Figure 2.3.: Flexure Hinges according to their mobility (a) 1 DOF, (b) 2 DOF, (c) 3 DOF [Lin15].

## 2.1.2. Applications

Mainly used in compliant mechanisms, flexure hinges have demonstrated their performance in diverse applications during recent years. This is due to the great advantages compared to common joints in application where high positioning accuracy is required [Lob01; Tia10]. Flexure hinges are widely used in micro mechanical systems such as micro-machining, micro/nano positioning stages and micro/nano manipulators (x-ray lithography, micro-manufacturing, biomedicine, micro-surgery and nano-metrology) [Tia10; Zhu15].

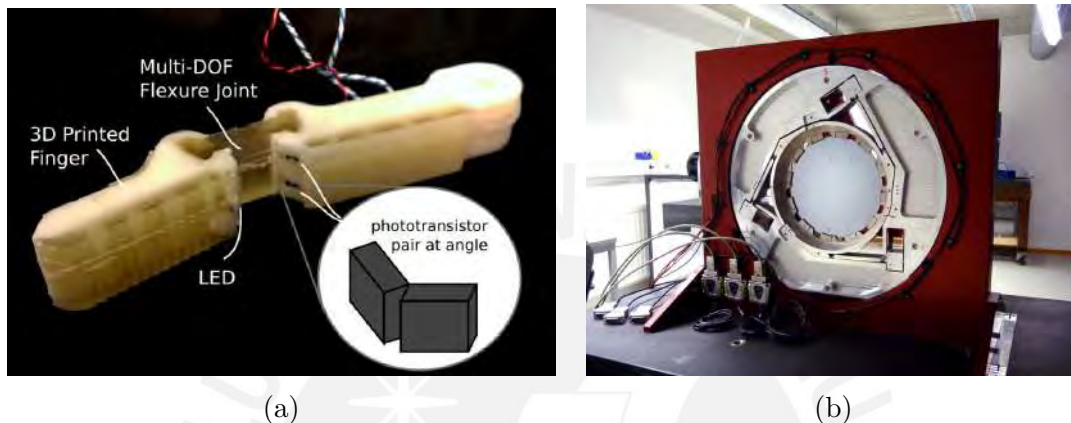


Figure 2.4.: Flexure Hinge Applications (a) Biomedicine [Jen14] (b) Micro/Nano Positioning Stages  
 (<https://www.janssenprecisionengineering.com/page/module-design-3dof-optical-motion-stage/>)

## 2.2. Experimental setups

This section focuses on experiments with flexure hinges with the aim of determining their mechanical properties. Flexure hinges are typically made from aluminum- or steel-alloys. In all revised cases, the analysis is done for short deformations in flexure hinges, in other words, only the elastic range of behavior is considered. To contribute to compliant mechanisms performance, an analysis of flexure hinge of larger deformation has been developed [Du16]. The material used is a metal alloy of nickel and titanium called Nitinol, the main property is the fact that parts made of this material recover their original form, after it has deformed when they are heated despite of being plastically deformed, they are known as super elasticity materials or shape memory alloy (SMA). The analytical part consists of relating the deformation angle and the torque applied according to mechanical calculations (material nonlinearities and geometrical considerations were taken into account). Further, verification part is carried out with the help of the experimental setup. It was proposed to apply a bending load on a flexure hinge

( $H=10$  mm;  $b=5$  mm;  $h=0.4$  mm and  $l=20$  mm constant cross section according to Fig. 2.1); the schematic diagram is shown below in Fig. 2.5.

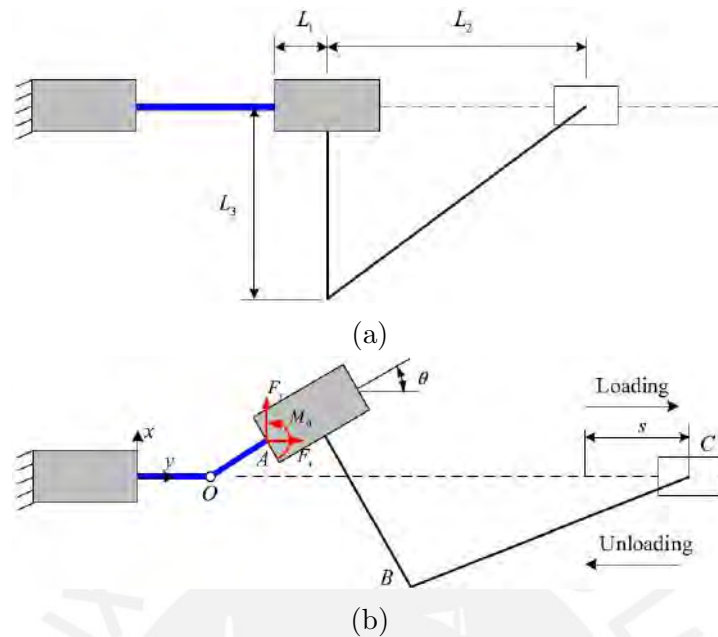


Figure 2.5.: Schematic setup to test flexure hinges made of shape memory alloy [Du16]

The force applied by the motor is in the range of 0 to 1.32 N approximately. It is measured continuously by a force/torque sensor; through the simple system, this force and the torque generated are transmitted to the free end of the hinge, and the bending angle is obtained geometrically. In Fig. 2.6 experimental setup is shown. Therefore, it was concluded that SMA material provide wider bending angle range in comparison to the conventional material (approximately 6 times). About stiffness, it was found that the stiffness of the hinge keeps constant for greater deformations to then decreases after the elastic behavior.

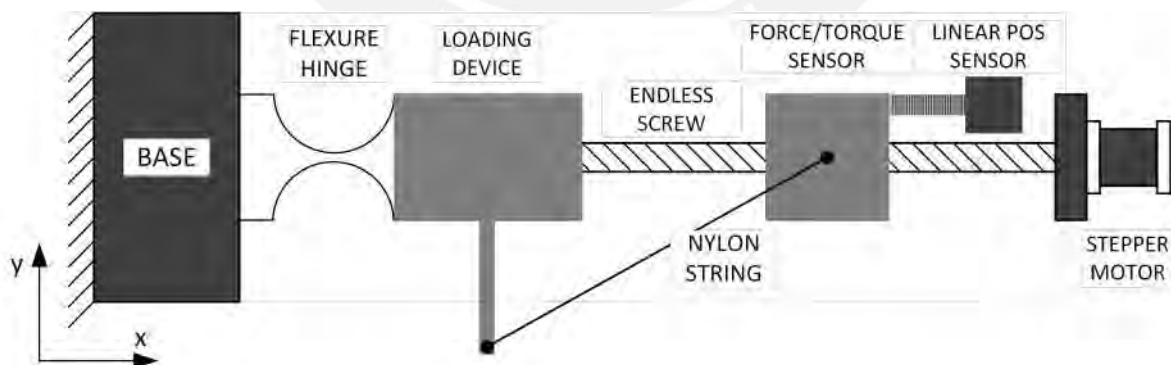


Figure 2.6.: Schematic experimental setup components [Du16]

Another investigations was carried out to test three circular flexure hinges of different

geometries ( $h=0.5, 0.7$  and  $0.84$  mm;  $l=6, 3.74$  and  $2.2$  mm constant cross section respectively) are analyzed, it consists of validating compliance determined by FEA with experimental values. Experimental values are determined by a setup that is on an anti-vibration table and the hinges are loaded by hanging weights that are applied at known distance from the center of rotation of the hinge. Rotational compliance, with respect to the  $z$ -axis, is obtained by the quotient of bending angle and the torque applied. Torque is calculated multiplying the gravitational force of the hanging weight and rectangular distance to the center of rotation. The angle is calculated geometrically through the distance measured by the two sensors whose operating principle is based on eddy current. On the other hand, compliance respect to the  $y$ -axis, is calculated due to the displacement of hanging weight, it is measured by an optical sensor that detect the rotation of the mirror attached to the hinge [YL09].

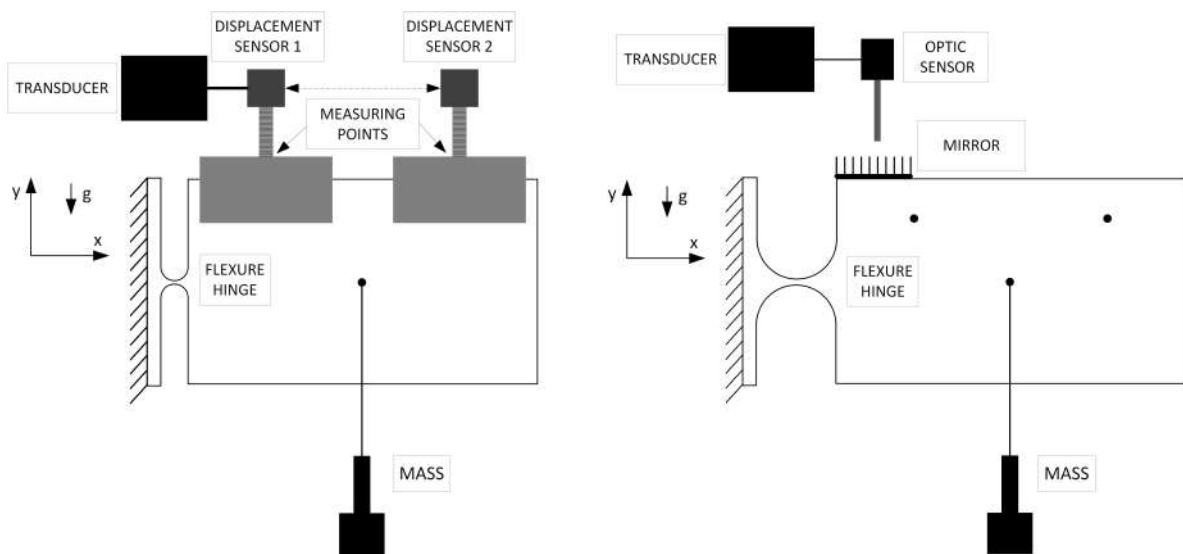


Figure 2.7.: Schematic of the experimental of both setups built in [YL09]

It can be notice that there is no way to measure the angle between the hinge and the hanging weight but it is assumed 90 degrees in all cases. In addition, to calculate the bending stiffness, the accuracy of eddy current sensors is not as significant as an optical sensor.

With the purpose to enhance the motion capacity of compliant mechanisms, a research is focused on validate theoretical models by experimentation [DYD16]. In this case, flexure hinge of ellipse-parabola shape ( $H=10\text{mm}$ ;  $b=5\text{mm}$ ;  $h=0.4$  mm;  $l=15, 20$  and  $25$  mm) are analyzed. As is shown in Fig. 2.8, setup schematic is basically formed by a flexure hinge fixed vertically on the top end and subjected of a loading device on the bottom end, where a mass is suspended on the end of the lever arm. Torque applied in this system is approximately  $72$  Nmm. The deflection angle and the vertical deformation are obtained by computer vision measurement system, it consists of a high-resolution camera with a resolution of  $8\ \mu\text{m}$  in straight deformations and  $1$  mrad on rotational deformations. The

hinges tested were rotated in the range of 10 to 20 degrees [DYD16].

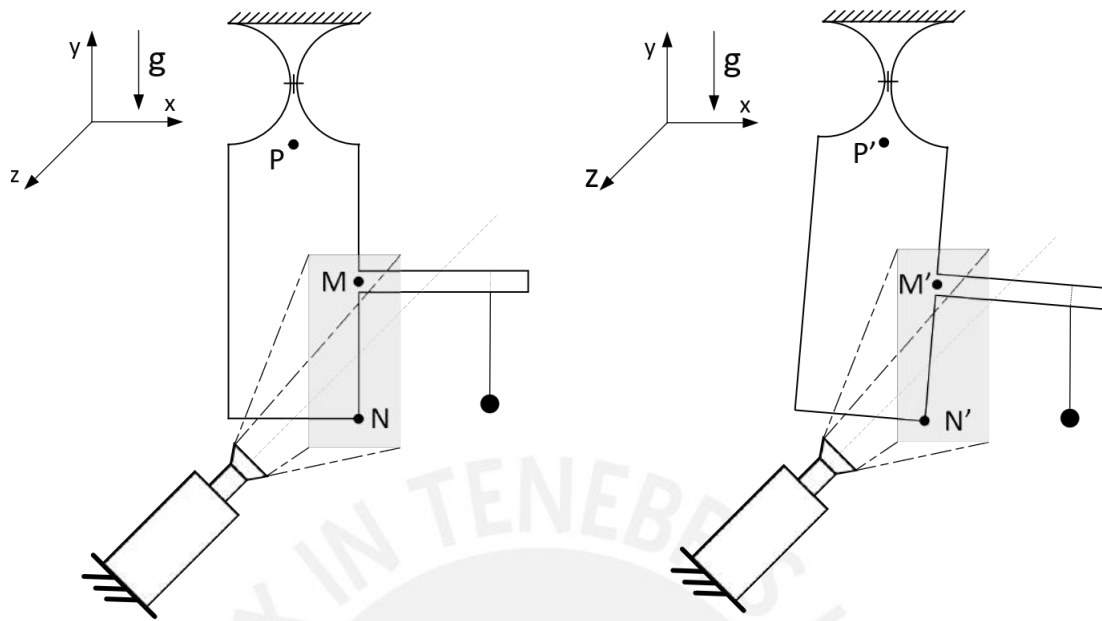


Figure 2.8.: Schematic of the experimental setup built in [DYD16]

In the state of the art presented above, experimental setups were developed to test flexure hinges with a thickness in the order of millimeters or fractions of a millimeter. The contribution of this thesis to the state of the art is that it is presented an experimental setup for the evaluation of rotational stiffness of thin flexure hinges with thickness in the order of micrometers. The setup allows the continuous load application. Also, it provides high resolution in both angle measurement and torque application. Furthermore, the torque applied avoids changes of axial loads.

## 3. Design of the setup

In this chapter, all the considerations for the design of the setup are detailed. It starts with the requirements, followed by conceptual design, then the dimensioning of the setup according to the requirements is specified. Later, the mechanic assembly is explained and represented, and finally a description of the movement system is made.

### 3.1. Requirements definition

The start point is the definition of the scope of the investigation. In particular, the aim of this thesis is to produce deflection on aluminum circular notch hinges of 50  $\mu\text{m}$ , 75  $\mu\text{m}$  and 100  $\mu\text{m}$  of thickness to obtain their experimental stiffness behavior in the elastic operation range. For this purpose, it is necessary to know the yield strength of the aluminum alloy, calculate the bending stress and finally determine the maximum bending angle in the elastic range based on the equations adapted from [LSZ17].

$$\frac{M}{\varphi} = \frac{2Ebh^{5/2}}{9\pi R^{1/2}} \quad (3.1)$$

$$k_b = \left(1 + \frac{h}{2R}\right)^{9/2} \quad (3.2)$$

$$\sigma_b = \frac{k_b M h}{2I} \quad (3.3)$$

$$s = \frac{\sigma_Y}{\sigma_b} \quad (3.4)$$



where:

$M$ - bending moment	$R$ - radius of the notch	$h$ - thickness of the notch
$\varphi$ - bending angle	$\sigma_b$ - bending stress applied	$I$ - moment of inertia
$E$ - Young's Modulus	$k_b$ - stress concentration factor	$s$ - factor of safety
$b$ - width of the notch		$\sigma_Y$ - yield strength

Solving equations 3.1, 3.2, 3.3 and 3.4, the maximum bending angle and the maximum bending torque for each notch is determined to limit the range of measurement and performance in the elastic region. In Table 3.1, " $M_{an}$ " indicates the maximum torque obtained by the equations presented above, and " $M_{FEA}$ "<sup>1</sup> indicates the maximum torque obtained by finite element analysis.

Table 3.1.: Maximum analytical requirements for torque and angle

$h$ ( $\mu\text{m}$ )	$M_{an}$ (Nmm)	$M_{FEA}$ (Nmm)	$\varphi_{max}$ ( $^\circ$ )
50	1.15	1.27	4.07
75	2.59	2.85	3.32
100	4.60	5.02	2.87

The values from Table 3.1 serve as a foundation for the development of a suitable measurement setup. They limit the range of operation of the elements that are the object of our study.

## 3.2. Conceptual design and operation

The purpose of this research is to study the bending behavior of thin flexure hinges in the elastic range. The parameter to be determined is the rotational stiffness ( $k_\varphi$ ). It is calculated dividing the torque with the bending angle. To get both variables, one of them must be applied and the other measured. Due to the high accuracy of the available optical measurement devices on high precision applications, it is rather to use them to measure the bending angle than to apply a specific bending angle to the hinge. Therefore, torque is applied.

There is more than one way to apply this kind of load on the hinge element, Fig. A.1, in Appendix A, contains some load configurations with which it is possible to achieve bending in the flexure hinge. Some of these configurations produce, in addition to bending

<sup>1</sup>Torres Melgarejo, Mario: Modeling of the elastic mechanical behavior of thin compliant joints under load for highest-precision applications (Ilmenau,2018)

moment, additional forces that would affect the measurements. Others may be difficult to implement or their implementation requires the coupling of more mechanical elements. It would increase costs and mainly affect uncertainties in measurements. And some others that do not provide symmetrical application of the loads that can induce shifts on rotation axis and different kind of stresses on each side of the hinge [Du16; Lin11]. Concluding, options A9 and A10 of Appendix A are more suited to the requirements of measurement despite of the existence of tension forces in the joint due to gravitational force and the external forces that produce bending. In Fig. 3.1 the most appropriate solution for the implementation due to its symmetry is presented. The resulting bending moment is the difference of both applied forces. The advantage lies in the fact that the moments applied do not need to be small but approximate to each other. Another advantage is that the axial load on the joint remains constant

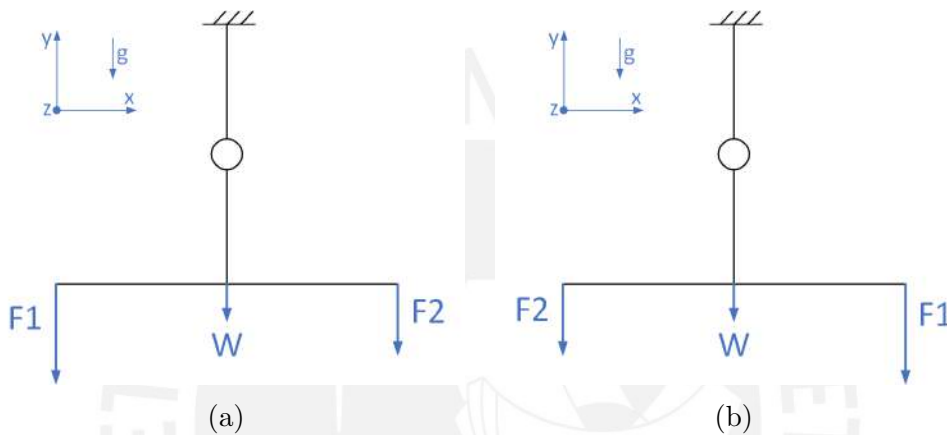


Figure 3.1.: Option of load application (a) turn anti-clockwise (b) turn clockwise

Omitting the direct application of electromagnetic and electrostatic forces on the system. Forces  $\vec{F}_1$  and  $\vec{F}_2$  could be generated in different ways, however some of these alternatives could involve complex and independent mechanisms between each end. We start from the premise of creating a *simple and functional* system. The inspiration for a purely mechanical solution was taken from the experimental setup presented in [Har68] to create an absolute length scale in the region of  $10^{-10}\text{m}$ , the system is based on the basic concept of torque generated by a force  $\vec{F}$  at a distance  $\vec{d}$ , specifically a body suspended at one end of a beam. To do this, a tape is suspended from one end to the other at an angle of  $90^\circ$  with respect to the plane and supported in the middle by a pulley that regulate the length of the tape from side to side. The rotation of the pulley is propelled by a motor-gearbox assembly. The rotation of the pulley modifies the length of the tape on both sides and the difference of masses between both sides cause the bending of the joint. Mirrors are placed on both ends to work with an angle measurement device. The schematic of the whole setup is shown in Fig. 3.2.

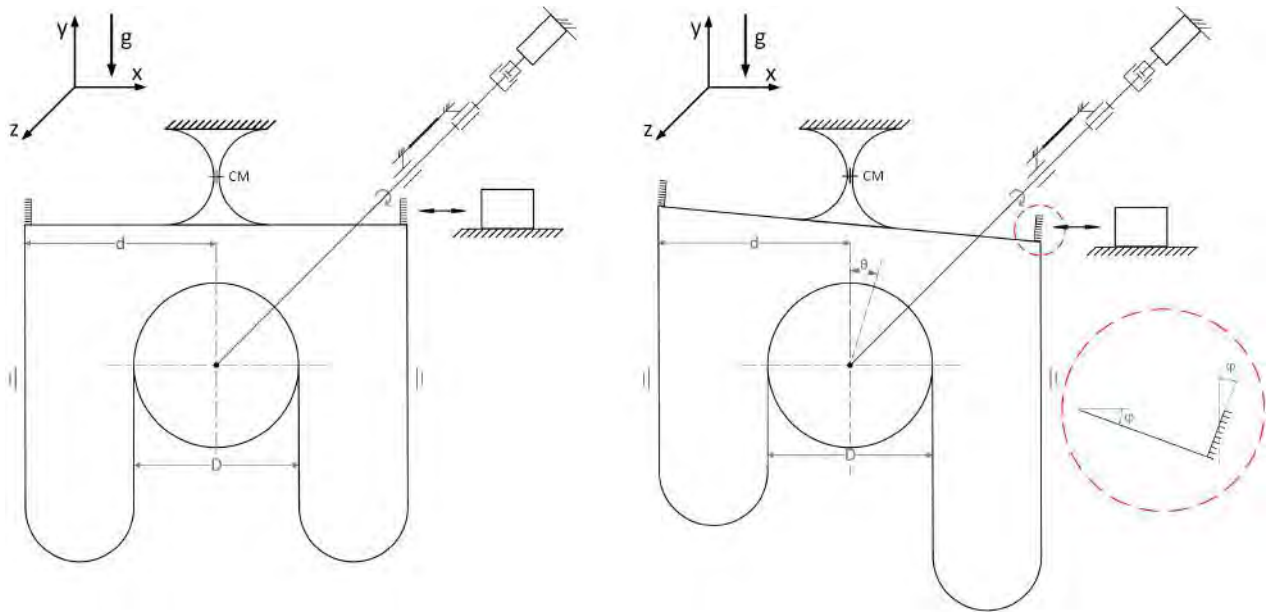


Figure 3.2.: Schematic of the Setup Resting (left) - Operating (right)

### 3.3. Setup design and dimensioning

In this section, the setup design is detailed. The function of main parts of the setup are explained. The mathematical formula to estimate the torque applied by the setup is exposed. Nominal values and uncertainties of the main variables are calculated.

**Coupling beam/hinge element:** To facilitate the torque application, according to the Fig. 3.2, it is necessary to extend the lever arm symmetrically from side to side. There are two ways to do this. The first is to combine the flexure hinge and the lever arm in a single element; the second is to build two independent elements (flexure hinge / lever arm) that can be coupled to accomplish the same function as the previous one. Each alternative has advantages and disadvantages. The first option has the advantage of reducing coupling errors that reduce the precision of the setup, but the elements under test that need to be manufactured with high precision (required for the thickness of the flexure hinge) would be larger and thus costly. The second eliminates this need. It allows to use a standard element of lever arm for each test. That way costs can be minimized, with the disadvantage that the repeatability of the measurements is dependent on the quality of the coupling.

For this work, the second option with the coupling was found to be more appropriate than the first one. Due to its frequent use in precision applications, kinematic couplings are the most suitable. They attach two structures by constraining six degrees of freedom (DOF), its basic principle of operation is to use a contact point per degree of freedom to constrain. The main types are shown below in Fig. 3.3, one of them consists of three

V-grooves radially oriented towards the center and symmetrically distributed on a flat structure. Three balls fixed to one structure which together define six constraints (two constraints per V-groove); the other type uses a V-groove (to constraints 2 DOF), a concave tetrahedron (to constrain 3 DOF) and a flat plate (to constrain 1 DOF), all of them instead of three V-grooves [Slo10; HS01; Slo10; Cul04].

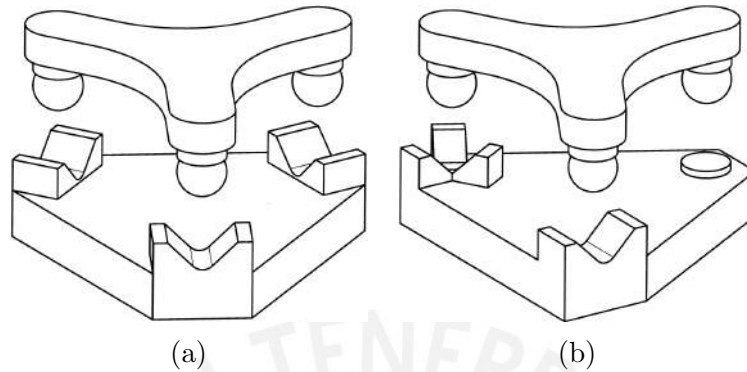


Figure 3.3.: Main kinematic couplings (a) Maxwell clamp (b) Kelvin clamp [HS01]

The kinematic coupling should have certain features as low mass, low cost, easy to manufacture and easy implementation. Hence, there would be some difference with respect to the standard ones. First of all, spheres will be orthogonally constrained on the lever arm structure by cylindrical holes; second, there will be a V-groove where two spheres will be sitting on; third, the third ball will be located on the other side on a flat section; and forth, both elements will be pressed with a point ball screw. Thus it is possible to constrain the relative displacement in the x-axis and y-axis between both elements without overconstraining which is important for the setup; it is achieved to do not increase the mass with complex couplings; it is possible to make the coupling easy to manufacture and with repeatability. However, constraint in z-axis can not be achieved, although it can be neglected because there are no loads in that direction and the position can be defined by stops during the mounting process.

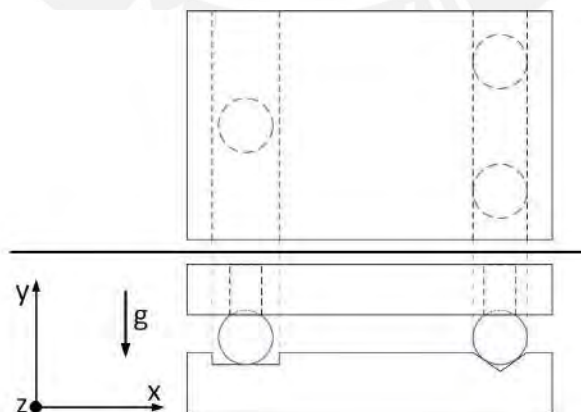


Figure 3.4.: Schematic of the Setup Resting (left) - Operating (right)

**Tape shape:** As is mentioned above, the main idea for the conceptual design is to take advantage of suspending equal lengths of tape on both sides of the rotation axis. These generate symmetrical torques, the form it adopts is catenary curve. Historically used, the catenary curve is the shape adopted by cables and/or chains when suspended from their ends and deformed due to their own weight over their length [GO04]. In theory, when considering a wire without stiffness, the equation of the catenary is defined as indicated in equation 3.5.

$$y(x) = a \cosh\left(\frac{x}{a} + C_1\right) + C_2 \quad (3.5)$$

Setting  $C_1$  and  $C_2$  equal to zero, the catenary curve would be centered in x-axis and with its lowest point at a distance "a" from the coordinate axis (see Fig. 3.5 ).

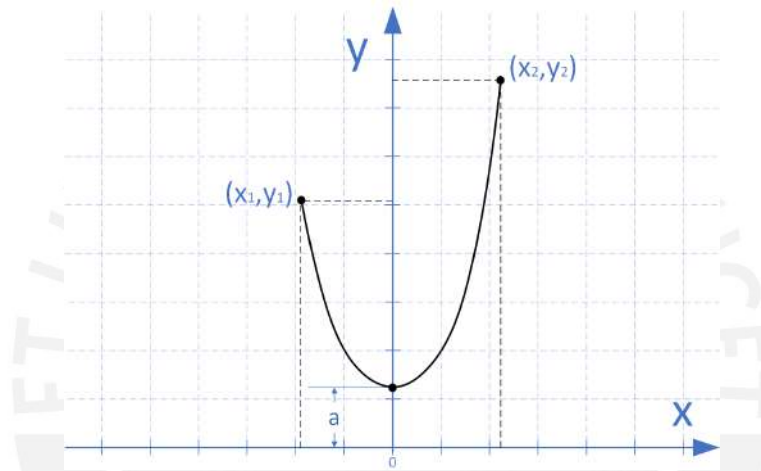


Figure 3.5.: Catenary curve

To have a better approximation of reality, it is necessary to consider the bending stiffness of the tape material. This consideration is made in [HP14] for a wire suspended of two points separated by a distance ( $L$ ), Young's modulus ( $E$ ), moment of inertia ( $I$ ) and constant horizontal tensile force ( $H$ ). The resulting dimensionless equation that describes its shape is expressed below.

$$\bar{y} = \frac{q \sec \theta}{2} (\bar{x}^2 - \bar{x}) + \tan \theta \bar{x} + \frac{q \sec \theta}{\xi^2} [1 - \cosh(\xi \bar{x}) + \tanh\left(\frac{\xi}{2}\right) \sinh(\xi \bar{x})] \quad (3.6)$$

where:  $\xi^2 = HL^2/EI$ ;  $\theta = \arctan[(y_2 - y_1)/(x_2 - x_1)]$  and  $L = x_2 - x_1$  [HP14].

For the design of this setup, we use the properties presented by a catenary curve and consider  $\beta = \dot{y}(x_2) \approx \pi/2$  so that the application of force at that point has almost null horizontal component and thus simplify calculations of the moment.

**Angle:** In accordance with Table 3.1, the maximum permissible clearance to the stops should be 2.87 degrees. Due to geometrical considerations, the clearance of the design is 2.08 degrees. To make sure that tests will be limited to the elastic operation region, there is going to be considered only the 10% of the elastic operation region; the worst case will be for the flexure hinge of 100  $\mu\text{m}$  thickness, it is  $0.29^\circ \approx 1033''$ , which means that the system must be designed to provide no more than  $1033''$ .

For bending angle on flexure hinge of 100  $\mu\text{m}$  thickness. The angle that is going to be measured is  $\varphi$  as is shown in Fig. 3.2 for which there are two high precision angle measuring devices available, they are *ELCOMAT 3000* and *SP-TR Interferometer*. Characteristics of both devices are shown in the Table 3.2.

Table 3.2.: High-precision angular measuring devices [MW; Gmb]

Device	Range (arcsec)	Resolution (arcsec)	Mirror (mm)	Beam features $\eta\text{m}$	Flatness $\eta\text{m}$
ELCOMAT 3000	$\pm 1000$	0.05	$> 5$	660	$\lambda/10$
SIOS Interferometer	$\pm 90$	0.002	$> 12$	632.8	-

Instead of thinking on design a setup that can only achieve limited angular displacement and to contribute to the research, it would be more beneficial to design a setup that can carry out larger angle. This idea can be explained by the fact that this way both angle measuring devices will be able to be used depending on the tasks of the current researches. In this manner, *ELCOMAT 3000* is chosen due to the wide range of measuring instead of its resolution, the setup is designed to produce bending angle until  $1000''$  on the notch of 50  $\mu\text{m}$  or apply 0.087 Nmm of moment (M). Hence, the measurement of the other hinges would be limited by the maximum moment the setup can achieve, because the greater their stiffness, the less bending angle. Therefore, according to the Table 3.1, both the hinge of 75 $\mu\text{m}$  and 100 $\mu\text{m}$ , would achieve theoretically  $365.2''$  and  $179.1''$  respectively. However, these values would change when the analytical torque is determined. Two mirrors are glued on both ends of the lever arm, they are constrained by a plane determined by three contact points and a V-groove as is shown in Fig. 3.6.

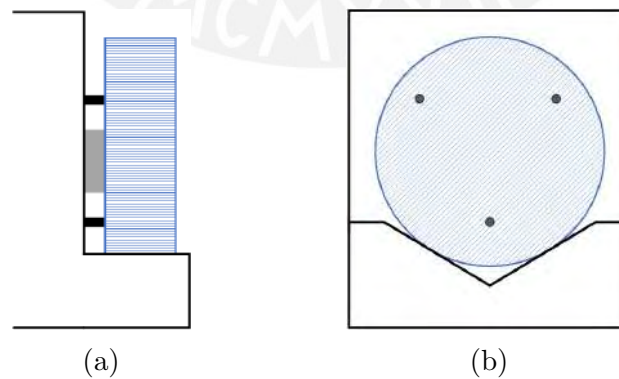


Figure 3.6.: Mirror positioning (a) Side view (b) Front view

**Pulley and motor arrangement:** According to Fig. 3.2, a system that turn the pulley needs to be defined. Bearings will play a crucial role for the shafts alignment and the role play of the arrange motor/gearbox is to transmit movement. Fortunately, there is a complete arrangement that can be use in this research. The main features of this are listed below in Table 3.3. In addition, the pulley is assembled to the shaft with a fixing screw, it needs a threaded hole into the hub and a flattened area on the shaft.

Table 3.3.: Devices for Motor/Gearbox arrangement

Device	Brand	Model	Characteristics
Motor	Faulhaber	3242GBX4	RPM: 8500 Encoder: 10000 counts/rev Ratio: 100
Gearbox	Harmonicdrive	CSF-11-100-2XH	No backlash 2 Bearings incorporated

**Torque:** The most important variable for the setup operation is the torque that can be applied to the flexure hinges. In order to facilitate torque calculation and due to the small variations on the tape geometry while it is in operation, some considerations have been taken into account to determine the bending moment applied for the setup. It starts with the free-body diagram of the notch and lever arm assembly, then there would be some geometrical assumptions to take into account and finally obtain the approximate formula of the bending moment.

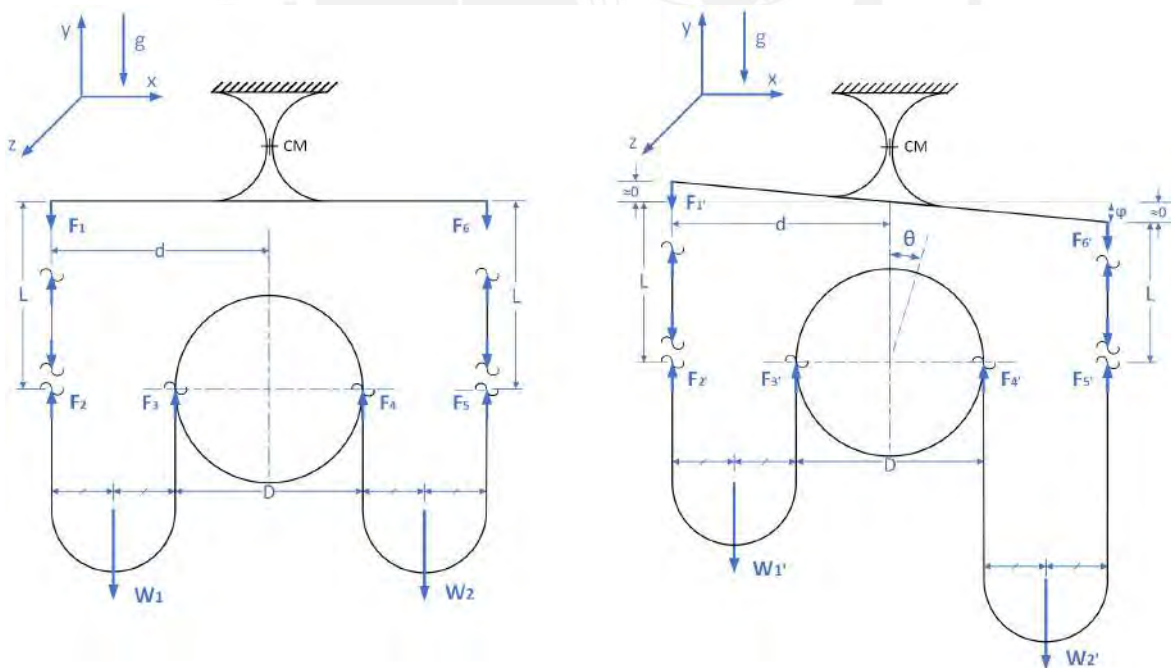


Figure 3.7.: Free-body diagram of the tape: resting (left) - operating (right)

Applying the second equilibrium condition with respect to CM, Eq. (3.7) is obtained.

$$\sum \tau_{CM} = M$$

$$(F_{6'} - F_{1'}) d = M \quad (3.7)$$

Then, it is considered no height variation of the application points of  $F_{1'}$  and  $F_{6'}$  as is indicated in Fig. 3.7 (right). In consequence, the following is arranged:

$$F_{1'} = F_{2'} + W_L \quad \text{and} \quad F_{6'} = F_{5'} + W_L \quad (3.8)$$

Where  $W_L$  is the weight of the segment of length  $L$ . Also, from Eq. (3.8) it can be deduced that  $F_{6'} - F_{1'} = F_{5'} - F_{2'}$ . The relation between those forces is taken into account to deduce Eq. (3.7). In the initial resting position, the tape is equally distributed on both sides of the pulley. Thus, it can be said the following:

$$W_1 = W_2 \quad (3.9)$$

Then, it is assumed that weight of the tape on both sides of the pulley acts in the middle axis of each concave section. In consequence, according to Fig. 3.7 and applying the first and second equilibrium conditions respect to the  $y$ -axis and CM respectively, it is possible to deduce the following:

$$F_2 + F_3 = W_1 \quad \text{and} \quad F_2 = F_3 \longrightarrow F_2 = \frac{W_1}{2} \quad (3.10)$$

$$F_4 + F_5 = W_2 \quad \text{and} \quad F_4 = F_5 \longrightarrow F_5 = \frac{W_2}{2} \quad (3.11)$$

When performing the rotation of the pulley, variation of the length of the tape is given by  $\Delta l = \theta \frac{D}{2}$ . Then, taking into account the considerations for obtaining the equations 3.10 and 3.11, the first and second equilibrium conditions are applied when the pulley is already rotated to obtain:

$$F_{2'} + F_{3'} = W_{1'} \quad \text{and} \quad F_{2'} = F_{3'} \longrightarrow F_{2'} = \frac{W_{1'}}{2} \quad (3.12)$$



$$F_{4'} + F_{5'} = W_{2'} \quad \text{and} \quad F_{4'} = F_{5'} \longrightarrow F_{5'} = \frac{W_{2'}}{2} \quad (3.13)$$

The weight variations of the tape on both sides of the pulley, before and after carrying out the experiment, is defined by the weight difference of each side of the tape. This is expressed in equation 3.14.

$$W_{1'} - W_1 = -\rho wt\Delta l g \quad \text{and} \quad W_{2'} - W_2 = \rho wt\Delta l g \quad (3.14)$$

Where the mass of the displaced tape is defined by  $\Delta m = \rho wt\Delta l$ . Inserting Eq. (3.9) in Eq. (3.14), the following equation is obtained (Eq. (3.15)).

$$W_{2'} - W_{1'} = 2\rho wt\Delta l g \quad (3.15)$$

Then,  $W_{1'}$  and  $W_{2'}$  are cleared from Eq. (3.12) and Eq. (3.13) respectively. Further, they are inserted in Eq. (3.15) to get the following equation:

$$F_{5'} - F_{2'} = \rho wt\Delta l g \quad (3.16)$$

Multiplying Eq. (3.16) by the lever arm length ( $d$ ) and inserting the length variation of the (tape ( $\Delta l$ ), it can be obtained the following.

$$(F_{5'} - F_{2'})d = \rho wt\theta \frac{D}{2}gd$$

Finally, Eq. (3.7) is deduced. The moment applied is defined by Eq. (3.17).

$$M = \rho wt\theta \frac{D}{2}gd \quad (3.17)$$

$M$  - bending moment

$\theta$  - pulley rotation angle

$\rho$  - tape density

$D$  - pulley diameter

$w$  - tape width

$g$  - acceleration of gravity

$t$  - tape thickness

$d$  - moment of inertia

There are two kind of experimental magnitudes. First, there are quantities obtained directly by measurement operation, like measuring the length of a segment, the mass of an object or the temperature of an environment. Second, some quantities are derivated from others.

These physical magnitudes depend of the mathematical relation between the others. Thus, it is understood that the errors of the variables considered in the calculation are propagated and affect its precision and accuracy [HH10]. Let us suppose measure of some quantities  $x_1, x_2, x_3, \dots, x_n$  with uncertainties  $\sigma_{x_1}, \sigma_{x_2}, \sigma_{x_3}, \dots, \sigma_{x_n}$ . Then suppose we need to calculate the value of the uncertainty of  $f = f(x_1, x_2, x_3, \dots, x_n)$  denoted by  $\sigma_f$ , it can be determined as follow in the equation 3.18.

$$\sigma_f = \sqrt{\left(\frac{\partial f}{\partial x_1}\right)^2 \sigma_{x_1}^2 + \left(\frac{\partial f}{\partial x_2}\right)^2 \sigma_{x_2}^2 + \left(\frac{\partial f}{\partial x_3}\right)^2 \sigma_{x_3}^2 + \dots + \left(\frac{\partial f}{\partial x_n}\right)^2 \sigma_{x_n}^2} \quad (3.18)$$

Thus, the standard form to represent the variable is  $f \pm \sigma_f$ . For our purpose, the value of the moment  $M$  is already determined as is shown in Eq. (3.17), likewise the moment uncertainty might be calculated using equation 3.18 and adapting the independent variables to get equation 3.19.

$$\sigma_M = \sqrt{\left(\frac{\partial M}{\partial \theta}\right)^2 \sigma_\theta^2 + \left(\frac{\partial M}{\partial D}\right)^2 \sigma_D^2 + \left(\frac{\partial M}{\partial d}\right)^2 \sigma_d^2 + \left(\frac{\partial M}{\partial w}\right)^2 \sigma_w^2 + \left(\frac{\partial M}{\partial t}\right)^2 \sigma_t^2} \quad (3.19)$$

$\sigma_M$  - bending moment uncertainty

$\sigma_d$  - lever arm uncertainty

$\sigma_\theta$  - pulley rotation angle uncertainty

$\sigma_w$  - tape width uncertainty

$\sigma_D$  - pulley diameter uncertainty

$\sigma_t$  - tape thickness uncertainty

Whereas, the bending angle  $\varphi$  can be obtained from equations 3.1 and 3.17 as is shown below.

$$\varphi = \frac{9\pi g\rho}{4E\sqrt{2}} \frac{\theta D d w t l^{1/2}}{b h^{5/2}} \quad (3.20)$$

Then uncertainty of bending angle  $\varphi$  results in  $\sigma_\varphi$  as follows:

$$\sigma_\varphi = \left[ \left(\frac{\partial \varphi}{\partial \theta}\right)^2 \sigma_\theta^2 + \left(\frac{\partial \varphi}{\partial D}\right)^2 \sigma_D^2 + \left(\frac{\partial \varphi}{\partial d}\right)^2 \sigma_d^2 + \left(\frac{\partial \varphi}{\partial w}\right)^2 \sigma_w^2 + \left(\frac{\partial \varphi}{\partial t}\right)^2 \sigma_t^2 + \left(\frac{\partial \varphi}{\partial l}\right)^2 \sigma_l^2 + \left(\frac{\partial \varphi}{\partial b}\right)^2 \sigma_b^2 + \left(\frac{\partial \varphi}{\partial h}\right)^2 \sigma_h^2 \right]^{1/2} \quad (3.21)$$

$\sigma_\varphi$ - bending angle uncertainty	$\sigma_t$ - tape thickness uncertainty
$\sigma_\theta$ - pulley rotation angle uncertainty	$\sigma_l$ - hinge diameter uncertainty
$\sigma_D$ - pulley diameter uncertainty	$\sigma_b$ - hinche width uncertainty
$\sigma_d$ - lever arm uncertainty	$\sigma_h$ - hinge thickness uncertainty
$\sigma_w$ - tape width uncertainty	

**Numerical calculation:** After having defined the overall aspects and qualitative procedures taken into account for the design of this setup, the quantitative parameters and numerical results obtained are calculated and presented.

There are numerous assumptions which have to be taken into account to set the dimensions of the hole setup as the fact that the tape is hung up tangentially on both sides of the pulley (see Fig. 3.2) or, probably the most important, assume that the maximum rotation of the pulley is  $\theta = 10^\circ$ . It was decided in order to make sure that both tangential points are located at an approximate height. Otherwise, it would cause that the lengths of the tape on both sides differ not only by the pulley rotation, but also for the difference between their heights.

According to the Eq. (3.17) it is necessary to define the characteristics of the tape. This must be flexible enough to take the shape of the rope seen in Eq. (3.17) and not influenced by magnetic fields. It was considered two accessible materials that, depending on the length and the distance between their support points, could be suitable for the experiment; these are the audio tapes or brass precision tapes, their features are detailed in Table 3.4.:

Table 3.4.: Available tapes dimensions [Per16; Sta03; Has]

Material	Density ( $g/cm^3$ )	Width (mm)	Thickness (mm)
Audio tape	1.61 - 4.06	6.35 - 50.8	0.007 - 0.03
Brass tape	8.45	1 - 150	0.05 - 0.50

As is mentioned above, a moment  $M = 0.087$  Nmm is required. Then, according to the Eq. (3.17), moment  $M$  depends of tape characteristics (density ( $\rho$ ) and cross section ( $w, t$ )), pulley diameter ( $D$ ), pulley rotation angle ( $\theta$ ), lever arm ( $d$ ) and acceleration of gravity ( $g$ ). If some of these parameters ( $\rho, g, \theta$ ) are constants and considering the range of values of ' $w$ ' and ' $t$ ' for each material; then the range of values for the pulley radius ' $D/2$ ' and ' $d$ ' can be calculated. In Fig. 3.8, it can be seen on a x-y graph the distribution of  $D/2$  and  $d$  (*black* for brass tape and *gray* for audio tape) that satisfy the requirements of torque. Values of  $d$  are limited between 50 mm and 300 mm in order to not increase excessively the weight that is going to be hung from the flexure hinge. Another consideration taken into account was to fit the setup without problems

in the work environment. Finally, reordering all variables of Eq. (3.17) it is possible to find the relation between the pulley radius ( $D/2$ ) and the length of the lever arm ( $d$ ) to get Eq. (3.22). This way it is possible to determine all possible combinations of pulley diameter and length of lever arm to achieve the required torque.

$$\frac{D}{2}d = \frac{M}{\rho w t \theta g} \longrightarrow \frac{D}{2}d = \text{const.} \quad (3.22)$$

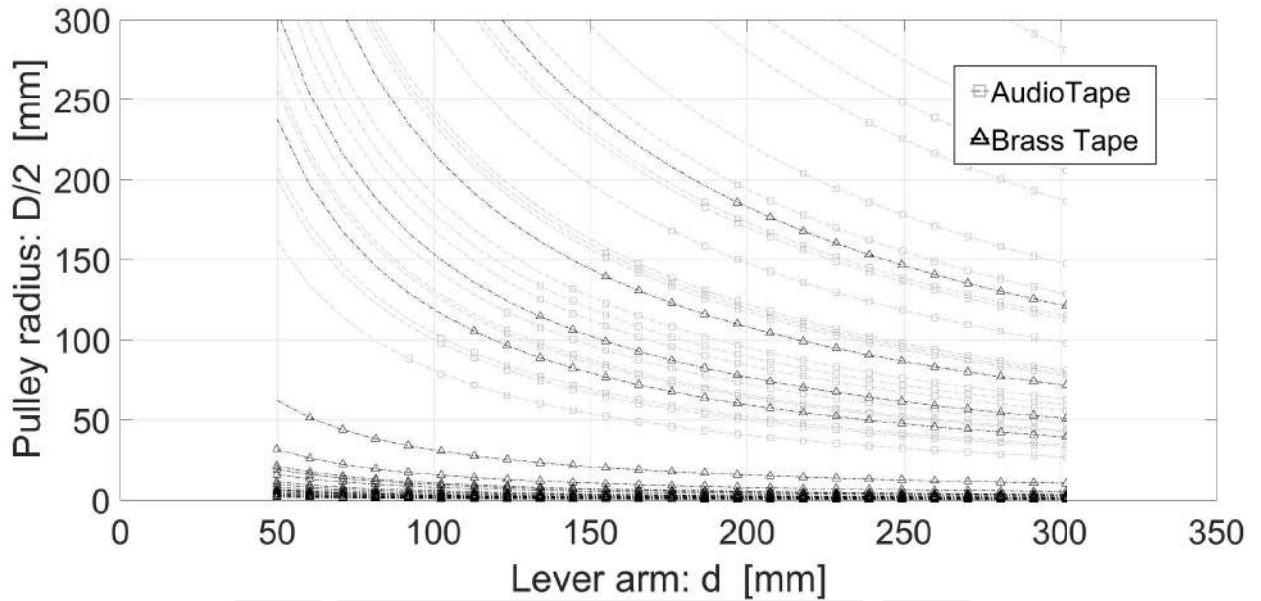


Figure 3.8.: Dispersion of Pulley Radio and Lever Arm values to get the required torque due to the tape cross section and material Brass tape (black) - Audio tape (gray)

As seen in Fig. 3.8, using audio tape instead of brass tape, there are required larger sizes of pulley and lever arm to achieve the torque. For this reason, it becomes more convenient to use brass tape rather than audio tape, this last could be more useful for shorter torques. Therefore, with all these considerations, the values of all the variables in equation 3.17 are the following:  $\rho = 8.45 \text{ g/cm}^3$ ,  $w = 40 \text{ mm}$ ,  $t = 0.02 \text{ mm}$ ,  $\theta = 10^\circ$ ,  $D = 110 \text{ mm}$ ,  $d = 135 \text{ mm}$ ,  $g = 9.81 \text{ m/s}^2$  to get a torque of  $M = 0.0859 \text{ Nmm}$ .

After determining the value of the variables, the behavior of a tape supported at its ends and hanging only its own weight was tested in *ANSYS 18.2*. This calculation provided the position of the points from which the tape is supported. The shape of the tape is shown in Fig. 3.9.

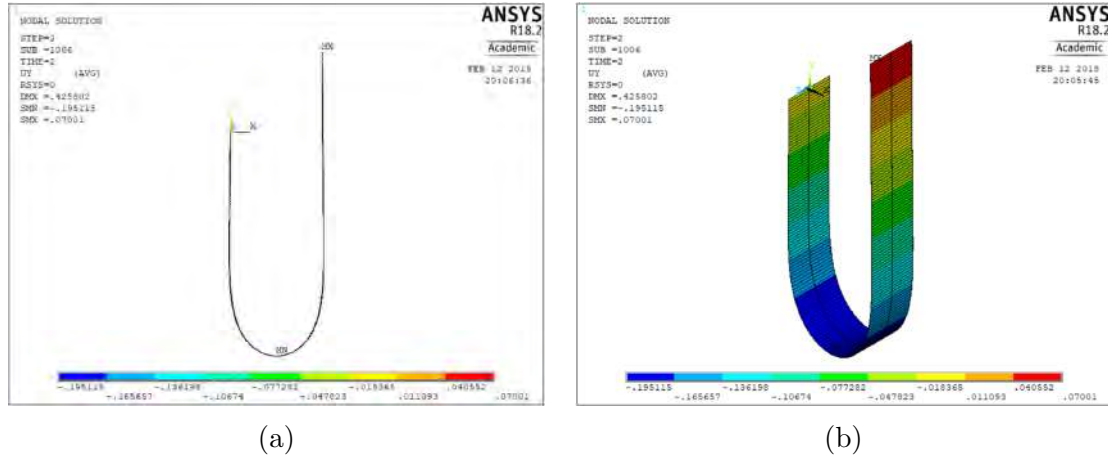


Figure 3.9.: Tape shape simulation (a) front view (b) isometric view

According to the equation 3.19, the propagation of torque uncertainty depends on the nominal values and the uncertainties of the variables that comprise it. Some of them, like the uncertainties of the tape, are given by the technical sheet of the manufacturer. But, others need to be established considering the manufacturer protocols that are taken into account to produce them. Also, the influence of their uncertainties on torque uncertainty should be considered.

In particular, pulley rotation angle uncertainty is directly obtained from the encoder resolution and the gearbox ratio. Values of the uncertainties are calculated in order to get less than ten percent of bending moment as uncertainty, these values are the following:  $\sigma_M = 0.008596$  Nmm;  $\sigma_\theta = 0.162$  arcsec;  $\sigma_D = 0.2$  mm;  $\sigma_d = 0.2$  mm;  $\sigma_w = 0.002$  mm and  $\sigma_t = 0.002$  mm.

Finally, these variables are expressed as follows in Table 3.5 according to the theory of errors and uncertainties.

Table 3.5.: Variables and uncertainties values

Variables	Nominal values	Tolerances	Units
M	0.086	$\pm 0.009$	Nmm
$\theta$	10.0000000	$\pm 5 \cdot 10^{-7}$	degrees
D	110.0	$\pm 0.2$	mm
d	135.0	$\pm 0.2$	mm
w	40.000	$\pm 0.002$	mm
t	0.020	$\pm 0.002$	mm

Variables previously shown do not represent the behavior of bending angle during the setup operation. Equation 3.21 can be evaluated to get equation 3.23 and to notice that analytical bending angle uncertainty ( $\sigma_\varphi$ ) depends on the rotation angle of the pulley ( $\theta$ ).

$$\sigma_\varphi = \frac{9\pi g\rho}{4E\sqrt{2}} \left[ \left( \frac{Ddwtl^{1/2}}{bh^{5/2}} \right)^2 \sigma_\theta + \left( \frac{\theta dwtl^{1/2}}{bh^{5/2}} \right)^2 \sigma_D + \left( \frac{\theta Dwtl^{1/2}}{bh^{5/2}} \right)^2 \sigma_d + \left( \frac{\theta Ddtl^{1/2}}{bh^{5/2}} \right)^2 \sigma_w + \right. \\ \left. + \left( \frac{\theta Ddwtl^{1/2}}{bh^{5/2}} \right)^2 \sigma_t + \left( \frac{1}{2} \frac{\theta Ddwtl^{-1/2}}{bh^{5/2}} \right)^2 \sigma_l + \left( -\frac{\theta Ddwtl^{1/2}}{b^2 h^{5/2}} \right)^2 \sigma_b + \left( -\frac{5}{2} \frac{\theta Ddwtl^{1/2}}{b^2 h^{7/2}} \right)^2 \sigma_h \right]^{1/2} \quad (3.23)$$

In Table 3.6, there are organized the values of bending angles and bending angle uncertainties for the flexure hinges for pulley rotation from 0 to 10 degrees. Calculations demonstrate that the more rotation of pulley, the more uncertainty of bending angle.

Table 3.6.: Analytical bending angle and uncertainties according to pulley rotation for each flexure hinge

$\theta$ (o)	T (Nmm)	h=50 $\mu$ m		h=75 $\mu$ m		h=100 $\mu$ m	
		$\varphi$ (arcsec)	$\sigma_\varphi$ (arcsec)	$\varphi$ (arcsec)	$\sigma_\varphi$ (arcsec)	$\varphi$ (arcsec)	$\sigma_\varphi$ (arcsec)
0	0	0	0	0	0	0	0
1	0.0086	109.36	0.06	39.69	0.02	19.332	0.0097
2	0.0172	218.72	0.12	79.37	0.04	38.664	0.019
3	0.0258	328.08	0.18	119.05	0.06	57.996	0.029
4	0.0344	437.44	0.24	158.74	0.08	77.329	0.039
5	0.0430	546.79	0.30	198.42	0.10	96.661	0.048
6	0.0516	656.15	0.36	238.11	0.12	115.993	0.058
7	0.0602	765.51	0.42	277.79	0.14	135.325	0.068
8	0.0688	874.82	0.47	317.48	0.16	154.657	0.077
9	0.0773	984.23	0.53	357.16	0.18	173.989	0.087
10	0.0859	1093.59	0.59	396.85	0.20	193.321	0.097

After calculating the main variables involved in sizing of the setup, the following section contains the detail of the functions of each part.

### 3.4. Components and assembly

Details of the parts and assembly elements that were considered necessary for the implementation are shown and explained below. Drawings and dimensions are detailed in the appendix.

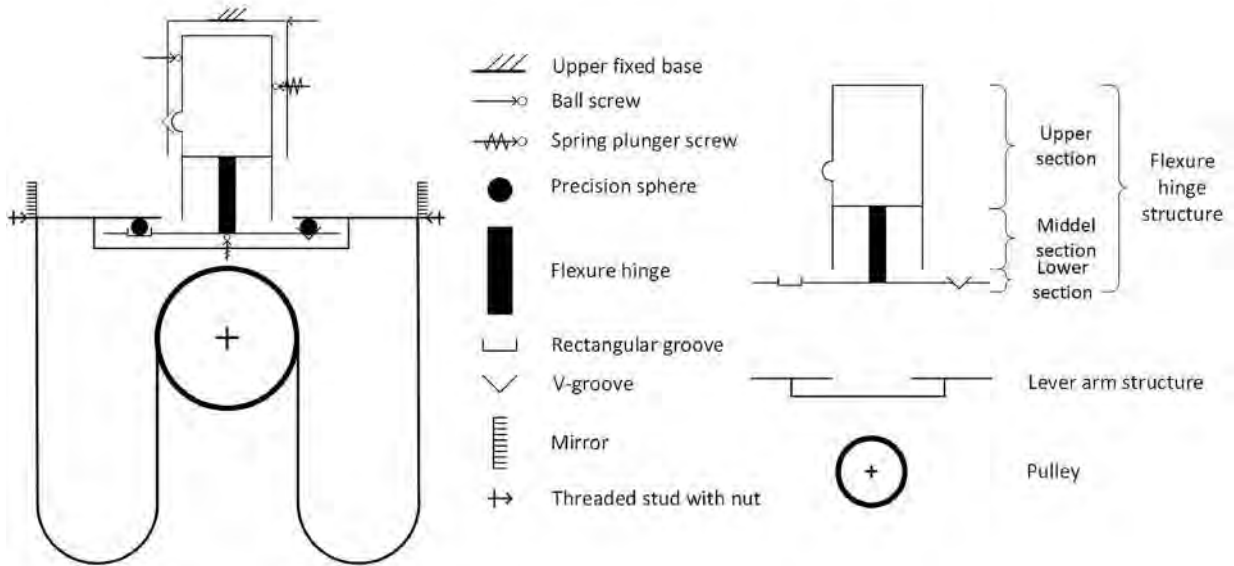


Figure 3.10.: Basic scheme of the setup and main assembly components

**Flexure hinge structure:** It is the main element on the setup made of aluminum alloy. It is composed in its central section by the flexure hinge and two stops on both sides, on left side of upper section spread out a rectangular profile with a semi-circular relief and on the lower part extends a rectangular section as a grooved beam (rectangular groove and V-groove). This element will be fixed on top with a spring plunger screw. A second screw are used for adjustment. Also, it is to align the main element with the frame with greater precision. In the middle part the flexure hinge is protected of yielding by two stops on each side that limit the bending angle to 2.36 degrees (according to Table 3.1, yield point is achieved on 2.87 degrees for flexure hinge of 100  $\mu\text{m}$ ), and in its lower section, the grooves serve to align this element with the lever arm structure.

**Lever arm structure:** Made of aluminum, the only functions of this structure is to extend the lever arm to reach the torque needed with the selected tape and to place the mirrors properly. The characteristics to be considered for this structure are rigidity, lightweight design, ease of construction and symmetry. In that sense, the most appropriate structure is a planar truss. It because of this kind of triangular structures provide enough rigidity to prevent it of deformations caused by its own weight and by external loads. Another advantage is that due to the triangular shapes inside, the weight of the structure of the lever arm is reduced. The center section of the truss is connected to the lower section of Flexure Hinge structure by a kinematic mount. On the lateral ends there are two V-grooves to rest the mirrors on them.

**Top Holder:** The functions of these elements is to fix the system to the external frame to hold the system by pressing. It consists on a L-shape piece of aluminum alloy with two holes on the shorter segment and a threaded hole and V-groove (for the alignment the Flexure Hinge structure vertically) on the longer segment. Also, a short beam with two threaded holes, one is used to put both pieces together. The other, to insert the spring plunger ball screw for applying point pressure to the upper section of the Flexure Hinge structure.

**Pulley, mirrors, precision spheres and screws:** Pulley is designed considering the external diameter and minimizing its weight, for this reason it is made of aluminum alloy with a large pocket to reduce the weight. It is connected with the gear-box shaft using a setscrew. Mirrors are made of silica substrate with 15 mm diameter, 3 mm thickness, beam wavelength  $\lambda = 250 - 700 \text{ nm}$  and  $\lambda/10$  surface flatness. They are glued to both ends of the lever arm. Finally, three stainless steel precision spheres are used for the alignment of flexure hinge and lever arm structures.

Following, in Fig. 3.11 there are shown the final design of the experimental setup.

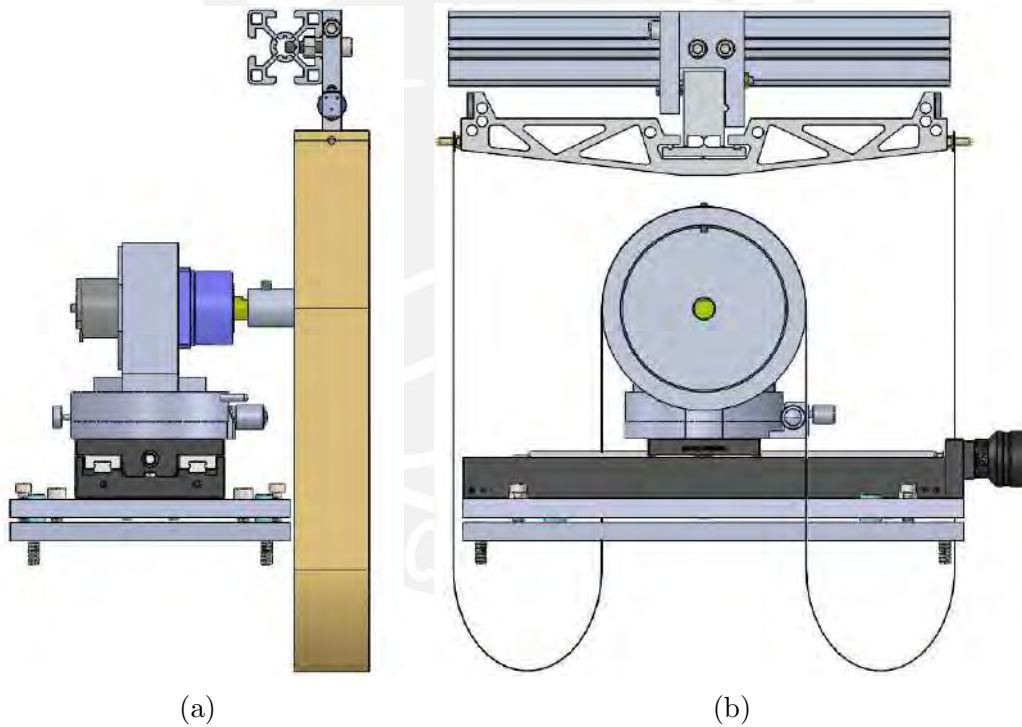


Figure 3.11.: Experimental setup Ddesign (a) side view (b) front view



## 3.5. Motion setup system

After having established the mechanical components of the setup, it is necessary to specify the elements that manage the movement and data collection of the system. This section start with a complete overview of the experimental setup. Then, wiring and connections between all devices are indicated. Finally, the main configurations of the electronic equipments are explained in order to stablish their best performance.

### 3.5.1. Schematic overview

The setup operates turning the motor from  $\theta = 0^\circ$  to  $\theta = 10^\circ$ . To do this, motor requires to read some configuration and movement instructions, then send response commands to indicate the current encoder position. While torque is applied and bending on the flexure hinge occurs, the angle measurement device needs to collect angle data and send them to the computer. At a last step, all data is processed and arranged to obtain the behavior of torque respect to the bending angle. In Fig. 3.12, communication diagram is shown.

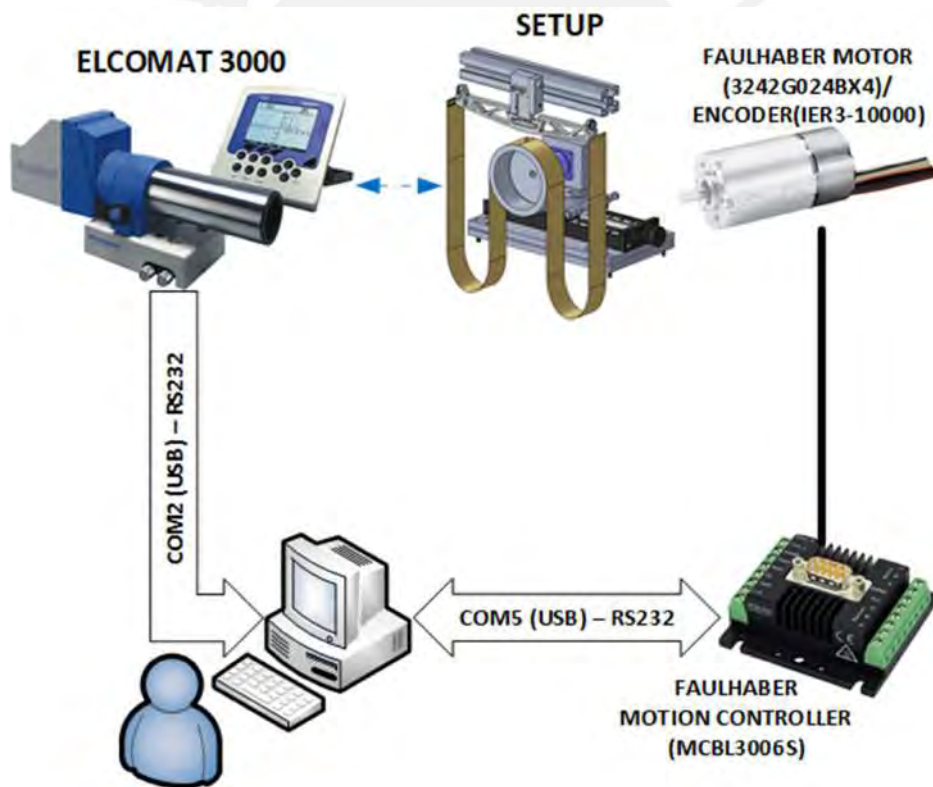


Figure 3.12.: Communication diagram

The correct wiring between all devices is made in accordance with the manuals in order to avoid electrical errors and prevent the devices from being damaged.

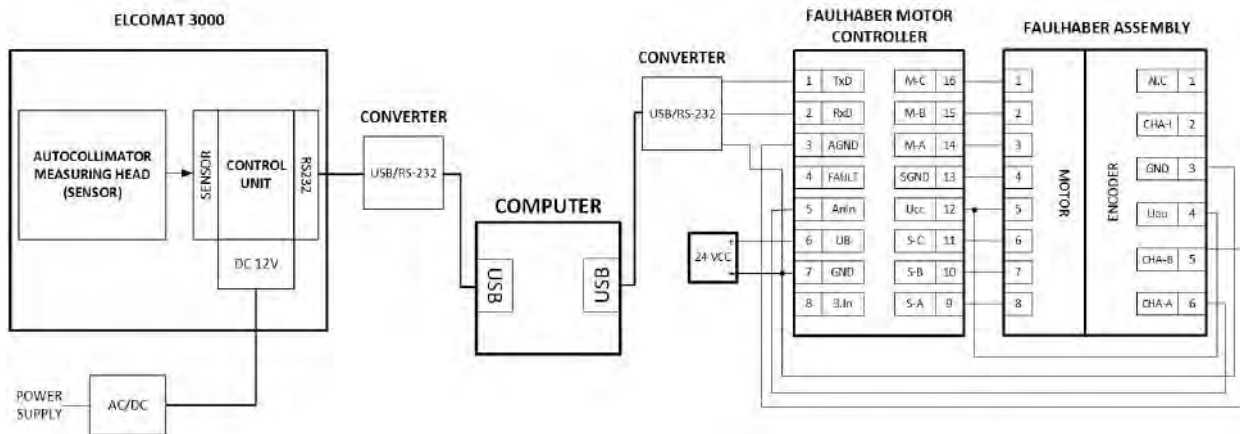


Figure 3.13.: Wiring between computer and Faulhaber controller

### 3.5.2. Physical connections

In order to make it easier for users operate the system and to avoid connection errors that could damage electronic equipment, this section shows the physical connections necessary for the proper functioning of each device used. It starts with the power supply Statron 64V/12A, it provides continuous voltage that powers the Faulhaber Motion Controller with the voltage needed by the Faulhaber motor (24V). The blue cable contains the supply voltage and the yellow wire is the ground. See Fig. 3.14.



Figure 3.14.: Power supply Statron 64V/12A

According to the wiring indicated in Fig. 3.13, the Faulhaber controller is connected as shown in Fig. 3.15. Black cables are connected to the pins dedicated to transmit information between the motor and the computer. White cables energize the encoder

and are connected to the pins of data transmission of this with the computer. The blue and yellow wires are those that come from the power supply to powering up the controller and the motor.



Figure 3.15.: Faulhaber controller - connections

To mount the Elcomat 3000, first, it is necessary to fix the Autocollimation Head in the adjustable mounting support. Then, plug in one end of the wire in the socket of the autocollimation measuring head (see Fig. 3.16) and the other end in the Sensor socket of the Control Unit. Second, plug in one end of the RS232 connection cable in the RS232 socket of the Control Unit, then connect the other via converter to USB to the computer.

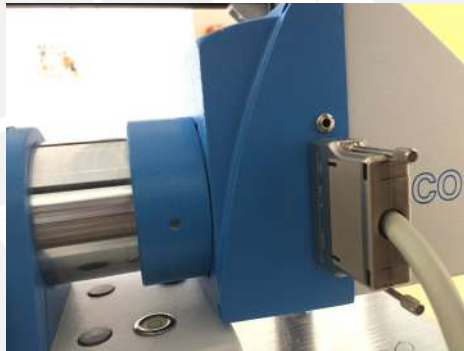


Figure 3.16.: Elcomat 3000 - connection

Third, plug in the plug supply unit in the power connector socket (DC 12V) to finally get what is shown in Fig. 3.17.



Figure 3.17.: Control Unit of Elcomat 3000 - Connections

After having made all the connections, the next step is to configure the Control Unit for the proper data transmission and the way it is displayed in the LCD-display (see Elcomat 3000 user manual to know this information [MW].)



Figure 3.18.: Control unit of Elcomat 3000 - configuration display

### 3.5.3. Operation modes

All devices used in the system have a wide range of application as is indicated in their manuals and datasheets. In this section, operation modes there are specified for each device for further tests.

**ELCOMAT 3000 configuration:** Before starting with the measurements, we need to set some parameters that have been chosen by experimentation to facilitate data reception and visualization. First, "Finder Mode" needs to be configured in control unit of *ELCOMAT* 3000 due to it allows faster detection, and set the type of reflector on "very small" due to the mirror size. Second, the control unit also provides of two RS232 protocol types to communicate with a computer, they are *TextProtocol* and *CompatibleProtocol*. In *CompatibleProtocol*, data is transmitted in 25 blocks of 8 bytes per second and transmission parameters need to be set with a transfer rate of 2400 baud, 8 data bit, no parity and 1 stop bit. Each block contains information about yaw and pitch angle, this is arranged as is indicated in Fig. 3.19.

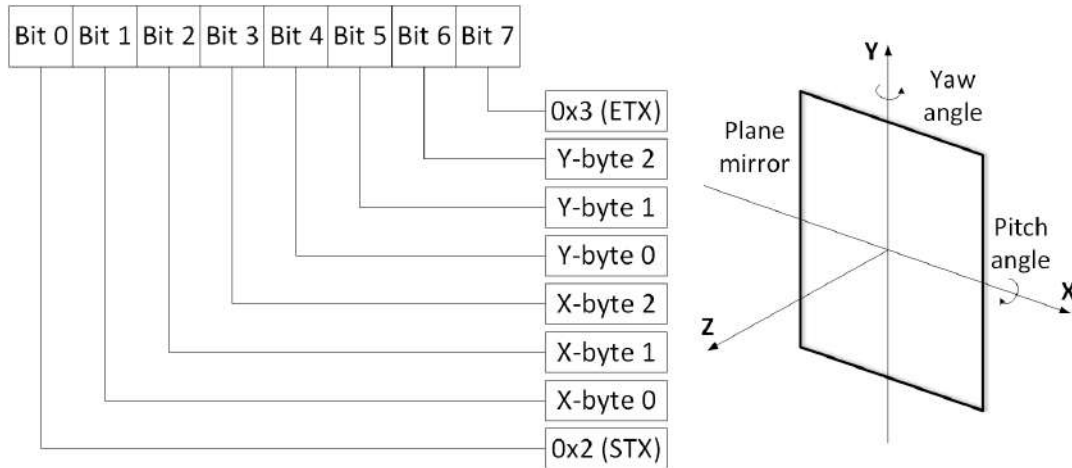


Figure 3.19.: Compatible protocol data block architecture

In order to obtain the angle measurements in "arcsec", first it is necessary to extract the information from the data block that correspond to the yaw angle (Bit 4, Bit 5 and Bit 6), and then apply the equation 3.24. The function of bits 0 and 7 is to recognize the start and the end of the data block respectively. However, when negative angles are measured, some errors could happen and it is possible that wrongs measurements exist.

$$Y[arcsec] = \frac{Bit4 + Bit5 * 256 + Bit6 * 65536}{100} \tag{3.24}$$

Another mode of data transmission via serial port that is supported by the ELCOMAT 3000 control unit on *TextMode*. In this mode, the control unit sends and receives messages in ASCII code. To request information about the current measurement, it is necessary to send certain characters depending on the configuration used. In our particular case, to request the absolute measure of the measured angles (pitch or yaw angle) it is necessary to send the character "a" and automatically the control unit will send a Type 4 message whose structure is detailed in Fig. 3.20. Because of the convenient way to get angle measurements directly expressed in arcsec, *TextProtocol* mode looks as the best option for our purpose.

Message Structure	Type field	Status	Pitch Ang.Meas X	Yaw Ang.Meas Y
Example	[4]	[003]	[-32.469]	[62.874]

Figure 3.20.: Text protocol data block architecture

**FAULHABER motion controller and motor:** The brushless 24 VDC motor and the incremental encoder attached send the information of motor position to the motion controller (driver), it reads data and send instructions to control the motor movement. The motor driver can operate as Position controller or Velocity controller. For our purpose, in order to achieve the torque with high accuracy, the rotational angle of the pulley must be as accurate as possible. Instead, velocity does not need to be that precise. Therefore, configure the motor drive as Position controller turns out to be the most suitable option.

As a Position controller, motor driver allows the user to know the final position before starting the movement, because target position is an input parameter. There are two alternatives if motion controller is configured as Position controller. They are APC-MOD (Analogue positioning mode) and ENCMOD (External encoder as actual position value). ENCMOD is chosen because is the most suitable for high-precision applications on which motor position is determined from encoder. Most frequently used commands are presented in Table 3.7.

Table 3.7.: Main instruction Faulhaber motion controller [Fau]

Command	Argument	Function	Description
EN	-	Enable drive	Activate drive
DI	-	Disable drive	Deactivate drive
LA	$-1.8 \cdot 10^9 \dots 1.8 \cdot 10^9$	Load absolute position	Load new absolute target position
LR	$-2.14 \cdot 10^9 \dots 2.14 \cdot 10^9$	Load relative position	Load new relative target position
M	-	Initiate motion	Activate position control and start positioning
HO	- / $-1.8 \cdot 10^9 \dots 1.8 \cdot 10^9$	Define home position	Without argument: set actual pos. to 0. With argument: set actual position to specified value.
POS	-	Read encoder position	Get current position

## 4. Experiment and results

In the previous chapter, the mechanical characteristics of the experimental system have been specified. Physical dimensions of its components were defined and torque scope was specified. In addition, the main characteristics of the electronic devices like setup, wiring and operation, are explained. In this chapter, setup functionality is evaluated experimentally. Then, experimental results of the stiffness behavior of the flexure hinges are presented.

### 4.1. Rotational system behavior

The rotational system is integrated by the Faulhaber motor in combination with an incremental encoder and controlled by a motion controller from the same company, as well as a high performance gearhead of the Harmonic Drive company. For our understanding, the controller was tested with the software FAULHABER Motion Manager 6 in order determine the most adequate configuration to achieve successfully the motion controlling of the motor. Physically the encoder coupled to the motor is subdivided into 10000 accounts. It indicates that when the encoder turns a full revolution, 10000 steps of the encoder are sensed. Particularly, with the configuration of the ACWS1 mode, the encoder virtually increases the number of steps per revolution up to 40000 steps, as indicated in the communication manual [Fau]. The controller has several operating modes that are indicated in 4.1:

Table 4.1.: Operation modes of Faulhaber controller

Operating Modes	Description
Continuous mode	Motor rotates indefinitely until it is disabled.
Stepper mode	Motor is config. as stepper motor.
Analog position control mode	Analogue voltage is used to achieve the target position.
Encoder mode	External encoder is used as a position detector.
Gearing mode	Activate gearing mode.
Set voltage mode	Activate voltage regulator mode.
Set IxR mode	Activate IxR control.

For our purpose, the controller is set to encoder mode. In this mode of operation, target positions can be preset via the serial interface. For high precision applications, the external encoder as actual position value (ENCMOD) can be used properly because the encoder is directly attached to the motor shaft and can therefore be used as a position detector since each encoder step corresponds to a certain angle of rotation on the motor.

To transmit movement to the motor, it is necessary to send instructions in a certain order. First, the instruction indicating the position to be reached is sent ( $LA$  [ $Position$ ] or  $LR$  [ $Position$ ]). Second, the instruction that orders the execution of the movement to the position indicated above (M) is transmitted in the following manner.

- LR 800
- M

As is indicated in Fig. 4.1, the dashed line in POS vs  $t$  drawing represents the target position to be reached and the solid line represents the real position response of the output controller in which target position is achieved at the end of the ramp curve. In  $V$  vs  $t$  is represented the behavior of the velocity along the operation time in which it is limited by the maximum velocity set before. Each time a target position is required to achieve, the position of the motor in time is given as indicated in Fig. 4.1. However this target position is not reached instantaneously but it is incrementally carried out. Due to controller parameters, there are overshoots before stabilizing the system so the time to reach the proper position will be longer.

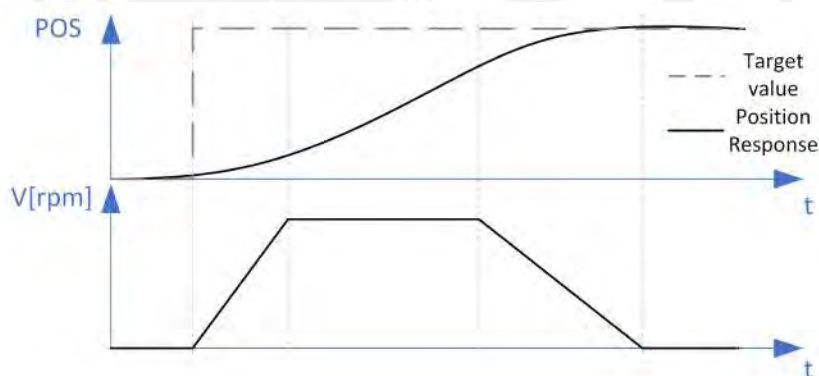


Figure 4.1.: FAULHABER controller - behavior of position and velocity signals in time

Based on experiments carried out with Motion Manager 6 and considering the default parameters of the controller, the rotation system was tested to verify its performance. After configured the controller as is mentioned above in order to know the establishment time, tests were performed. Tests consist of rotation of the motor with a mirror attached to output shaft of the gearbox. In this way because of virtually no backlash of the shaft, ELCOMAT 3000 directly detects the position of the shaft without significant variations. It was set up as is shown in 4.2.



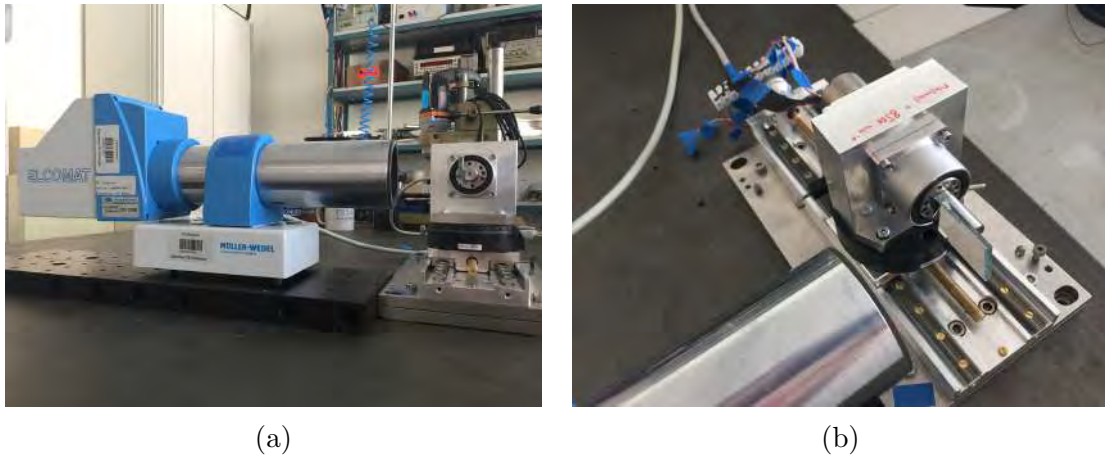


Figure 4.2.: Setup implemented to verify the establishment time of the controller

As we can see in the following graphics, according to the RS232 serial communication manual of the controller, when configuring the parameter CORRIDOR we are limiting the maximum acceptable variation to consider the encoder reading as valid with respect to the target position. That is, as indicated in Fig. 4.3, if it is intend to move from position 0 to position 600 and consider the parameter  $CORRIDOR = 20$ , positions will be taken as valid values 20 units below or 20 units above 600 (if position between 580 and 620 is reached, means that the controller has reached the target position). If the CORRIDOR has not been previously configured, the controller will continue to work until reaching the desired position, this process can take a many minutes.

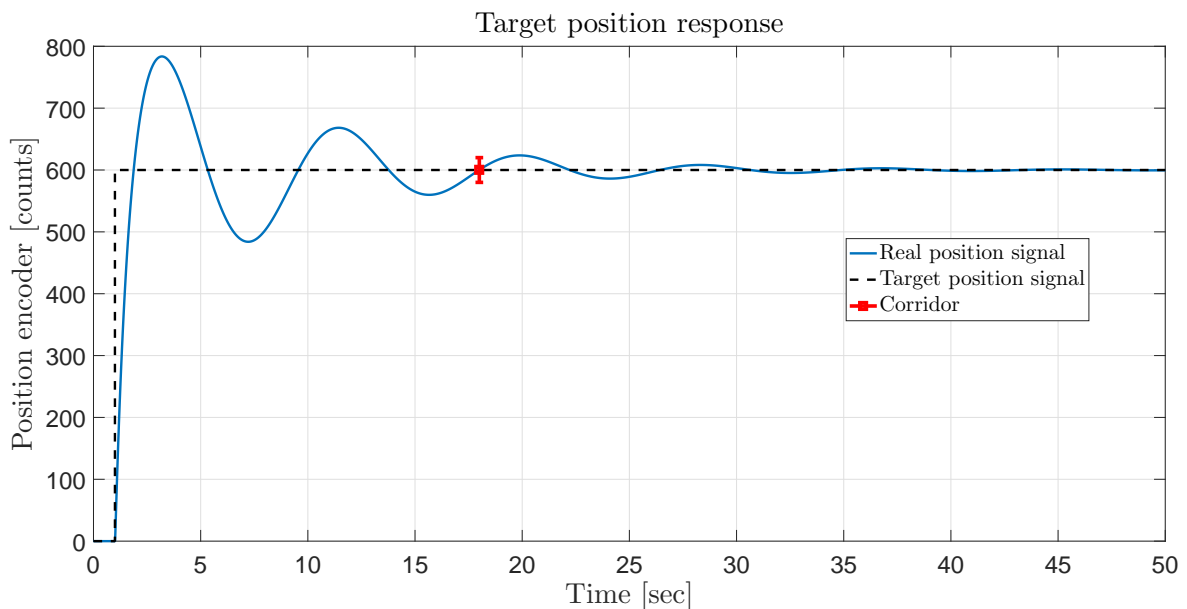


Figure 4.3.: Representation of real position signal behavior along the time with the CORRIDOR parameter

The operating time for each measurement could take several minutes if we let the controller work until reaching the target position, this time can be variable if we consider different rotation angles and directions. In order to determine the most optimal movement to be carried out in the final tests, motor rotation tests have been performed from 0 to 3100 encoder counts clockwise and counterclockwise, which is equivalent to a rotation of approximately 1000 arcsec on the gearhead shaft, in three different ways considering the CORRIDOR of 10 and of 20 as shown in Fig. 4.4.

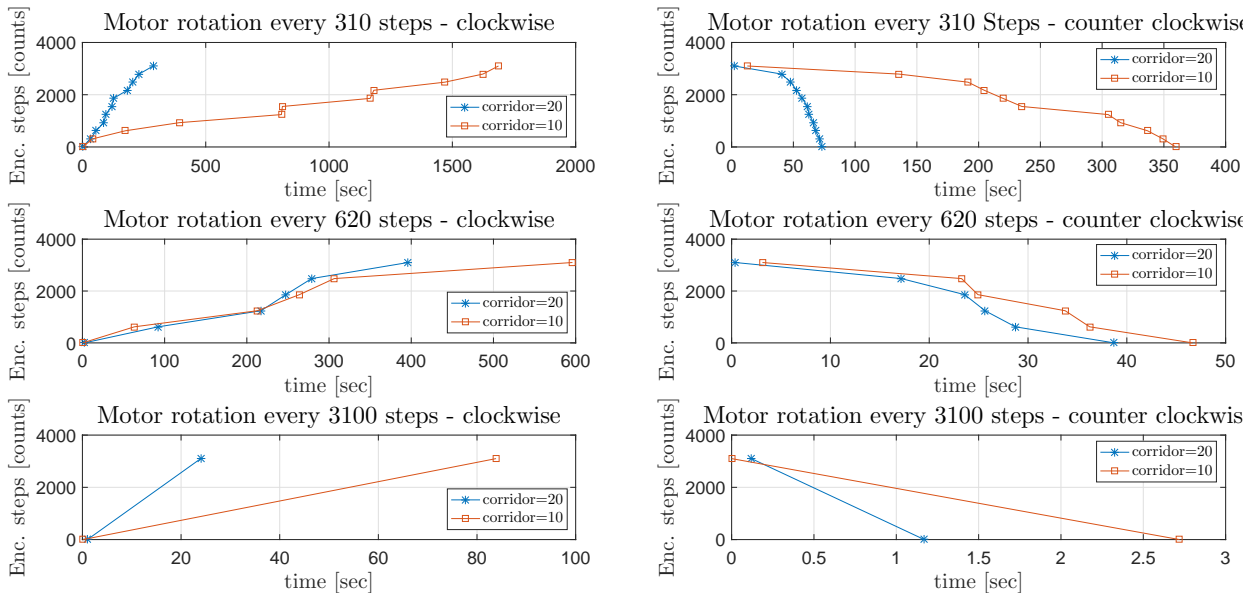


Figure 4.4.: Gearhead shaft rotation performance

Each row of subplots in the Fig. 4.4 presents the waypoints of the movements discretized in steps of 310, 620 and 3100 counts respectively, the graphs of the left column represent movement in the clockwise direction and those in the right column represent movement in the counterclockwise direction. Within each graph there are two graphs, which represent the point-to-point development of the movement for two different values of the CORRIDOR (10 and 20). As it can be seen in each graph, there is no constant linearity between all the waypoints that build each draw, which means that although it moves by equal steps, the time between one and the other is different. These times depend on the variation that is selected (CORRIDOR) and on the electromechanical variations of the gearhead and the motor friction effects.

In spite of ordered to return to its initial position, it can be seen that the points of rotation are not the same. The points represented in the previous graphic come from a list of time values obtained experimentally. Each of these values come from a list of 65 iterations for each type of movement. It should be noted that in the firsts experiments, the value of the CORRIDOR parameter was not taken into account and, by default (CORRIDOR=1), the controller executed its function until finding the exact value of

the target position, this process required much more time than on these graphics. For example, when iterating for only 10 times in steps of 620 counts, it took up to 12 hours to complete the iteration, therefore it was necessary to reduce the time of experimentation.

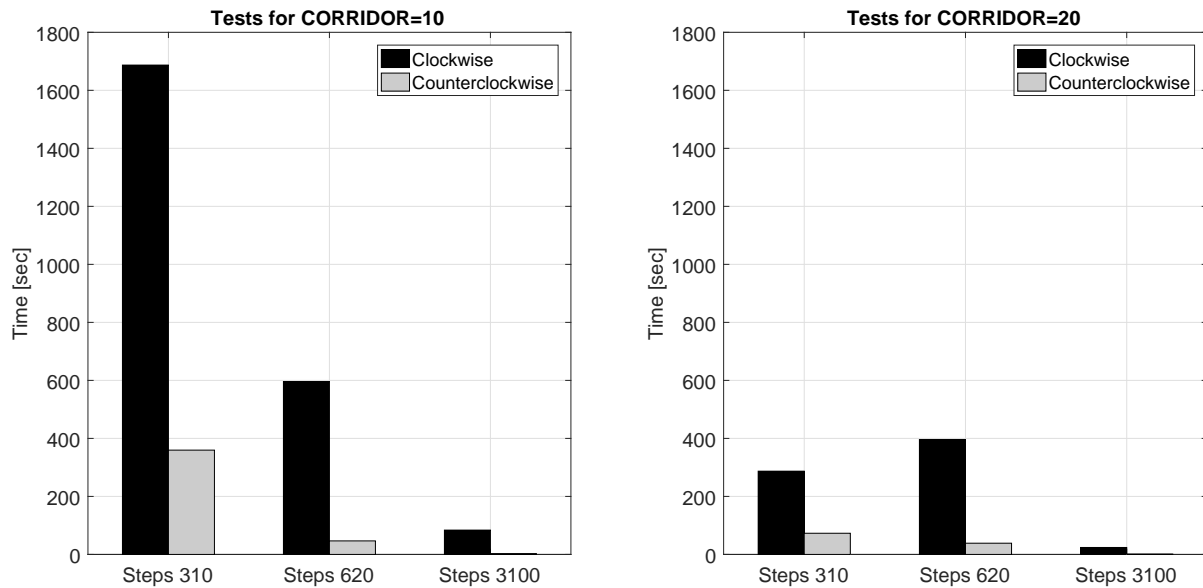


Figure 4.5.: Comparison of operation time setting CORRIDOR 10 or 20

To help to compare the operating times needed to rotate the gearhead shaft approximately 1000 arcsec, the Fig. 4.5 clearly shows that setting the CORRIDOR to 20 decreases significantly the execution time with respect to the value of 10. Another characteristic of the tests performed, is that by rotating counterclockwise to return to the initial position, less time is required.

In the Table 4.2, it can be seen the values of the mean establishment times and the standard deviation for the cases shown above. It can be noted that despite moving at constant steps, the average time differs from the others with a high deviation from its mean value. This fact could be explained by several factors. For example, when there are external vibrations that affect the detection of the angle. Another way of explaining these variations is by referring to the internal temperature of the rotation system, which due to electromechanical factors such as internal current and friction can affect the normal displacement of the encoder and its reading. Thus directly affecting the position control. Some values can be observed including deviations greater than the mean value, and this happens because the tests performed, establishment times ranged from fractions of seconds to a few minutes. However, for values of the variable CORRIDOR of 10 and 20, it can be assured that in the first case it requires longer establishment times.

Table 4.2.: Comparison chart of establishment times for corridor values of 10 and 20.

	POS 0 - 0(arcsec)	POS 1 - 310(arcsec)	POS 2 - 620(arcsec)	POS 3 - 930(arcsec)	POS 4 - 1240(arcsec)	POS 5 - 1550(arcsec)	POS 6 - 1860(arcsec)	POS 7 - 2170(arcsec)	POS 8 - 2480(arcsec)	POS 9 - 2790(arcsec)	POS 10 - 3100(arcsec)	
Corridor 10	Mean	1.60	39.29	133.45	218.22	414.30	3.89	356.18	14.57	287.65	154.69	63.19
	Std.Dev	4.23	53.10	162.16	168.54	156.16	6.51	161.74	11.50	345.09	221.93	128.15
	Mean	0.23		62.99		149.58		51.12		42.41		289.75
	Std.Dev	0.89		60.37		69.24		69.46		45.09		225.47
	Mean	1.01										22.98
	Std.Dev	3.11										32.80
Corridor 10	Mean	10.35	12.48	21.81	10.01	69.93	15.31	15.13	13.09	56.03	122.75	12.70
	Std.Dev	9.83	14.91	21.93	6.64	173.09	17.31	39.54	13.35	194.03	228.08	31.55
	Mean	9.99		3.07		2.06		6.42		16.82		0.35
	Std.Dev	11.66		1.19		1.43		15.01		23.01		0.83
	Mean	2.72										0.00
	Std.Dev	1.77										0.00
Corridor 20	Mean	0.44	31.97	23.22	31.41	6.91	24.90	7.14	55.46	22.81	25.47	57.30
	Std.Dev	1.41	52.85	32.33	32.03	5.59	19.09	5.60	31.01	29.53	44.29	83.80
	Mean	2.24		90.05		124.91		30.27		31.36		117.34
	Std.Dev	12.21		76.28		118.82		37.90		31.71		175.11
	Mean	0.10										83.76
	Std.Dev	0.55										50.36
Corridor 20	Mean	1.61	3.60	1.59	3.39	1.43	4.23	4.47	4.90	7.36	38.22	2.22
	Std.Dev	2.26	2.00	1.27	4.01	1.11	8.40	4.61	11.44	24.54	78.87	10.04
	Mean	10.42		2.48		8.83		1.66		20.15		3.12
	Std.Dev	11.62		1.16		38.68		2.40		19.35		12.16
	Mean	1.05										0.12
	Std.Dev	1.47										0.49

## 4.2. Experimental tests

As mentioned in previous chapters, flexure hinges of different thickness are tested within the scope of the present work (50  $\mu\text{m}$ , 75  $\mu\text{m}$  and 100  $\mu\text{m}$ ). For this purpose, two sets of flexure hinges from two different precision manufacturing companies have been manufactured. The experimental setup implemented is shown in Fig. 4.6.

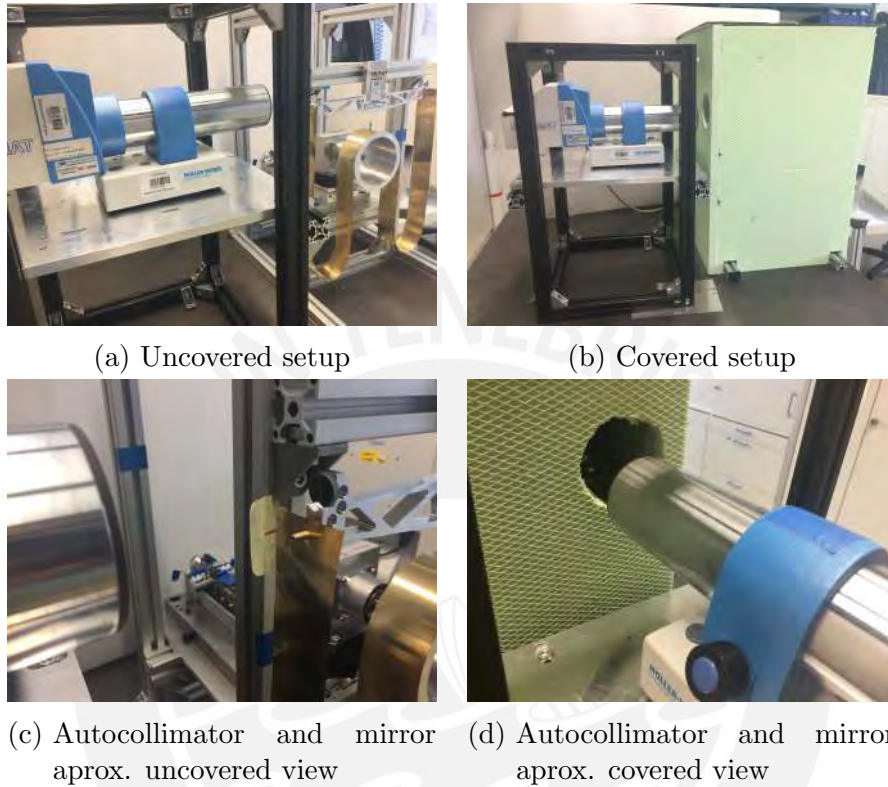


Figure 4.6.: Final experimental setup

Despite the importance of implementing the setup in a especially conditioned environment for its optimal functionality, the setup was implemented in a common place as is shown in Fig. 4.6. Under these experimental conditions, the setup is exposed to external vibrations and to the effects of air turbulence. They make produce oscillations in the tape. Also, the setup is exposed to the adherence of particles on all its parts that can cause errors in data recording.

### 4.2.1. Tests of flexure hinges manufactured by manufacturer A

The first set consists of three flexure hinges manufactured by manufacturer A (see Fig. 4.7). According to the measurement protocol, the company provides the information of the measured thickness for each hinge.

This information is shown below.

Flexure hinge  $50\mu m \rightarrow h = 46.3\mu m$

Flexure hinge  $75\mu m \rightarrow h = 73.8\mu m$

Flexure hinge  $100\mu m \rightarrow h = 98.3\mu m$

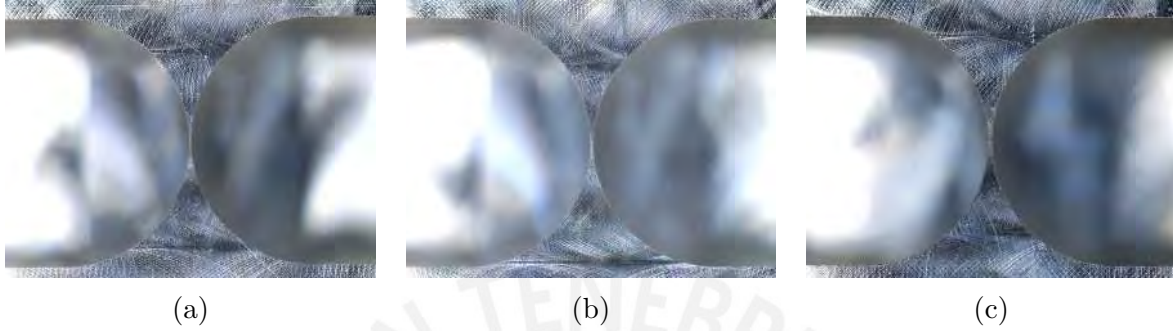


Figure 4.7.: Manufacturer A flexure hinges: (a)  $50\mu m$  (b)  $75\mu m$  (c)  $100\mu m$

The initial rotational stiffness calculations were made for nominal thickness values of flexure hinges ( $50\mu m$ ,  $75\mu m$  and  $100\mu m$ ) solving equations 3.1, 3.2, 3.3 and 3.4. These stiffness values are denoted as analytical rotational stiffness ( $k_{\varphi_{an}}$ ). Then, the estimated rotational stiffness value ( $k_{\varphi_{esti}}$ ) is determined by the quotient that results from dividing applied torque according to Eq. (3.17) and rotation angles for each hinge ( $1000$  arcsec,  $365.2$  arcsec and  $179.1$  arcsec for  $50\mu m$ ,  $75\mu m$  and  $100\mu m$  hinges respectively). The values obtained in each case for nominal thickness of flexure hinges are presented below in Table 4.3.

Table 4.3.: Rotational stiffness of the first set of flexure hinges (estimated and calculated analytically)

$h$ ( $\mu m$ )	$k_{\varphi_{esti}}$ (Nmm/rad)	$k_{\varphi_{analy}}$ (Nmm/rad)
50	17.73	16.21
75	48.54	44.67
100	98.98	91.69

However, due to the tolerances that are generated for manufacturing process we must recalculate the analytical rotational stiffness since the thickness differs from its nominal value. Then, the analytical values of stiffness are updated to those indicated in Table 4.4 and its respective hinge thickness. Experimental rotational stiffness are compared with these.

Table 4.4.: Analytical rotational stiffness for measured thickness of manufacturer A flexure hinges

<b>h</b> <b>(<math>\mu\text{m}</math>)</b>	<b><math>k_{\varphi_{an}}</math></b> <b>(Nmm/rad)</b>
46.3	13.37
73.8	42.90
98.3	87.85

The experimental tests of the three flexure hinges were carried out with the purpose of determining the stiffness of each joint when the system produces a torque on it. This is the experimental value of estimated stiffness  $k_{\varphi_{esti}}$ .

Four different types of tests are carried out in which applied torque and bending angle data, necessary to determine the stiffness of the hinge, are collected. For each test the pulley rotates 10 degrees (clockwise from 0 to 10 degrees, then counterclockwise to go back). For the first case, the rotation is carried out in 20 steps of 0.5 degrees. In the second case, the number of steps is reduced to 10, but it increases to 1 degree per step. For the third case, there are 5 steps of 2 degrees. Finally, the fourth case, the pulley is rotated from its initial position to 10 degrees in a single movement. For each experiment, the initial position is the one in which 0 arcsec is recorded because the lever arm element is completely horizontal and there are equal lengths of tape on both sides of the pulley. Then these experimental results are compared with the analytical ones. Further, some comments are made.

Each type of test was carried out on each joint with 20 iterations per experiment. Table 4.5, Table 4.6 and Table 4.7 contain the statistical data that results from collecting the stiffness information of all the experiments. Table 4.5 contains the statistical data of the complete movement for each position (both clockwise and counterclockwise). Table 4.6 contains the statistical data for each position when moving in a clockwise direction and Table 4.7 contains the statistical data for each position when it moves counterclockwise. In all cases, rotational stiffness is calculated dividing the torque applied for the system and the bending angle measured.

Table 4.5.: Experimental values of stiffness for manufacturer A flexure hinge of 50  $\mu\text{m}$ , 75  $\mu\text{m}$  and 100  $\mu\text{m}$  thickness. Mean and standard deviation per pulley position (total experimental values, clockwise and counterclockwise rotation) from 0 to 10 degrees

	POS 1 - 0.5(°)	POS 2 - 1(°)	POS 3 - 1.5(°)	POS 4 - 2(°)	POS 5 - 2.5(°)	POS 6 - 3(°)	POS 7 - 3.5(°)	POS 8 - 4(°)	POS 9 - 4.5(°)	POS 10 - 5(°)	POS 11 - 5.5(°)	POS 12 - 6(°)	POS 13 - 6.5(°)	POS 14 - 7(°)	POS 15 - 7.5(°)	POS 16 - 8(°)	POS 17 - 8.5(°)	POS 18 - 9(°)	POS 19 - 9.5(°)	POS 20 - 10(°)	
Mean	10.68	10.13	10.36	10.31	10.51	10.5	10.47	10.36	10.33	10.38	10.49	10.53	10.47	10.49	10.42	10.55	10.56	10.57	10.57	11.57	13.42
Std.Dev	1.93	0.91	0.41	0.35	0.54	0.34	0.33	0.26	0.17	0.17	0.18	0.2	0.17	0.18	0.13	0.16	0.12	0.12	0.12	1.71	2.94
Mean	10.46	10.46	10.45	10.45	10.49	10.49	10.5	10.5	10.46	10.46	10.58	10.58	10.54	10.54	10.6	10.6	10.6	10.6	10.6	10.63	10.63
Std.Dev	0.39	0.39	0.13	0.13	0.13	0.13	0.1	0.1	0.07	0.07	0.09	0.09	0.06	0.06	0.04	0.04	0.05	0.05	0.05	0.03	0.03
Mean	11.65	11.65	11.65	11.65	11.65	11.65	11.03	11.03	11.03	10.83	10.83	10.83	10.84	10.84	10.84	10.84	10.84	10.84	10.84	10.86	10.86
Std.Dev	0.86	0.86	0.86	0.86	0.86	0.86	0.19	0.19	0.19	0.13	0.13	0.13	0.14	0.14	0.14	0.14	0.14	0.14	0.14	0.11	0.11
Mean	10.74	10.74	10.74	10.74	10.74	10.74	10.74	10.74	10.74	10.74	10.74	10.74	10.74	10.74	10.74	10.74	10.74	10.74	10.74	10.74	10.74
Std.Dev	0.26	0.26	0.26	0.26	0.26	0.26	0.26	0.26	0.26	0.26	0.26	0.26	0.26	0.26	0.26	0.26	0.26	0.26	0.26	0.26	0.26
Mean	31.6	32.61	32.94	33.58	33.68	33.78	33.8	33.81	33.78	34.02	34.06	34	33.99	33.99	33.95	33.92	33.94	33.94	33.94	33.9	33.91
Std.Dev	0.77	0.41	0.35	0.62	0.5	0.43	0.39	0.29	0.26	0.1	0.08	0.08	0.11	0.07	0.05	0.05	0.06	0.06	0.06	0.06	0.05
Mean	33.37	33.37	33.94	33.94	34.02	34.02	34.01	34.01	34.26	34.26	34.16	34.16	34.08	34.08	34.06	34.06	34.05	34.05	34.05	33.99	33.99
Std.Dev	0.44	0.44	0.61	0.61	0.45	0.45	0.27	0.27	0.1	0.1	0.04	0.04	0.15	0.15	0.06	0.06	0.07	0.07	0.07	0.05	0.05
Mean	33.33	33.33	33.33	33.33	33.33	33.33	33.8	33.8	33.8	33.99	33.99	33.99	33.98	33.98	33.98	33.98	33.98	33.98	33.98	33.9	33.9
Std.Dev	0.29	0.29	0.29	0.29	0.29	0.29	0.28	0.28	0.28	0.06	0.06	0.06	0.09	0.09	0.09	0.09	0.09	0.09	0.09	0.05	0.05
Mean	33.99	33.99	33.99	33.99	33.99	33.99	33.99	33.99	33.99	33.99	33.99	33.99	33.99	33.99	33.99	33.99	33.99	33.99	33.99	33.99	33.99
Std.Dev	0.13	0.13	0.13	0.13	0.13	0.13	0.13	0.13	0.13	0.13	0.13	0.13	0.13	0.13	0.13	0.13	0.13	0.13	0.13	0.13	0.13
Mean	56.58	58.04	58.86	59.44	59.72	59.82	60.14	60.12	60.23	60.2	60.26	60.27	60.26	60.33	60.33	60.37	60.34	60.36	60.4	60.4	60.42
Std.Dev	2.32	1.23	1.06	0.66	0.54	0.5	0.49	0.46	0.32	0.34	0.3	0.25	0.18	0.23	0.25	0.24	0.23	0.27	0.22	0.19	0.19
Mean	59.35	59.35	59.74	59.74	60.21	60.21	60.46	60.46	60.44	60.44	60.48	60.48	60.68	60.68	60.5	60.5	60.57	60.57	60.6	60.6	60.6
Std.Dev	0.66	0.66	0.63	0.63	0.35	0.35	0.29	0.29	0.23	0.23	0.34	0.34	0.36	0.36	0.15	0.15	0.25	0.25	0.17	0.17	0.17
Mean	60.55	60.55	60.55	60.55	60.55	60.55	61.17	61.17	61.02	61.02	61.02	61.02	61.29	61.29	61.29	61.29	61.29	61.29	61.28	61.28	61.28
Std.Dev	0.24	0.24	0.24	0.24	0.24	0.24	0.44	0.44	0.31	0.31	0.31	0.31	0.08	0.08	0.08	0.08	0.08	0.08	0.07	0.07	0.07
Mean	61.39	61.39	61.39	61.39	61.39	61.39	61.39	61.39	61.39	61.39	61.39	61.39	61.39	61.39	61.39	61.39	61.39	61.39	61.39	61.39	61.39
Std.Dev	0.15	0.15	0.15	0.15	0.15	0.15	0.15	0.15	0.15	0.15	0.15	0.15	0.15	0.15	0.15	0.15	0.15	0.15	0.15	0.15	0.15



Table 4.6.: Experimental values of stiffness for manufacturer A flexure hinge of 50  $\mu\text{m}$ , 75  $\mu\text{m}$  and 100  $\mu\text{m}$  thickness. Mean and standard deviation per pulley position (clockwise rotation) from 0 to 10 degrees

	POS 1 - 0.5(°)	POS 2 - 1(°)	POS 3 - 1.5(°)	POS 4 - 2(°)	POS 5 - 2.5(°)	POS 6 - 3(°)	POS 7 - 3.5(°)	POS 8 - 4(°)	POS 9 - 4.5(°)	POS 10 - 5(°)	POS 11 - 5.5(°)	POS 12 - 6(°)	POS 13 - 6.5(°)	POS 14 - 7(°)	POS 15 - 7.5(°)	POS 16 - 8(°)	POS 17 - 8.5(°)	POS 18 - 9(°)	POS 19 - 9.5(°)	POS 20 - 10(°)
Mean	10.62	10.43	10.61	10.43	10.47	10.36	10.42	10.35	10.35	10.39	10.55	10.58	10.47	10.55	10.39	10.61	10.57	10.58	11.81	12.92
Std.Dev	1.36	1.13	0.28	0.19	0.17	0.2	0.19	0.17	0.23	0.2	0.14	0.11	0.16	0.21	0.14	0.17	0.13	0.15	1.81	2.79
Mean	10.72	10.45	10.58	10.52	10.49	10.54	10.5	10.59	10.63	10.63	10.63	10.63	10.63	10.63	10.63	10.63	10.63	10.63	10.63	10.63
Std.Dev	0.2	0.09	0.09	0.08	0.04	0.06	0.06	0.02	0.02	0.02	0.02	0.02	0.02	0.02	0.02	0.02	0.02	0.02	0.03	0.03
Mean	11.63	11.63	11.63	11.63	11.63	11.63	11.63	11.63	11.63	11.63	11.63	11.63	11.63	11.63	11.63	11.63	11.63	11.63	11.63	11.63
Std.Dev	0.66	0.66	0.66	0.66	0.66	0.66	0.66	0.66	0.66	0.66	0.66	0.66	0.66	0.66	0.66	0.66	0.66	0.66	0.66	0.66
Mean																				
Std.Dev																				
Mean	31.65	32.52	32.89	33	33.26	33.41	33.46	33.55	33.54	34.02	34.06	34.02	33.96	34	33.94	33.91	33.92	33.92	33.89	33.92
Std.Dev	0.64	0.48	0.34	0.22	0.2	0.27	0.17	0.14	0.12	0.09	0.08	0.06	0.14	0.09	0.03	0.07	0.07	0.06	0.05	0.05
Mean	33.37	33.55	33.61	33.75	34.25	34.16	34.03	34.03	34.03	34.03	34.03	34.03	34.03	34.03	34.03	34.03	34.03	34.03	34.03	34.03
Std.Dev	0.46	0.2	0.19	0.07	0.1	0.04	0.18	0.18	0.18	0.18	0.18	0.18	0.18	0.18	0.18	0.18	0.18	0.18	0.18	0.18
Mean	33.3	33.3	33.3	33.3	33.3	33.3	33.3	33.3	33.3	33.3	33.3	33.3	33.3	33.3	33.3	33.3	33.3	33.3	33.3	33.3
Std.Dev	0.13	0.13	0.13	0.13	0.13	0.13	0.13	0.13	0.13	0.13	0.13	0.13	0.13	0.13	0.13	0.13	0.13	0.13	0.13	0.13
Mean																				
Std.Dev																				
Mean	56.87	57.91	59.15	59.56	59.85	59.92	60	60.23	60.15	60.21	60.29	60.3	60.26	60.32	60.34	60.39	60.34	60.35	60.42	60.41
Std.Dev	2.31	1.2	0.72	0.44	0.47	0.24	0.37	0.32	0.31	0.36	0.32	0.28	0.17	0.2	0.23	0.27	0.21	0.32	0.24	0.2
Mean	59.07	59.97	60.38	60.45	60.38	60.45	60.38	60.45	60.38	60.38	60.53	60.53	60.53	60.53	60.53	60.42	60.59	60.59	60.59	60.59
Std.Dev	0.31	0.89	0.41	0.37	0.41	0.37	0.37	0.37	0.37	0.32	0.48	0.48	0.48	0.52	0.52	0.15	0.26	0.26	0.21	0.21
Mean	60.59	60.59	60.59	60.59	60.59	60.59	60.59	60.59	60.59	60.59	60.59	60.59	60.59	60.59	60.59	60.59	60.59	60.59	60.59	60.59
Std.Dev	0.2	0.2	0.2	0.2	0.2	0.2	0.2	0.2	0.2	0.2	0.2	0.2	0.2	0.2	0.2	0.2	0.2	0.2	0.2	0.2
Mean																				
Std.Dev																				

Table 4.7.: Experimental values of stiffness for manufacturer A flexure hinge of 50  $\mu\text{m}$ , 75  $\mu\text{m}$  and 100  $\mu\text{m}$  thickness. Mean and standard deviation per pulley position (counterclockwise rotation) from 0 to 10 degrees

	POS 1 - 0.5( $\circ$ )	POS 2 - 1( $\circ$ )	POS 3 - 1.5( $\circ$ )	POS 4 - 2( $\circ$ )	POS 5 - 2.5( $\circ$ )	POS 6 - 3( $\circ$ )	POS 7 - 3.5( $\circ$ )	POS 8 - 4( $\circ$ )	POS 9 - 4.5( $\circ$ )	POS 10 - 5( $\circ$ )	POS 11 - 5.5( $\circ$ )	POS 12 - 6( $\circ$ )	POS 13 - 6.5( $\circ$ )	POS 14 - 7( $\circ$ )	POS 15 - 7.5( $\circ$ )	POS 16 - 8( $\circ$ )	POS 17 - 8.5( $\circ$ )	POS 18 - 9( $\circ$ )	POS 19 - 9.5( $\circ$ )	POS 20 - 10( $\circ$ )	
Mean	10.74	9.82	10.11	10.19	10.54	10.64	10.52	10.37	10.31	10.37	10.43	10.47	10.47	10.44	10.45	10.49	10.54	10.56	10.56	11.33	13.93
Std.Dev	2.45	0.51	0.35	0.44	0.76	0.4	0.44	0.33	0.1	0.13	0.19	0.25	0.18	0.14	0.11	0.14	0.11	0.09	1.66	3.14	
Mean	10.19	10.45	10.4	10.47	10.43	10.58	10.62	10.62	10.58	10.62	10.62	10.62	10.62	10.62	10.62	10.62	10.62	10.62	10.62	10.62	10.62
Std.Dev	0.36	0.16	0.11	0.11	0.09	0.03	0.05	0.05	0.03	0.03	0.03	0.03	0.03	0.03	0.03	0.03	0.03	0.03	0.03	0.03	0.03
Mean	11.67	10.99	10.89	10.91	10.91	10.91	10.91	10.91	10.91	10.91	10.91	10.91	10.91	10.91	10.91	10.91	10.91	10.91	10.91	10.91	10.91
Std.Dev	1.05	0.15	0.12	0.12	0.12	0.12	0.12	0.12	0.12	0.12	0.12	0.12	0.12	0.12	0.12	0.12	0.12	0.12	0.12	0.12	0.12
Mean	31.56	32.7	32.98	34.15	34.1	34.14	34.14	34.07	34.01	34.01	34.06	33.99	34.02	33.99	33.95	33.93	33.96	33.97	33.97	33.91	33.91
Std.Dev	0.91	0.34	0.37	0.17	0.3	0.14	0.15	0.1	0.08	0.12	0.08	0.09	0.07	0.05	0.07	0.04	0.04	0.06	0.07	0.05	0.05
Mean	33.37	34.33	34.44	34.27	34.27	34.27	34.27	34.27	34.27	34.27	34.17	34.13	34.13	34.13	34.05	34.05	34.06	34.06	34.06	34.06	34
Std.Dev	0.44	0.64	0.14	0.14	0.04	0.04	0.04	0.04	0.11	0.11	0.05	0.08	0.08	0.08	0.05	0.05	0.06	0.06	0.06	0.06	0.06
Mean	33.35	33.35	34.06	34.06	34.06	34.06	34.06	34.06	34.01	34.01	34.01	34.01	34.01	34.01	34.01	34.01	34.01	34.01	34.01	34.01	34.01
Std.Dev	0.4	0.09	0.09	0.09	0.09	0.09	0.09	0.09	0.05	0.05	0.05	0.05	0.05	0.05	0.05	0.05	0.05	0.05	0.05	0.05	0.05
Mean	56.3	58.17	58.57	59.31	59.58	59.72	60.27	60.02	60.31	60.19	60.23	60.24	60.26	60.35	60.33	60.36	60.35	60.37	60.38	60.42	60.42
Std.Dev	2.36	1.28	1.27	0.82	0.58	0.66	0.56	0.56	0.33	0.33	0.29	0.22	0.19	0.27	0.28	0.2	0.26	0.21	0.2	0.19	0.19
Mean	59.63	59.51	60.03	60.47	60.49	60.44	60.54	60.54	60.54	60.54	60.54	60.54	60.54	60.54	60.57	60.57	60.54	60.54	60.62	60.62	60.62
Std.Dev	0.87	0.2	0.19	0.26	0.15	0.22	0.06	0.26	0.15	0.15	0.22	0.22	0.22	0.22	0.12	0.12	0.29	0.29	0.16	0.16	0.16
Mean	60.51	60.51	61.59	61.59	61.59	61.59	61.59	61.59	61.59	61.59	61.59	61.59	61.59	61.59	61.29	61.29	61.29	61.29	61.28	61.28	61.28
Std.Dev	0.27	0.1	0.1	0.1	0.1	0.12	0.12	0.12	0.12	0.12	0.12	0.12	0.12	0.12	0.1	0.1	0.1	0.1	0.07	0.07	0.07
Mean	61.42	61.42	61.42	61.42	61.42	61.42	61.42	61.42	61.42	61.42	61.42	61.42	61.42	61.42	61.42	61.42	61.42	61.42	61.42	61.42	61.42
Std.Dev	0.15	0.15	0.15	0.15	0.15	0.15	0.15	0.15	0.15	0.15	0.15	0.15	0.15	0.15	0.15	0.15	0.15	0.15	0.15	0.15	0.15

In order to summarize the experimental data obtained in the previous tables, Table 4.8 is presented. In this table it can be clearly observed that the stiffness values obtained remain stable in relation to their mean value. The standard deviation in each case is small in comparison to the average. Additionally, it can be seen that the behavior of the rotational stiffness of the joints are very similar in both directions of rotation.

Table 4.8.: Statistical summary of flexure hinges rotational stiffness

		$k_{\varphi 50_{exp}}$	$k_{\varphi 75_{exp}}$	$k_{\varphi 100_{exp}}$
		(Nmm/rad)	(Nmm/rad)	(Nmm/rad)
<b>Both directions</b>	<b>Mean</b>	10.74	33.86	60.64
	<b>Std.Dev</b>	0.31	0.19	0.31
<b>Clockwise</b>	<b>Mean</b>	10.77	33.79	60.62
	<b>Std.Dev</b>	0.3	0.13	0.28
<b>Counterclockwise</b>	<b>Mean</b>	10.72	33.93	60.67
	<b>Std.Dev</b>	0.28	0.15	0.27

Once the results of the rotational stiffness for each hinge have been obtained, we compare them with the analytical results for the real size of the hinges. It is shown in Table 4.9.

Table 4.9.: Comparative table of estimated and experimental rotational stiffness with respect to analytical results considering nominal and real values of thickness

			Nominal thickness			Real thickness		
$h_{nom}$	$h_{re}$	$h_{re}/h_{nom}$	$k_{\varphi_{an}}$	$k_{\varphi_{esti}}$	$k_{\varphi_{esti}}/k_{\varphi_{an}}$	$k_{\varphi_{an}}$	$k_{\varphi_{exp}}$	$k_{\varphi_{exp}}/k_{\varphi_{an}}$
( $\mu\text{m}$ )	( $\mu\text{m}$ )	(%)	(Nmm/rad)		(%)	(Nmm/rad)		(%)
50	46.3	<b>92.6</b>	16.21	17.73	<b>109.38</b>	13.37	10.74	<b>80.33</b>
75	73.8	<b>98.4</b>	44.67	48.54	<b>108.66</b>	42.90	33.86	<b>78.93</b>
100	98.3	<b>98.3</b>	91.69	98.98	<b>107.95</b>	87.85	60.64	<b>69.03</b>

Due to the thickness variation of the joints, the analytical results and the estimated by the setup results can vary in different ways for each of the elements. Comparing the experimental and analytical formulas of the rotational stiffness, it is observed that for nominal values of thickness the experimental system gives values of stiffness approximately 10% higher than analytical values. When analyzing the experiment, it is observed that the experimental system give values of rotational stiffness lower than those obtained analytically, approximately 30% less.

Then, stiffness errors are generated by the thickness variations of the flexure hinges and experimental errors of the setup. Misalignment between the rotation system and the frame that holds the rest of the setup is considered as experimental error. There are also errors in the wrong distribution of weight of the lever arm element. Further, there are errors on brass tape, because it was not cut properly with the designed width along its entire length. Finally, external vibrations also influence on the stiffness determination.

In Fig. 4.8, it can be observed the linear behavior of the rotational stiffness for the three flexure hinges analyzed. Mean values of torque applied and angle of rotation detected by Elcomat 3000 were selected to create the graph.

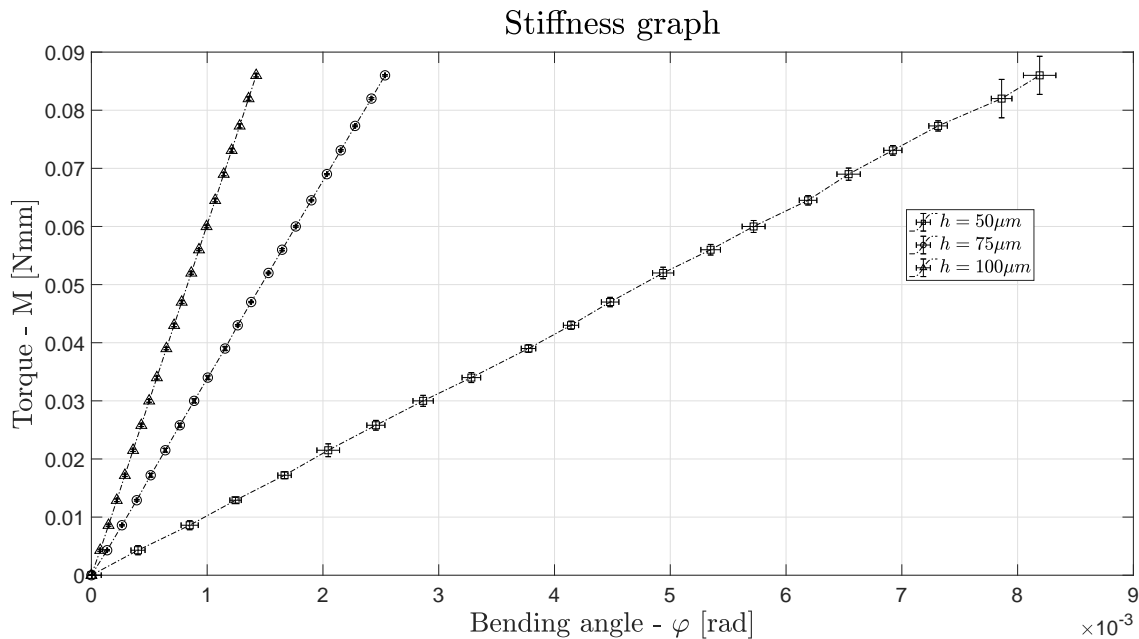


Figure 4.8.: Stiffness behavior of manufacturer A flexure hinges for 10 degree of pulley rotation

In the previous graph, there are two singular points that concern to the 50  $\mu\text{m}$  flexure hinge. They are located on the top-right of the graph. Greater variations in torque and bending angles, with respect to the other points, are observed. It can be explained because of sudden vibrations in the work environment where the experiments were carried out.

After performing experiments to evaluate the rotational stiffness of the joints when applying torques from 0 to 0.086 Nmm, the next step to accomplish is the evaluation of this parameter when the applied torque is ten times lower. This is made to determine possible nonlinear behaviors that could occur for smaller deformations. Each type of test was carried out on each joint with 20 iterations per experiment. Table 4.10, Table 4.11 and Table 4.12 contain the statistical data that results from collecting the stiffness information of all the experiments. Table 4.10 contains the statistical data of the complete movement for each position (both clockwise and counterclockwise). Table 4.11 contains the statistical data for each position when moving in a clockwise direction and Table 4.12 contains the statistical data for each position when it moves counterclockwise.

Table 4.10.: Experimental values of stiffness for manufacturer A flexure hinge of 50  $\mu\text{m}$ , 75  $\mu\text{m}$  and 100  $\mu\text{m}$  thickness. Mean and standard deviation per pulley position (total experimental values, clockwise and counterclockwise rotation) from 0 to 1 degree

	POS 1 - 0.05(°)	POS 2 - 0.10(°)	POS 3 - 0.15(°)	POS 4 - 0.20(°)	POS 5 - 0.25(°)	POS 6 - 0.30(°)	POS 7 - 0.35(°)	POS 8 - 0.40(°)	POS 9 - 0.45(°)	POS 10 - 0.50(°)	POS 11 - 0.55(°)	POS 12 - 0.60(°)	POS 13 - 0.65(°)	POS 14 - 0.70(°)	POS 15 - 0.75(°)	POS 16 - 0.80(°)	POS 17 - 0.85(°)	POS 18 - 0.90(°)	POS 19 - 0.95(°)	POS 20 - 1(°)
Mean	10.58	10.57	10.61	10.62	10.65	10.42	10.51	10.58	10.48	10.54	10.52	10.54	10.53	10.46	10.52	10.55	10.51	10.48	10.45	10.51
Std.Dev	1.32	1.17	0.6	0.57	0.45	0.25	0.32	0.26	0.18	0.15	0.23	0.17	0.23	0.14	0.18	0.13	0.09	0.11	0.11	0.07
Mean	10.63	10.63	12.06	12.06	10.05	10.05	10.94	10.94	10.49	10.49	10.74	10.74	10.65	10.65	10.43	10.43	10.55	10.55	10.42	10.42
Std.Dev	4.23	4.23	5.03	5.03	1.37	1.37	1.74	1.74	0.67	0.67	0.81	0.81	0.64	0.64	0.34	0.34	0.29	0.29	0.17	0.17
Mean	10.58	10.58	10.22	10.22	1.79	1.79	1.56	1.56	10.58	10.58	10.29	10.29	10.28	10.28	10.56	10.56	0.67	0.67	10.56	10.56
Std.Dev	1.79	1.79	1.79	1.79	1.79	1.79	1.56	1.56	1.56	1.56	0.72	0.72	0.56	0.56	0.56	0.56	0.67	0.67	10.57	10.57
Mean	10.57	10.57	10.57	10.57	10.57	10.57	10.57	10.57	10.57	10.57	10.57	10.57	10.57	10.57	10.57	10.57	10.57	10.57	10.57	10.57
Std.Dev	0.77	0.77	0.77	0.77	0.77	0.77	0.77	0.77	0.77	0.77	0.77	0.77	0.77	0.77	0.77	0.77	0.77	0.77	0.77	0.77
Mean	21.42	26.11	28.08	29.01	29.75	30.57	30.9	31.05	31.2	31.45	31.8	31.86	31.81	31.92	32.22	32.34	32.45	32.45	32.47	32.52
Std.Dev	2.42	2.19	1.66	1.24	0.95	0.72	0.83	0.68	0.7	0.52	0.45	0.51	0.39	0.44	0.47	0.39	0.26	0.27	0.27	0.32
Mean	28.15	28.15	29.43	29.43	31.22	31.22	31.5	31.5	31.9	31.9	32.16	32.16	32.44	32.44	32.91	32.91	32.97	32.97	32.9	32.9
Std.Dev	6.5	6.5	2.93	2.93	1.25	1.25	1.08	1.08	0.88	0.88	0.81	0.81	0.78	0.78	0.63	0.63	0.44	0.44	0.46	0.46
Mean	30.99	30.99	30.99	30.99	31.84	31.84	31.84	31.84	32.54	32.54	32.54	32.54	33.06	33.06	33.06	33.06	33.06	33.06	33.09	33.09
Std.Dev	1.15	1.15	1.15	1.15	0.98	0.98	0.98	0.98	0.37	0.37	0.37	0.37	0.41	0.41	0.41	0.41	0.38	0.38	0.38	0.38
Mean	136.49	106.38	83.41	76.46	72.43	69.96	68.12	67.27	66.72	66.39	65.81	65.37	64.92	64.71	64.56	64.29	64.12	63.85	63.71	63.63
Std.Dev	27.6	28.79	12.56	7.29	4.72	3.65	2.91	2.6	2.15	2.07	1.74	1.6	1.41	1.25	1.1	1.18	1.07	0.97	0.92	0.84
Mean	94.79	94.79	73.72	73.72	68.46	68.46	65.93	65.93	65.53	65.53	64.51	64.51	64.5	64.5	63.99	63.99	63.66	63.66	63.34	63.34
Std.Dev	11.29	11.29	3.81	3.81	1.97	1.97	1.26	1.26	1.02	1.02	1.07	1.07	0.42	0.42	0.59	0.59	0.71	0.71	0.68	0.68
Mean	72.37	72.37	72.37	72.37	66.25	66.25	66.25	66.25	64.14	64.14	64.14	64.14	0.87	0.87	0.83	0.83	0.83	0.83	0.83	0.83
Std.Dev	3.1	3.1	3.1	3.1	1.44	1.44	1.44	1.44	0.87	0.87	0.87	0.87	0.46	0.46	0.46	0.46	0.46	0.46	0.46	0.46
Mean	62.56	62.56	62.56	62.56	62.56	62.56	62.56	62.56	62.56	62.56	62.56	62.56	62.56	62.56	62.56	62.56	62.56	62.56	62.56	62.56
Std.Dev	0.43	0.43	0.43	0.43	0.43	0.43	0.43	0.43	0.43	0.43	0.43	0.43	0.43	0.43	0.43	0.43	0.43	0.43	0.43	0.43

Table 4.11.: Experimental values of stiffness for manufacturer A flexure hinge of 50  $\mu\text{m}$ , 75  $\mu\text{m}$  and 100  $\mu\text{m}$  thickness. Mean and standard deviation per pulley position (clockwise rotation) from 0 to 1 degree

	POS 1 - 0.05(°)	POS 2 - 0.10(°)	POS 3 - 0.15(°)	POS 4 - 0.20(°)	POS 5 - 0.25(°)	POS 6 - 0.30(°)	POS 7 - 0.35(°)	POS 8 - 0.40(°)	POS 9 - 0.45(°)	POS 10 - 0.50(°)	POS 11 - 0.55(°)	POS 12 - 0.60(°)	POS 13 - 0.65(°)	POS 14 - 0.70(°)	POS 15 - 0.75(°)	POS 16 - 0.80(°)	POS 17 - 0.85(°)	POS 18 - 0.90(°)	POS 19 - 0.95(°)	POS 20 - 1(°)	
Mean	10.92	10.73	10.75	10.69	10.59	10.46	10.58	10.55	10.48	10.57	10.55	10.53	10.54	10.52	10.53	10.57	10.48	10.52	10.48	10.48	10.49
Std.Dev	0.73	0.71	0.58	0.24	0.25	0.15	0.18	0.16	0.13	0.11	0.12	0.07	0.12	0.1	0.08	0.05	0.08	0.06	0.09	0.08	0.08
Mean	10.16	10.54	10.54	10.54	10.69	10.69	10.69	10.69	10.69	10.49	10.61	10.61	10.61	10.61	10.42	10.42	10.42	10.49	10.49	10.49	10.4
Std.Dev	3.77	2.37	2.37	2.37	1.01	1.01	1.01	1.01	1.01	0.55	0.21	0.21	0.21	0.65	0.23	0.23	0.32	0.32	0.32	0.32	0.2
Mean	9.94	10.77	10.77	10.77	10.77	10.77	10.77	10.77	10.77	10.55	10.55	10.55	10.55	10.19	10.19	10.19	10.19	10.19	10.19	10.19	10.3
Std.Dev	1.87	1.87	1.87	1.87	1.64	1.64	1.64	1.64	1.64	0.8	0.8	0.8	0.8	0.56	0.56	0.56	0.56	0.56	0.56	0.56	0.62
Mean	10.51	10.51	10.51	10.51	10.51	10.51	10.51	10.51	10.51	10.51	10.51	10.51	10.51	10.51	10.51	10.51	10.51	10.51	10.51	10.51	10.51
Std.Dev	1.02	1.02	1.02	1.02	1.02	1.02	1.02	1.02	1.02	1.02	1.02	1.02	1.02	1.02	1.02	1.02	1.02	1.02	1.02	1.02	1.02
Mean	22.02	26.51	28.23	29.15	29.89	30.78	31	31.22	31.54	31.72	32.04	32	31.9	32.13	32.35	32.43	32.53	32.49	32.59	32.56	32.56
Std.Dev	2.06	2.17	1.76	1.23	0.92	0.52	0.77	0.73	0.75	0.43	0.37	0.46	0.36	0.37	0.41	0.33	0.24	0.33	0.25	0.34	0.34
Mean	29.6	29.6	29	29	31.82	31.82	32.02	32.02	32.32	32.32	32.52	32.52	32.52	32.48	33.19	33.19	33.08	33.08	32.95	32.95	32.95
Std.Dev	8.62	8.62	3.71	3.71	0.47	0.47	0.69	0.69	0.94	0.94	0.83	0.83	0.83	0.97	0.67	0.67	0.52	0.52	0.49	0.49	0.49
Mean	30.62	30.62	30.62	30.62	31.69	31.69	31.69	31.69	32.72	32.72	32.72	32.72	32.72	32.81	32.81	32.81	32.81	32.81	33.08	33.08	33.08
Std.Dev	0.92	0.92	0.92	0.92	0.41	0.41	0.41	0.41	0.32	0.32	0.32	0.32	0.32	0.17	0.17	0.17	0.17	0.17	0.39	0.39	0.39
Mean	33.17	33.17	33.17	33.17	33.17	33.17	33.17	33.17	33.17	33.17	33.17	33.17	33.17	33.17	33.17	33.17	33.17	33.17	33.17	33.17	33.17
Std.Dev	0.22	0.22	0.22	0.22	0.22	0.22	0.22	0.22	0.22	0.22	0.22	0.22	0.22	0.22	0.22	0.22	0.22	0.22	0.22	0.22	0.22
Mean	140.84	103.8	81.96	74.84	72.29	70.04	67.88	67.27	66.58	66.4	65.97	65.27	64.81	64.68	64.51	64.24	63.97	63.79	63.69	63.59	63.59
Std.Dev	31.02	28.8	13.21	5.79	4.76	3.22	2.59	2.69	1.91	1.95	1.7	1.46	1.19	1.26	1.1	1.13	1	1.03	0.93	0.87	0.87
Mean	97.36	97.36	74.28	74.28	69.22	69.22	66.23	66.23	65.8	65.8	64.76	64.76	64.76	64.51	63.93	63.73	63.73	63.73	63.13	63.13	63.13
Std.Dev	11.27	11.27	3.43	3.43	2.06	2.06	1.4	1.4	0.94	0.94	0.55	0.55	0.55	0.41	0.48	0.48	0.79	0.79	0.39	0.39	0.39
Mean	73.05	73.05	73.05	73.05	66.18	66.18	66.18	66.18	64.01	64.01	64.01	64.01	64.01	63.26	63.26	63.26	63.26	63.26	63.12	63.12	63.12
Std.Dev	2.85	2.85	2.85	2.85	1.6	1.6	1.6	1.6	0.96	0.96	0.96	0.96	0.96	0.78	0.78	0.78	0.78	0.78	0.48	0.48	0.48
Mean	62.53	62.53	62.53	62.53	62.53	62.53	62.53	62.53	62.53	62.53	62.53	62.53	62.53	62.53	62.53	62.53	62.53	62.53	62.53	62.53	62.53
Std.Dev	0.53	0.53	0.53	0.53	0.53	0.53	0.53	0.53	0.53	0.53	0.53	0.53	0.53	0.53	0.53	0.53	0.53	0.53	0.53	0.53	0.53

Table 4.12.: Experimental values of stiffness for manufacturer A flexure hinge of 50  $\mu\text{m}$ , 75  $\mu\text{m}$  and 100  $\mu\text{m}$  thickness. Mean and standard deviation per pulley position (counterclockwise rotation) from 0 to 1 degree

	POS 1 - 0.05(°)	POS 2 - 0.10(°)	POS 3 - 0.15(°)	POS 4 - 0.20(°)	POS 5 - 0.25(°)	POS 6 - 0.30(°)	POS 7 - 0.35(°)	POS 8 - 0.40(°)	POS 9 - 0.45(°)	POS 10 - 0.50(°)	POS 11 - 0.55(°)	POS 12 - 0.60(°)	POS 13 - 0.65(°)	POS 14 - 0.70(°)	POS 15 - 0.75(°)	POS 16 - 0.80(°)	POS 17 - 0.85(°)	POS 18 - 0.90(°)	POS 19 - 0.95(°)	POS 20 - 1(°)
Mean	10.24	10.42	10.47	10.54	10.7	10.39	10.44	10.62	10.48	10.51	10.49	10.55	10.52	10.41	10.51	10.52	10.53	10.44	10.42	10.54
Std.Dev	1.7	1.52	0.63	0.78	0.59	0.33	0.42	0.35	0.23	0.19	0.3	0.23	0.31	0.15	0.24	0.18	0.1	0.14	0.12	0.05
Mean	11.09	13.57	13.57	13.57	10.64	10.64	11.2	11.2	11.2	10.49	10.88	10.88	10.68	10.68	10.43	10.43	10.61	10.61	10.44	10.44
Std.Dev	4.81	6.53	6.53	6.53	1.47	1.47	1.86	1.86	1.86	0.8	1.14	1.14	0.66	0.66	0.43	0.43	0.26	0.26	0.15	0.15
Mean	10.5	10.5	10.5	10.5	10.39	10.39	10.39	10.39	10.39	10.02	10.02	10.02	10.37	10.37	10.37	10.37	10.37	10.37	10.82	10.82
Std.Dev	1.76	1.76	1.76	1.76	1.54	1.54	1.54	1.54	1.54	0.54	0.54	0.54	0.58	0.58	0.58	0.58	0.58	0.58	0.65	0.65
Mean	10.63	10.63	10.63	10.63	10.63	10.63	10.63	10.63	10.63	10.63	10.63	10.63	10.63	10.63	10.63	10.63	10.63	10.63	10.63	10.63
Std.Dev	0.46	0.46	0.46	0.46	0.46	0.46	0.46	0.46	0.46	0.46	0.46	0.46	0.46	0.46	0.46	0.46	0.46	0.46	0.46	0.46
Mean	20.82	25.71	27.93	28.88	29.6	30.35	30.8	30.88	30.85	31.18	31.56	31.72	31.71	31.71	31.71	32.09	32.25	32.38	32.41	32.35
Std.Dev	2.71	2.26	1.63	1.3	1.01	0.86	0.92	0.62	0.47	0.46	0.41	0.55	0.41	0.42	0.5	0.43	0.26	0.22	0.24	0.32
Mean	26.71	29.86	29.86	29.86	30.61	30.61	30.97	30.97	30.97	31.48	31.8	31.8	32.39	32.39	32.62	32.62	32.86	32.86	32.85	32.85
Std.Dev	3.2	1.97	1.97	1.97	1.5	1.5	1.16	1.16	1.16	0.6	0.65	0.65	0.58	0.58	0.45	0.45	0.33	0.33	0.45	0.45
Mean	31.35	31.35	31.35	31.35	32	32	32	32	32	32.36	32.36	32.36	33.3	33.3	33.3	33.3	33.3	33.3	33.1	33.1
Std.Dev	1.28	1.28	1.28	1.28	1.35	1.35	1.35	1.35	1.35	0.34	0.34	0.34	0.43	0.43	0.43	0.43	0.43	0.43	0.39	0.39
Mean	178.14	108.96	84.86	78.08	72.57	69.88	68.36	67.26	66.85	66.37	65.66	65.47	65.02	64.73	64.62	64.34	64.27	63.91	63.74	63.67
Std.Dev	49.13	30.09	12.41	8.53	4.94	4.2	3.33	2.65	2.45	2.3	1.86	1.81	1.67	1.3	1.16	1.29	1.17	0.96	0.96	0.85
Mean	92.22	92.22	73.16	73.16	67.7	67.7	65.63	65.63	65.25	65.25	64.25	64.25	64.25	64.5	64.5	64.05	64.05	63.6	63.54	63.54
Std.Dev	11.29	11.29	4.27	4.27	1.64	1.64	1.08	1.08	1.06	1.06	1.4	1.4	0.45	0.45	0.45	0.7	0.7	0.66	0.86	0.86
Mean	71.7	71.7	71.7	71.7	66.33	66.33	66.33	66.33	66.33	64.27	64.27	64.27	63.63	63.63	63.63	63.63	63.63	63.07	63.07	63.07
Std.Dev	3.35	3.35	3.35	3.35	1.35	1.35	1.35	1.35	1.35	0.8	0.8	0.8	0.87	0.87	0.87	0.87	0.87	0.46	0.46	0.46
Mean	62.59	62.59	62.59	62.59	62.59	62.59	62.59	62.59	62.59	62.59	62.59	62.59	62.59	62.59	62.59	62.59	62.59	62.59	62.59	62.59
Std.Dev	0.34	0.34	0.34	0.34	0.34	0.34	0.34	0.34	0.34	0.34	0.34	0.34	0.34	0.34	0.34	0.34	0.34	0.34	0.34	0.34

In order to summarize the experimental data obtained in the previous tables, Table 4.13 is presented. In this table it can be clearly observed that the stiffness values obtained remain stable with respect to their mean value. It is explained because the standard deviation in each case is small in comparison to the average. Additionally, it can be seen that the behavior of the rotational stiffness of the joints are very similar in both directions of rotation.

Table 4.13.: Statistical summary of flexure hinges rotational stiffness

		$k_{\varphi 50_{exp}}$	$k_{\varphi 75_{exp}}$	$k_{\varphi 100_{exp}}$
		(Nmm/rad)	(Nmm/rad)	(Nmm/rad)
<b>Both directions</b>	<b>Mean</b>	10.55	31.88	67.26
	<b>Std.Dev</b>	0.93	0.81	2.34
<b>Clockwise</b>	<b>Mean</b>	10.46	32	67.33
	<b>Std.Dev</b>	0.86	0.8	2.28
<b>Counterclockwise</b>	<b>Mean</b>	10.64	31.76	67.18
	<b>Std.Dev</b>	0.93	0.71	3.64

In Fig. 4.9 we can observe the linear behavior of the rotational stiffness for the three flexure hinges analyzed. Mean values of torque applied and angle of rotation detected by Elcomat3000 were selected to make the graph.

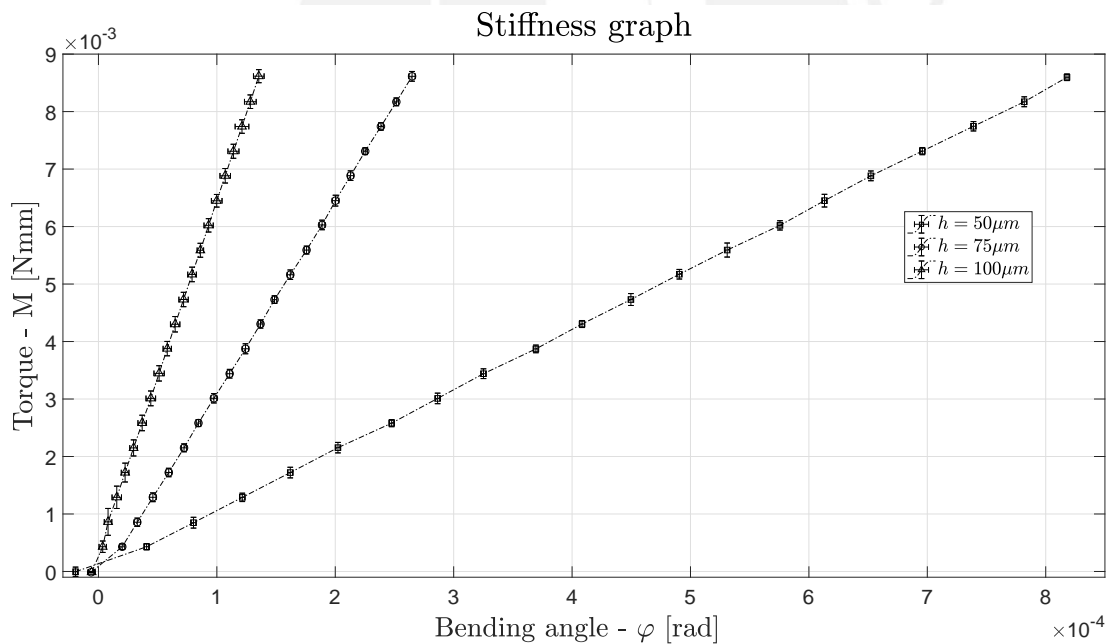


Figure 4.9.: Stiffness behavior of manufacturer A flexure hinges for 1 degree of pulley rotation



### 4.2.2. Tests of Flexure Hinges manufactured by manufacturer B

The second set consists of three flexure hinges manufactured by manufacturer B (see Fig. 4.10), according to the defined manufacturing tolerances. The company does not provide the information of the real thickness for each hinge, in consequence experimental results are compared with the analytical results considering only mean values of thickness ( $50\ \mu\text{m}$ ,  $75\ \mu\text{m}$  and  $100\ \mu\text{m}$ ).

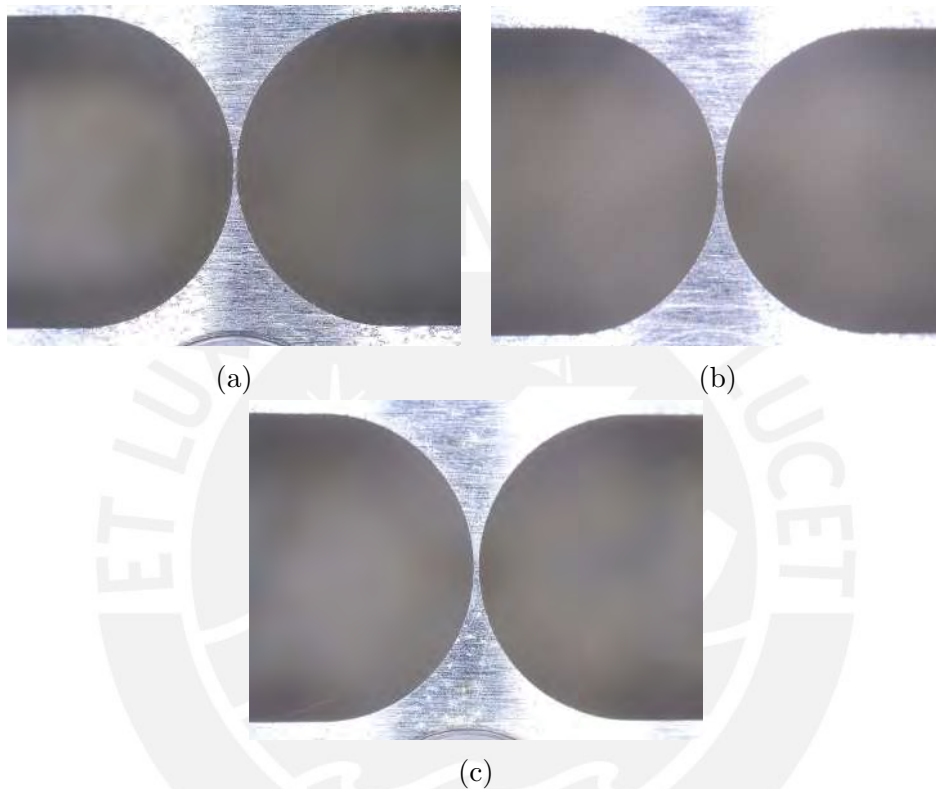


Figure 4.10.: Manufacturer B flexure hinges: (a)  $50\ \mu\text{m}$  (b)  $75\ \mu\text{m}$  (c)  $100\ \mu\text{m}$

The considerations that were taken into account for the first set of flexure hinge are contemplated for this second set. Proceeding in the same manner, four different types of tests are carried out in which applied torque and bending angle data are collected. There are the same made for manufacturer A flexure hinges to be compared under the same conditions. Each type of test was carried out on each joint with 20 iterations per experiment. Table 4.14, Table 4.15 and Table 4.16 contain the statistical data that results from collecting the stiffness information of all the experiments. Table 4.14 contains the statistical data of the complete movement for each position (both clockwise and counterclockwise). Table 4.15 contains the statistical data for each position when moving in a clockwise direction and Table 4.16 contains the statistical data for each position when it moves counterclockwise.

Table 4.14.: Experimental values of stiffness for manufacturer B flexure hinge of 50  $\mu\text{m}$ , 75  $\mu\text{m}$  and 100  $\mu\text{m}$  thickness. Mean and standard deviation per pulley position (total experimental values, clockwise and counterclockwise rotation) from 0 to 10 degrees

	POS 1 - 0.5(°)	POS 2 - 1(°)	POS 3 - 1.5(°)	POS 4 - 2(°)	POS 5 - 2.5(°)	POS 6 - 3(°)	POS 7 - 3.5(°)	POS 8 - 4(°)	POS 9 - 4.5(°)	POS 10 - 5(°)	POS 11 - 5.5(°)	POS 12 - 6(°)	POS 13 - 6.5(°)	POS 14 - 7(°)	POS 15 - 7.5(°)	POS 16 - 8(°)	POS 17 - 8.5(°)	POS 18 - 9(°)	POS 19 - 9.5(°)	POS 20 - 10(°)
Mean	18.21	18.65	19.01	18.95	18.94	19.02	19.02	19.02	19.05	19.05	19.05	19.05	19.06	19.07	19.07	19.04	19.07	19.09	19.09	19.07
Std.Dev	0.83	0.51	0.28	0.18	0.18	0.14	0.09	0.11	0.12	0.09	0.06	0.07	0.06	0.05	0.05	0.05	0.05	0.05	0.04	0.07
Mean	19.31	19.31	19.29	19.29	19.16	19.16	19.15	19.15	19.15	19.16	19.15	19.15	19.14	19.14	19.15	19.15	19.15	19.15	19.15	19.16
Std.Dev	0.49	0.49	0.29	0.29	0.25	0.25	0.13	0.13	0.12	0.09	0.09	0.11	0.11	0.09	0.08	0.08	0.08	0.08	0.08	0.09
Mean	19.06	19.06	19.06	19.06	19.07	19.07	19.07	19.07	19.07	19.05	19.05	19.05	19.05	19.05	19.1	19.1	19.1	19.1	19.1	19.12
Std.Dev	0.31	0.31	0.31	0.31	0.13	0.13	0.13	0.13	0.13	0.1	0.1	0.1	0.1	0.1	0.13	0.13	0.13	0.13	0.13	0.09
Mean	19.13	19.13	19.13	19.13	19.13	19.13	19.13	19.13	19.13	19.13	19.13	19.13	19.13	19.13	19.13	19.13	19.13	19.13	19.13	19.13
Std.Dev	0.03	0.03	0.03	0.03	0.03	0.03	0.03	0.03	0.03	0.03	0.03	0.03	0.03	0.03	0.03	0.03	0.03	0.03	0.03	0.03
Mean	57.63	53.6	52.28	51.79	51.28	51.23	51.11	51.01	50.77	50.73	50.75	50.66	50.62	50.6	50.59	50.54	50.52	50.57	50.54	50.5
Std.Dev	2.38	0.92	0.41	0.35	0.26	0.25	0.24	0.12	0.11	0.11	0.09	0.1	0.14	0.11	0.12	0.13	0.1	0.07	0.07	0.08
Mean	50.85	50.55	50.55	50.55	50.36	50.36	50.34	50.34	50.34	50.3	50.25	50.25	50.25	50.24	50.25	50.25	50.25	50.29	50.29	50.25
Std.Dev	0.63	0.33	0.33	0.33	0.21	0.21	0.24	0.24	0.24	0.2	0.1	0.1	0.1	0.05	0.08	0.08	0.04	0.04	0.04	0.04
Mean	50.1	50.1	50.1	50.1	50.16	50.16	50.16	50.16	50.16	50.18	50.18	50.18	50.18	50.14	50.14	50.14	50.14	50.14	50.19	50.19
Std.Dev	0.34	0.34	0.34	0.34	0.19	0.19	0.19	0.19	0.19	0.14	0.14	0.14	0.14	0.05	0.05	0.05	0.05	0.05	0.06	0.06
Mean	50.19	50.19	50.19	50.19	50.19	50.19	50.19	50.19	50.19	50.19	50.19	50.19	50.19	50.19	50.19	50.19	50.19	50.19	50.19	50.19
Std.Dev	0.07	0.07	0.07	0.07	0.07	0.07	0.07	0.07	0.07	0.07	0.07	0.07	0.07	0.07	0.07	0.07	0.07	0.07	0.07	0.07
Mean	88.18	94.1	96.23	97.31	99	99.26	99.62	99.76	99.94	100.3	100.9	100.7	100.8	100.8	100.8	100.9	100.9	100.9	100.9	100.7
Std.Dev	1.14	0.89	0.97	0.94	1.07	1.13	0.92	0.83	0.66	0.59	0.28	0.11	0.19	0.18	0.11	0.27	0.19	0.19	0.24	0.14
Mean	93.92	96.98	96.98	96.98	99.07	99.07	99.69	99.69	99.69	100.3	100.7	100.7	100.7	100.8	100.8	100.8	100.8	100.8	100.8	100.9
Std.Dev	1.73	0.48	0.48	0.48	1.07	1.07	0.76	0.76	0.76	0.59	0.28	0.28	0.28	0.39	0.3	0.3	0.22	0.22	0.21	0.21
Mean	97.33	97.33	97.33	97.33	99.7	99.7	99.7	99.7	99.7	100.9	100.9	100.9	100.9	101	101	101	101	101.0	101.0	101.0
Std.Dev	1.08	1.08	1.08	1.08	1.14	1.14	1.14	1.14	1.14	0.46	0.46	0.46	0.46	0.26	0.26	0.26	0.26	0.19	0.19	0.19
Mean	100.8	100.8	100.8	100.8	100.8	100.8	100.8	100.8	100.8	100.8	100.8	100.8	100.8	100.8	100.8	100.8	100.8	100.8	100.8	100.8
Std.Dev	0.17	0.17	0.17	0.17	0.17	0.17	0.17	0.17	0.17	0.17	0.17	0.17	0.17	0.17	0.17	0.17	0.17	0.17	0.17	0.17

Table 4.15.: Experimental values of stiffness for manufacturer B flexure hinge of 50  $\mu\text{m}$ , 75  $\mu\text{m}$  and 100  $\mu\text{m}$  thickness. Mean and standard deviation per pulley position (clockwise rotation) from 0 to 10 degrees

	POS 1 - 0.5(°)	POS 2 - 1(°)	POS 3 - 1.5(°)	POS 4 - 2(°)	POS 5 - 2.5(°)	POS 6 - 3(°)	POS 7 - 3.5(°)	POS 8 - 4(°)	POS 9 - 4.5(°)	POS 10 - 5(°)	POS 11 - 5.5(°)	POS 12 - 6(°)	POS 13 - 6.5(°)	POS 14 - 7(°)	POS 15 - 7.5(°)	POS 16 - 8(°)	POS 17 - 8.5(°)	POS 18 - 9(°)	POS 19 - 9.5(°)	POS 20 - 10(°)
Mean	18.47	18.66	19.01	19.01	19.02	19.08	19.08	19.06	19.1	19.1	19.04	19.05	19.08	19.07	19.07	19.05	19.06	19.08	19.08	19.07
Std.Dev	0.72	0.67	0.2	0.14	0.16	0.18	0.07	0.13	0.13	0.09	0.08	0.07	0.06	0.05	0.06	0.05	0.06	0.07	0.03	0.07
h = 90 $\mu\text{m}$	19.31	19.39	19.27	19.22	19.18	19.11	19.07	19.15	19.15	19.15	19.15	19.15	19.15	19.15	19.15	19.15	19.15	19.15	19.15	19.15
Std.Dev	0.63	0.37	0.29	0.09	0.09	0.11	0.07	0.05	0.05	0.05	0.05	0.05	0.05	0.05	0.05	0.05	0.05	0.05	0.05	0.05
Mean	19.16	19.16	19.16	19.16	19.16	19.16	19.16	19.16	19.16	19.16	19.16	19.16	19.16	19.16	19.16	19.16	19.16	19.16	19.16	19.16
Std.Dev	0.25	0.11	0.11	0.11	0.11	0.11	0.11	0.11	0.11	0.11	0.11	0.11	0.11	0.11	0.11	0.11	0.11	0.11	0.11	0.11
Mean	56.19	53.36	52.29	51.75	51.25	51.26	51.2	51	50.77	50.73	50.78	50.69	50.61	50.62	50.59	50.52	50.52	50.56	50.54	50.45
Std.Dev	2.22	1.14	0.48	0.43	0.28	0.32	0.26	0.12	0.11	0.11	0.07	0.07	0.17	0.12	0.15	0.07	0.09	0.07	0.07	0.05
Mean	50.68	50.56	50.33	50.37	50.35	50.35	50.35	50.35	50.35	50.35	50.35	50.35	50.35	50.35	50.35	50.35	50.35	50.35	50.35	50.35
Std.Dev	0.51	0.34	0.26	0.3	0.23	0.26	0.3	0.3	0.23	0.23	0.1	0.1	0.05	0.05	0.07	0.07	0.04	0.04	0.04	0.04
Mean	50.12	50.12	50.12	50.12	50.12	50.12	50.12	50.12	50.12	50.12	50.12	50.12	50.12	50.12	50.12	50.12	50.12	50.12	50.12	50.12
Std.Dev	0.26	0.26	0.26	0.26	0.26	0.26	0.26	0.26	0.26	0.26	0.14	0.14	0.14	0.14	0.14	0.14	0.14	0.14	0.14	0.14
Mean	88.62	94.19	95.97	97.75	98.06	98.27	98.9	98.99	99.37	99.79	101.1	100.7	100.9	100.8	100.8	100.9	100.9	100.8	100.8	100.8
Std.Dev	0.95	1.19	1.27	1.21	0.51	0.4	0.74	0.22	0.34	0.32	0.21	0.12	0.25	0.21	0.09	0.31	0.19	0.16	0.14	0.08
Mean	94.4	96.93	98.32	99.07	98.32	99.07	99.07	99.07	99.07	99.07	100.2	100.7	100.7	100.9	100.8	100.8	100.8	100.9	100.9	100.9
Std.Dev	1.36	0.51	0.84	0.48	0.84	0.48	0.48	0.48	0.48	0.58	0.27	0.27	0.16	0.16	0.24	0.24	0.23	0.23	0.19	0.19
Mean	97.5	97.5	97.5	97.5	97.5	97.5	97.5	97.5	97.5	97.5	101.0	101.0	101.0	101.0	100.8	100.8	100.8	100.9	100.9	100.9
Std.Dev	1.03	1.03	1.03	1.03	1.03	1.03	1.03	1.03	1.03	1.03	0.36	0.36	0.36	0.36	0.26	0.26	0.26	0.26	0.16	0.16
Mean	100.7	100.7	100.7	100.7	100.7	100.7	100.7	100.7	100.7	100.7	100.7	100.7	100.7	100.7	100.7	100.7	100.7	100.7	100.7	100.7
Std.Dev	0.18	0.18	0.18	0.18	0.18	0.18	0.18	0.18	0.18	0.18	0.18	0.18	0.18	0.18	0.18	0.18	0.18	0.18	0.18	0.18

Table 4.16.: Experimental values of stiffness for manufacturer B flexure hinge of 50  $\mu\text{m}$ , 75  $\mu\text{m}$  and 100  $\mu\text{m}$  thickness. Mean and standard deviation per pulley position (counterclockwise rotation) from 0 to 10 degrees

	POS 1 - 0.5( $\circ$ )	POS 2 - 1( $\circ$ )	POS 3 - 1.5( $\circ$ )	POS 4 - 2( $\circ$ )	POS 5 - 2.5( $\circ$ )	POS 6 - 3( $\circ$ )	POS 7 - 3.5( $\circ$ )	POS 8 - 4( $\circ$ )	POS 9 - 4.5( $\circ$ )	POS 10 - 5( $\circ$ )	POS 11 - 5.5( $\circ$ )	POS 12 - 6( $\circ$ )	POS 13 - 6.5( $\circ$ )	POS 14 - 7( $\circ$ )	POS 15 - 7.5( $\circ$ )	POS 16 - 8( $\circ$ )	POS 17 - 8.5( $\circ$ )	POS 18 - 9( $\circ$ )	POS 19 - 9.5( $\circ$ )	POS 20 - 10( $\circ$ )
Mean	17.95	18.65	19	18.9	18.86	18.97	18.96	18.98	19	19.01	19.05	19.05	19.03	19.06	19.06	19.03	19.07	19.09	19.07	19.11
Std.Dev	0.89	0.32	0.35	0.2	0.17	0.05	0.07	0.07	0.1	0.07	0.04	0.08	0.06	0.06	0.05	0.04	0.04	0.04	0.05	0.07
Mean	19.31	19.18	19.18	19.18	19.04	19.04	19.09	19.09	19.13	19.13	19.1	19.1	19.1	19.1	19.1	19.15	19.15	19.16	19.16	19.12
Std.Dev	0.32	0.13	0.13	0.13	0.15	0.15	0.13	0.13	0.1	0.1	0.08	0.08	0.06	0.1	0.11	0.11	0.05	0.05	0.08	0.08
Mean	18.97	18.97	18.97	18.97	19.03	19.03	19.03	19.03	19.03	19.02	19.02	19.02	19.02	19.11	19.11	19.11	19.11	19.11	19.11	19.13
Std.Dev	0.34	0.34	0.34	0.34	0.15	0.15	0.15	0.15	0.15	0.12	0.12	0.12	0.12	0.1	0.1	0.1	0.1	0.1	0.1	0.06
Mean	59.07	53.85	52.28	51.82	51.3	51.19	51.02	51.01	50.77	50.72	50.71	50.63	50.63	50.58	50.59	50.56	50.52	50.58	50.52	50.55
Std.Dev	1.55	0.59	0.36	0.26	0.24	0.15	0.2	0.13	0.12	0.13	0.1	0.12	0.11	0.1	0.09	0.18	0.11	0.08	0.08	0.07
Mean	51.01	50.55	50.55	50.55	50.39	50.39	50.32	50.32	50.25	50.25	50.25	50.25	50.23	50.23	50.24	50.24	50.29	50.29	50.25	50.25
Std.Dev	0.72	0.34	0.34	0.34	0.15	0.15	0.19	0.19	0.16	0.16	0.1	0.1	0.05	0.05	0.09	0.09	0.03	0.03	0.04	0.04
Mean	50.08	50.08	50.08	50.08	50.16	50.16	50.16	50.16	50.17	50.17	50.17	50.17	50.17	50.13	50.13	50.13	50.13	50.13	50.13	50.18
Std.Dev	0.43	0.43	0.43	0.43	0.23	0.23	0.23	0.23	0.13	0.13	0.13	0.13	0.13	0.04	0.04	0.04	0.04	0.04	0.07	0.07
Mean	87.73	94.01	96.5	96.88	99.95	100.25	100.3	100.5	100.5	100.8	100.8	100.7	100.75	100.8	100.8	100.7	100.9	101.0	101.0	101.0
Std.Dev	1.23	0.59	0.57	0.25	0.31	0.48	0.24	0.18	0.17	0.27	0.25	0.08	0.08	0.14	0.12	0.19	0.21	0.2	0.33	0.15
Mean	93.45	97.03	97.03	97.03	99.82	99.82	100.3	100.3	100.4	100.4	100.7	100.7	100.7	100.7	100.7	100.8	100.8	100.8	100.8	100.8
Std.Dev	1.99	0.48	0.48	0.48	0.67	0.67	0.36	0.36	0.61	0.61	0.3	0.3	0.52	0.52	0.36	0.36	0.22	0.22	0.23	0.23
Mean	97.13	97.13	97.13	97.13	100.6	100.6	100.6	100.6	100.7	100.7	100.7	100.7	100.7	100.7	100.9	100.9	100.9	101.0	101.0	101.0
Std.Dev	1.15	1.15	1.15	1.15	0.61	0.61	0.61	0.61	0.5	0.5	0.5	0.5	0.5	0.26	0.26	0.26	0.22	0.22	0.22	0.22
Mean	100.8	100.8	100.8	100.8	100.8	100.8	100.8	100.8	100.8	100.8	100.8	100.8	100.8	100.8	100.8	100.8	100.8	100.8	100.8	100.8
Std.Dev	0.17	0.17	0.17	0.17	0.17	0.17	0.17	0.17	0.17	0.17	0.17	0.17	0.17	0.17	0.17	0.17	0.17	0.17	0.17	0.17

In order to summarize the experimental data obtained in the previous tables, Table 4.17 is presented. In this table it can be clearly observed that the stiffness values obtained remain stable in relation to their mean value, it is explained because the standard deviation in each case is small in comparison to the average. Additionally, it can be seen that the behavior of the rotational stiffness of the joints are very similar in both directions of rotation.

Table 4.17.: Statistical summary of flexure hinges rotational stiffness

		$k_{\varphi 50_{exp}}$	$k_{\varphi 75_{exp}}$	$k_{\varphi 100_{exp}}$
		(Nmm/rad)	(Nmm/rad)	(Nmm/rad)
<b>Both directions</b>	<b>Mean</b>	19.09	50.52	99.81
	<b>Std.Dev</b>	0.13	0.18	0.49
<b>Clockwise</b>	<b>Mean</b>	19.12	50.5	99.7
	<b>Std.Dev</b>	0.13	0.18	0.4
<b>Counterclockwise</b>	<b>Mean</b>	19.07	50.54	99.91
	<b>Std.Dev</b>	0.11	0.17	0.4

Once the results of the rotational stiffness are obtained, they are compared with the analytical results. It is shown in Table 4.18.

Table 4.18.: Comparative table of estimated and experimental rotational stiffness respect to analytical results considering nominal values of thickness

<b>h</b>	<b>Analy. vs esti. Stiffness</b>			<b>Analy. vs exp. Stiffness</b>		
	$k_{\varphi_{an}}$	$k_{\varphi_{esti}}$	$k_{\varphi_{esti}}/k_{\varphi_{an}}$	$k_{\varphi_{an}}$	$k_{\varphi_{exp}}$	$k_{\varphi_{exp}}/k_{\varphi_{an}}$
( $\mu\text{m}$ )	(Nmm/rad)	(Nmm/rad)	(%)	(Nmm/rad)	(Nmm/rad)	(%)
50	16.21	17.73	<b>109.38</b>	16.21	19.09	<b>117.78</b>
75	44.67	48.54	<b>108.66</b>	44.67	50.52	<b>113.10</b>
100	91.69	98.98	<b>107.95</b>	91.69	99.81	<b>108.86</b>

Comparing the values of rotational stiffness obtained by estimating the experimental formula of the setup (see Table 4.3) with those calculated analytically, they increase its value in 10%. However, when comparing the experimental results of rotational stiffness with those calculated analytically, they increase in 13%. Due to the similarity of the results, flexure hinges manufactured by manufacturer B show mechanical properties closer to the ideal mechanical models than the hinges manufactured by manufacturer A.

In Fig. 4.11 we can observe the linear behavior of the rotational stiffness for the three flexure hinges analyzed. Mean values of torque applied and angle of rotation detected by Elcomat 3000 were selected to make the graph.

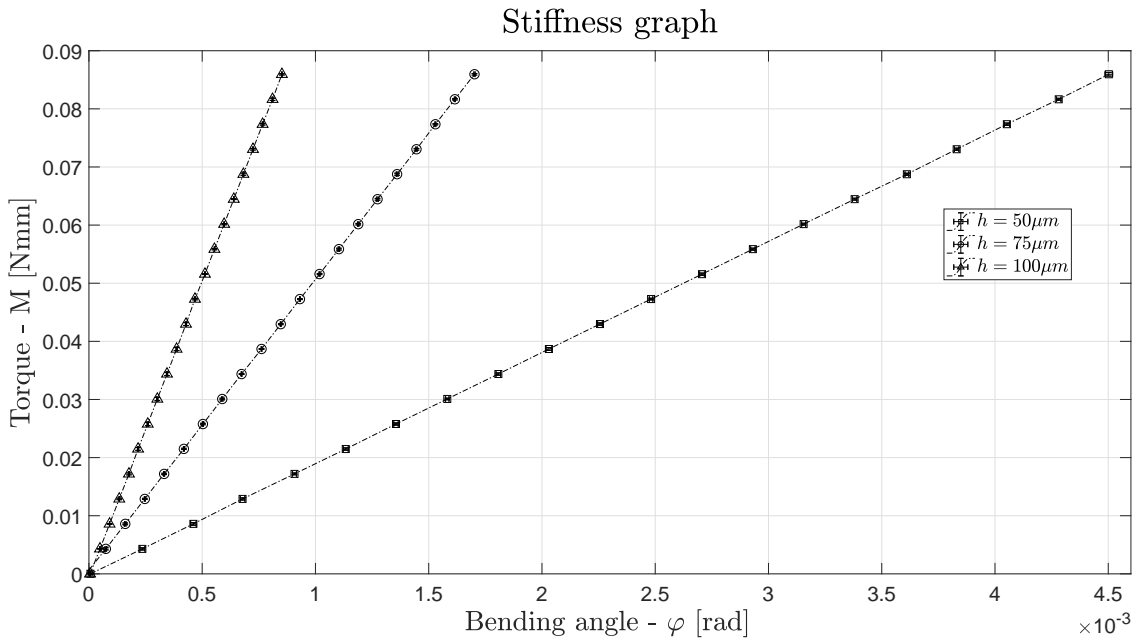


Figure 4.11.: Stiffness behavior of manufacturer B flexure hinges for 10 degrees of pulley rotation

After performing experiments to evaluate the rotational stiffness of the joints when applying torques from 0 to 0.086 Nmm, the next step is the evaluation of this parameter when the applied torque is ten times lower. This is made to determine possible nonlinear behaviors that could occur for smaller deformations. Each type of test was carried out on each joint with 20 iterations per experiment. Table 4.19, Table 4.20 and Table 4.21 contain the statistical data that results from collecting the stiffness information of all the experiments. Table 4.19 contains the statistical data of the complete movement for each position (both clockwise and counterclockwise). Table 4.20 contains the statistical data for each position when moving in a clockwise direction and Table 4.21 contains the statistical data for each position when it moves counterclockwise.

Table 4.19.: Experimental values of stiffness for manufacturer B flexure hinge of 50  $\mu\text{m}$ , 75  $\mu\text{m}$  and 100  $\mu\text{m}$  thickness. Mean and standard deviation per pulley position (total experimental values, clockwise and counterclockwise rotation) from 0 to 1 degree

	POS 1 - 0.05(°)	POS 2 - 0.10(°)	POS 3 - 0.15(°)	POS 4 - 0.20(°)	POS 5 - 0.25(°)	POS 6 - 0.30(°)	POS 7 - 0.35(°)	POS 8 - 0.40(°)	POS 9 - 0.45(°)	POS 10 - 0.50(°)	POS 11 - 0.55(°)	POS 12 - 0.60(°)	POS 13 - 0.65(°)	POS 14 - 0.70(°)	POS 15 - 0.75(°)	POS 16 - 0.80(°)	POS 17 - 0.85(°)	POS 18 - 0.90(°)	POS 19 - 0.95(°)	POS 20 - 1(°)
Mean	14.88	16.21	16.85	17.43	17.65	17.98	18	18.24	18.47	18.54	18.59	18.64	18.75	18.76	18.7	18.8	18.78	18.86	18.84	18.88
Std.Dev	3.68	1.08	0.93	0.8	0.58	0.32	0.32	0.37	0.28	0.26	0.2	0.2	0.22	0.19	0.18	0.18	0.13	0.11	0.14	0.12
Mean	14.09		15.76	16.87	17.37	17.7	18.03	18.29	18.59	18.81	18.98	19.24	19.31	19.31	19.31	19.31	19.31	19.31	19.31	19.31
Std.Dev	2.54		1.23	1.07	0.9	0.59	0.54	0.65	0.65	0.65	0.65	0.65	0.65	0.65	0.65	0.65	0.65	0.65	0.65	0.65
Mean	18.68		18.68	18.82	18.82	18.82	18.82	18.82	18.82	18.82	18.82	18.82	18.82	18.82	18.82	18.82	18.82	18.82	18.82	18.82
Std.Dev	2.59		2.59	1.51	1.51	1.51	1.51	1.51	1.51	1.51	1.51	1.51	1.51	1.51	1.51	1.51	1.51	1.51	1.51	1.51
Mean	19.17		19.17	1.28	1.28	1.28	1.28	1.28	1.28	1.28	1.28	1.28	1.28	1.28	1.28	1.28	1.28	1.28	1.28	1.28
Std.Dev	1.28		1.28	1.28	1.28	1.28	1.28	1.28	1.28	1.28	1.28	1.28	1.28	1.28	1.28	1.28	1.28	1.28	1.28	1.28
Mean	160.1	64.2	54.82	54.38	53.26	52.77	52.23	52	52.05	51.5	51.24	50.84	50.9	50.68	50.66	50.67	50.4	50.41	50.27	50.28
Std.Dev	198.75	18.96	9.23	6.84	5.73	4.9	3.72	3.64	2.92	2.74	2.33	2.08	2.07	1.77	1.59	1.63	1.33	1.27	1.26	1.15
Mean	54.19		50.38	49.66	49.66	49.33	49.89	49.9	49.33	49.33	49.33	49.89	49.89	49.73	49.58	49.58	49.6	49.6	49.54	49.54
Std.Dev	7.36		4.44	1.83	1.83	1.07	1.34	1.34	1.07	1.07	0.62	0.62	0.62	0.85	0.58	0.58	0.58	0.58	0.62	0.62
Mean	47.52		47.52	48.99	48.99	49.05	49.05	49.05	49.05	49.05	49.05	49.05	49.05	49.05	49.05	49.05	49.05	49.05	49.05	49.05
Std.Dev	2.45		2.45	1.94	1.94	0.62	0.62	0.62	0.62	0.62	0.62	0.62	0.62	0.62	0.62	0.62	0.62	0.62	0.62	0.62
Mean	261.3	131.4	119.16	112.1	109.4	108.8	107.3	106.9	105.9	104.9	104.9	104.6	104	104.1	104.1	103.4	103.6	103.1	102.7	102.7
Std.Dev	181.6	32.05	17.09	9.37	7.34	6.37	5.71	4.6	3.32	3.34	2.71	2.58	2.9	2.59	2.55	2.44	2.09	1.92	1.62	1.48
Mean	279.1		141.8	126.8	126.8	117.9	117.9	117.9	112.7	112.7	111.7	111.7	111.7	110.6	108.4	108.4	108.41	108.41	107.0	107.0
Std.Dev	129.6		10.28	6.18	6.18	4.5	4.5	3.01	3.01	3.01	2.38	2.38	2.38	1.44	1.41	1.41	1.02	1.02	0.82	0.82
Mean	134.4		134.4	115.1	115.1	109.7	109.7	109.7	109.7	109.7	109.7	109.7	109.7	107.65	107.65	107.65	107.65	107.65	106.4	106.4
Std.Dev	6.25		6.25	2.28	2.28	1.54	1.54	1.54	1.54	1.54	1.54	1.54	1.54	1.04	1.04	1.04	1.04	1.04	0.83	0.83
Mean	106.8		106.8	1.91	1.91	1.91	1.91	1.91	1.91	1.91	1.91	1.91	1.91	1.91	1.91	1.91	1.91	1.91	1.91	1.91
Std.Dev	1.91		1.91	1.91	1.91	1.91	1.91	1.91	1.91	1.91	1.91	1.91	1.91	1.91	1.91	1.91	1.91	1.91	1.91	1.91

Table 4.20.: Experimental values of stiffness for manufacturer B flexure hinge of 50  $\mu\text{m}$ , 75  $\mu\text{m}$  and 100  $\mu\text{m}$  thickness. Mean and standard deviation per pulley position (clockwise rotation) from 0 to 1 degree

	POS 1 - 0.05(°)	POS 2 - 0.10(°)	POS 3 - 0.15(°)	POS 4 - 0.20(°)	POS 5 - 0.25(°)	POS 6 - 0.30(°)	POS 7 - 0.35(°)	POS 8 - 0.40(°)	POS 9 - 0.45(°)	POS 10 - 0.50(°)	POS 11 - 0.55(°)	POS 12 - 0.60(°)	POS 13 - 0.65(°)	POS 14 - 0.70(°)	POS 15 - 0.75(°)	POS 16 - 0.80(°)	POS 17 - 0.85(°)	POS 18 - 0.90(°)	POS 19 - 0.95(°)	POS 20 - 1(°)
<b>Mean</b>	15.69	16.54	17.01	17.57	17.92	18.1	18.05	18.39	18.52	18.41	18.54	18.7	18.8	18.78	18.73	18.8	18.79	18.89	18.85	18.88
<b>Std.Dev</b>	4.88	1.11	0.89	0.78	0.46	0.22	0.29	0.37	0.24	0.14	0.19	0.19	0.15	0.16	0.14	0.19	0.15	0.11	0.15	0.11
<b>Mean</b>	14.32	15.84	15.12	16.9	16.9	16.9	17.3	17.3	17.79	17.79	18.02	18.02	18.46	18.46	18.15	18.15	18.39	18.39	18.52	18.52
<b>Std.Dev</b>	2.36	1.12	1.14	1.14	1.14	0.88	0.88	0.59	0.59	0.51	0.51	0.51	0.66	0.66	0.32	0.32	0.51	0.51	0.39	0.39
<b>Mean</b>	18.39	18.39	18.39	18.46	18.46	18.46	19.17	19.17	19.17	19.17	19.17	19.17	19.17	19.17	19.17	19.17	19.17	19.17	19.17	19.17
<b>Std.Dev</b>	2.49	2.49	2.49	1.65	1.65	1.65	0.79	0.79	0.79	0.79	0.79	0.79	0.79	0.79	0.79	0.79	0.79	0.79	0.79	0.79
<b>Mean</b>	18.63	18.63	18.63	18.63	18.63	18.63	18.63	18.63	18.63	18.63	18.63	18.63	18.63	18.63	18.63	18.63	18.63	18.63	18.63	18.63
<b>Std.Dev</b>	1.01	1.01	1.01	1.01	1.01	1.01	1.01	1.01	1.01	1.01	1.01	1.01	1.01	1.01	1.01	1.01	1.01	1.01	1.01	1.01
<b>Mean</b>	115.563	2855.97	53.53	52.84	52.45	51.93	51.46	51.25	51.01	50.84	50.78	50.72	50.57	50.61	50.27	50.4	50.18	50.32	50.18	50.32
<b>Std.Dev</b>	94.19	18.43	10.21	6.5	6.01	4.57	3.77	3.57	2.99	2.77	2.36	1.91	1.97	1.59	1.57	1.69	1.37	1.41	1.31	1.25
<b>Mean</b>	55.03	47.79	49.52	49.52	49.52	50.01	49.44	49.44	49.44	49.87	49.78	49.87	49.78	49.52	49.52	49.64	49.64	49.47	49.47	49.47
<b>Std.Dev</b>	5.75	2.11	1.28	1.28	1.28	1.14	1.06	1.06	1.06	0.5	0.8	0.5	0.8	0.56	0.56	0.73	0.73	0.59	0.59	0.59
<b>Mean</b>	47.16	47.16	47.16	47.16	47.16	48.64	48.64	48.64	48.64	48.92	48.92	48.92	48.92	48.65	48.65	49.18	49.18	49.18	49.18	49.18
<b>Std.Dev</b>	2.26	2.26	2.26	2.26	2.26	1.83	1.83	1.83	1.83	0.63	0.63	0.63	0.63	0.48	0.48	0.46	0.46	0.46	0.46	0.46
<b>Mean</b>	262.31	34.91	19.31	14.91	10.91	8.10	8.10	8.10	8.10	8.10	8.10	8.10	8.10	8.10	8.10	8.10	8.10	8.10	8.10	8.10
<b>Std.Dev</b>	195.3	30.1	11.6	8.04	6.41	5.26	5.62	4.39	2.74	2.97	2.48	2.69	2.65	2.47	2.97	2.58	2.48	2.14	1.76	1.53
<b>Mean</b>	249.6	249.6	141.3	127.6	127.6	116.6	112.19	112.19	112.19	111.31	109.9	108.2	108.1	108.2	108.2	108.1	108.1	106.8	106.8	106.8
<b>Std.Dev</b>	62.6	62.6	7.82	4.59	4.59	2.81	2.95	2.95	2.95	3.01	1.37	1.26	0.66	1.26	1.26	0.66	0.66	0.41	0.41	0.41
<b>Mean</b>	134.3	134.3	134.3	134.3	134.3	114.4	114.4	114.4	114.4	108.8	107.8	107.8	107.8	107.8	107.8	106.5	106.5	106.5	106.5	106.5
<b>Std.Dev</b>	7.52	7.52	7.52	7.52	7.52	2.76	2.76	2.76	2.76	1.36	1.36	0.92	0.92	0.92	0.92	1.08	1.08	1.08	1.08	1.08
<b>Mean</b>	106.4	106.4	106.4	106.4	106.4	106.4	106.4	106.4	106.4	106.4	106.4	106.4	106.4	106.4	106.4	106.4	106.4	106.4	106.4	106.4
<b>Std.Dev</b>	2.14	2.14	2.14	2.14	2.14	2.14	2.14	2.14	2.14	2.14	2.14	2.14	2.14	2.14	2.14	2.14	2.14	2.14	2.14	2.14



Table 4.21.: Experimental values of stiffness for manufacturer B flexure hinge of 50  $\mu\text{m}$ , 75  $\mu\text{m}$  and 100  $\mu\text{m}$  thickness. Mean and standard deviation per pulley position (counterclockwise rotation) from 0 to 1 degree

	POS 1 - 0.05( $\circ$ )	POS 2 - 0.10( $\circ$ )	POS 3 - 0.15( $\circ$ )	POS 4 - 0.20( $\circ$ )	POS 5 - 0.25( $\circ$ )	POS 6 - 0.30( $\circ$ )	POS 7 - 0.35( $\circ$ )	POS 8 - 0.40( $\circ$ )	POS 9 - 0.45( $\circ$ )	POS 10 - 0.50( $\circ$ )	POS 11 - 0.55( $\circ$ )	POS 12 - 0.60( $\circ$ )	POS 13 - 0.65( $\circ$ )	POS 14 - 0.70( $\circ$ )	POS 15 - 0.75( $\circ$ )	POS 16 - 0.80( $\circ$ )	POS 17 - 0.85( $\circ$ )	POS 18 - 0.90( $\circ$ )	POS 19 - 0.95( $\circ$ )	POS 20 - 1( $\circ$ )
Mean	14.08	15.88	16.69	17.29	17.38	17.87	17.95	18.1	18.41	18.66	18.63	18.58	18.69	18.73	18.68	18.79	18.76	18.84	18.82	18.89
Std.Dev	1.81	1	0.99	0.85	0.58	0.37	0.35	0.31	0.31	0.31	0.2	0.21	0.27	0.22	0.21	0.18	0.12	0.12	0.13	0.13
Mean	13.86	15.69	16.85	17.43	17.61	18.04	18.12	18.39	18.41	18.56	18.63	18.70	18.77	18.84	18.91	19.00	19.07	19.14	19.21	19.28
Std.Dev	2.82	1.39	1.06	0.96	0.6	0.59	0.63	0.63	0.63	0.63	0.63	0.63	0.63	0.63	0.63	0.63	0.63	0.63	0.63	0.63
Mean	18.96	19.18	19.14	19.14	19.14	19.14	19.14	19.14	19.14	19.14	19.14	19.14	19.14	19.14	19.14	19.14	19.14	19.14	19.14	19.14
Std.Dev	2.78	1.34	1.34	1.34	1.34	1.34	1.34	1.34	1.34	1.34	1.34	1.34	1.34	1.34	1.34	1.34	1.34	1.34	1.34	1.34
Mean	19.71	19.71	19.71	19.71	19.71	19.71	19.71	19.71	19.71	19.71	19.71	19.71	19.71	19.71	19.71	19.71	19.71	19.71	19.71	19.71
Std.Dev	1.34	1.34	1.34	1.34	1.34	1.34	1.34	1.34	1.34	1.34	1.34	1.34	1.34	1.34	1.34	1.34	1.34	1.34	1.34	1.34
Mean	204.78	65.13	53.66	55.22	53.69	53.1	52.52	52.05	52.63	51.74	51.46	50.85	51.01	50.65	50.75	50.73	50.54	50.43	50.36	50.23
Std.Dev	264.75	20.42	8.51	7.4	5.73	5.44	3.86	3.89	2.87	2.84	2.39	2.33	2.26	2.02	1.68	1.65	1.35	1.18	1.28	1.11
Mean	53.35	52.97	49.8	49.79	49.23	49.9	49.67	49.56	49.61	49.67	49.63	49.63	49.63	49.67	49.67	49.63	49.56	49.56	49.61	49.61
Std.Dev	8.93	4.71	2.31	1.58	1.12	0.76	0.93	0.41	0.67	0.62	0.62	0.62	0.62	0.62	0.62	0.62	0.62	0.62	0.67	0.67
Mean	47.88	49.34	49.17	49.17	49.17	49.17	49.17	49.17	49.17	49.17	49.17	49.17	49.17	49.17	49.17	49.17	49.17	49.17	49.17	49.17
Std.Dev	2.69	2.07	2.07	2.07	2.07	2.07	2.07	2.07	2.07	2.07	2.07	2.07	2.07	2.07	2.07	2.07	2.07	2.07	2.07	2.07
Mean	260.2	127.8	119.1	109.4	107.9	108.8	106.3	107.1	105.6	104.7	105.1	104.1	103.9	104.0	103.9	103.5	103.5	103.0	102.8	102.9
Std.Dev	177.5	35.14	22.0	10.21	8.22	7.61	5.9	5.02	3.94	3.81	3.04	2.53	3.27	2.84	2.21	2.42	1.75	1.77	1.55	1.48
Mean	308.6	142.4	125.9	119.2	113.19	112.1	111.2	108.6	108.7	108.6	108.6	108.6	108.6	108.6	108.6	108.6	108.6	108.6	108.6	108.6
Std.Dev	172.1	12.71	7.62	5.57	3.14	1.61	1.3	1.26	1.06	1.06	1.06	1.06	1.06	1.06	1.06	1.06	1.06	1.06	1.06	1.06
Mean	134.5	115.8	110.7	110.7	110.7	110.7	110.7	110.7	110.7	110.7	110.7	110.7	110.7	110.7	110.7	110.7	110.7	110.7	110.7	110.7
Std.Dev	5.1	1.47	1.47	1.47	1.47	1.47	1.47	1.47	1.47	1.47	1.47	1.47	1.47	1.47	1.47	1.47	1.47	1.47	1.47	1.47
Mean	107.3	107.3	107.3	107.3	107.3	107.3	107.3	107.3	107.3	107.3	107.3	107.3	107.3	107.3	107.3	107.3	107.3	107.3	107.3	107.3
Std.Dev	1.61	1.61	1.61	1.61	1.61	1.61	1.61	1.61	1.61	1.61	1.61	1.61	1.61	1.61	1.61	1.61	1.61	1.61	1.61	1.61

In order to summarize the experimental data obtained in the previous tables, Table 4.22 is presented. It is observed that the stiffness values obtained remain stable in relation to their mean value, it is explained because the standard deviation in each case is small in comparison to the average. Additionally, it can be seen that the behavior of the rotational stiffness of the joints are very similar in both directions of rotation.

Table 4.22.: Statistical summary of flexure hinges rotational stiffness

		$k_{\varphi 50_{exp}}$	$k_{\varphi 75_{exp}}$	$k_{\varphi 100_{exp}}$
		(Nmm/rad)	(Nmm/rad)	(Nmm/rad)
<b>Both directions</b>	<b>Mean</b>	18.40	51.42	117.28
	<b>Std.Dev</b>	0.98	4.34	8.76
<b>Clockwise</b>	<b>Mean</b>	18.29	50.71	116.41
	<b>Std.Dev</b>	0.92	2.86	7.11
<b>Counterclockwise</b>	<b>Mean</b>	18.50	52.12	118.17
	<b>Std.Dev</b>	0.98	5.32	9.85

In Fig. 4.12 we can observe the linear behavior of the rotational stiffness for the three flexure hinges analyzed. Mean values of torque applied and angle of rotation detected by Elcomat 3000 were selected to make the graph.

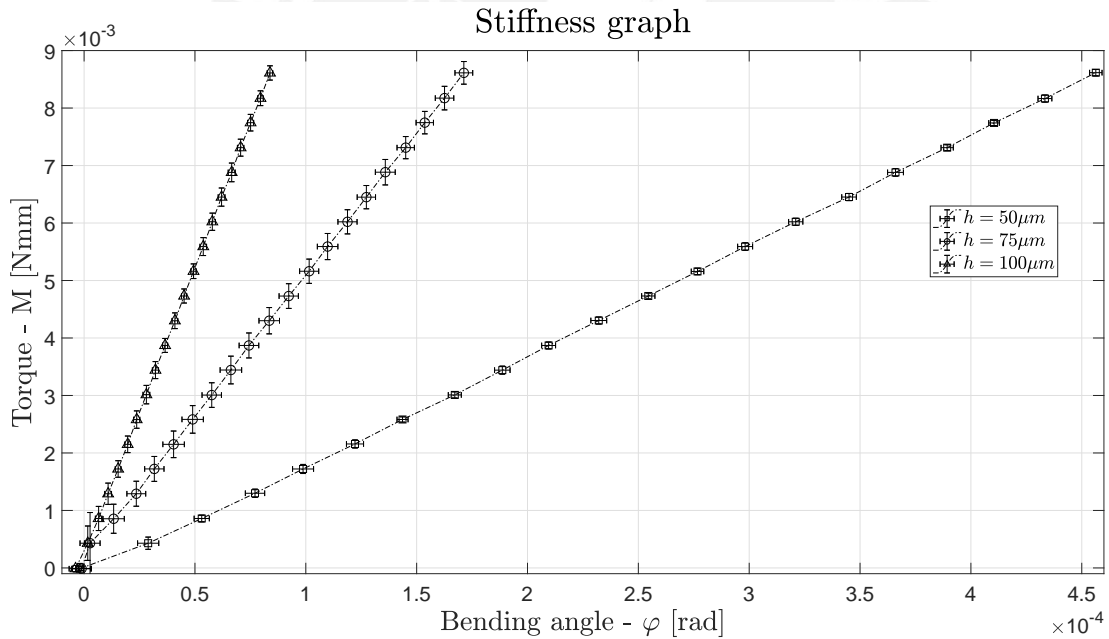


Figure 4.12.: Stiffness behavior of manufacturer B flexure hinges for 1 degree of pulley rotation

Observing Fig. 4.11 and Fig. 4.12, the linear behavior of the rotational stiffness of flexure hinges manufactured by manufacturer B is verified. Torque variations have less influence

on stiffness calculated for 10 degrees than 1 degree pulley rotation. That is why variations of torque and bending angle are more noticeable for the points plotted in Fig. 4.12.

### 4.2.3. Results Evaluation and Discussion

According to the work presented in the previous section, it was found that the rotational stiffness for the same nominal value of thickness differs depending of manufacturing company. To make a better evaluation of the obtained results, it was necessary to observe the elements microscopically. It was performed with the help of the wafer inspection microscope *Nikon Eclipse L300D* unit. It was of great importance to use this equipment because it showed physical details of the hinges that had not been considered until now. In Fig. 4.13 and Fig. 4.14 we can see in detail the shapes of the flexure hinges with magnifications of x10, x20 and x50.

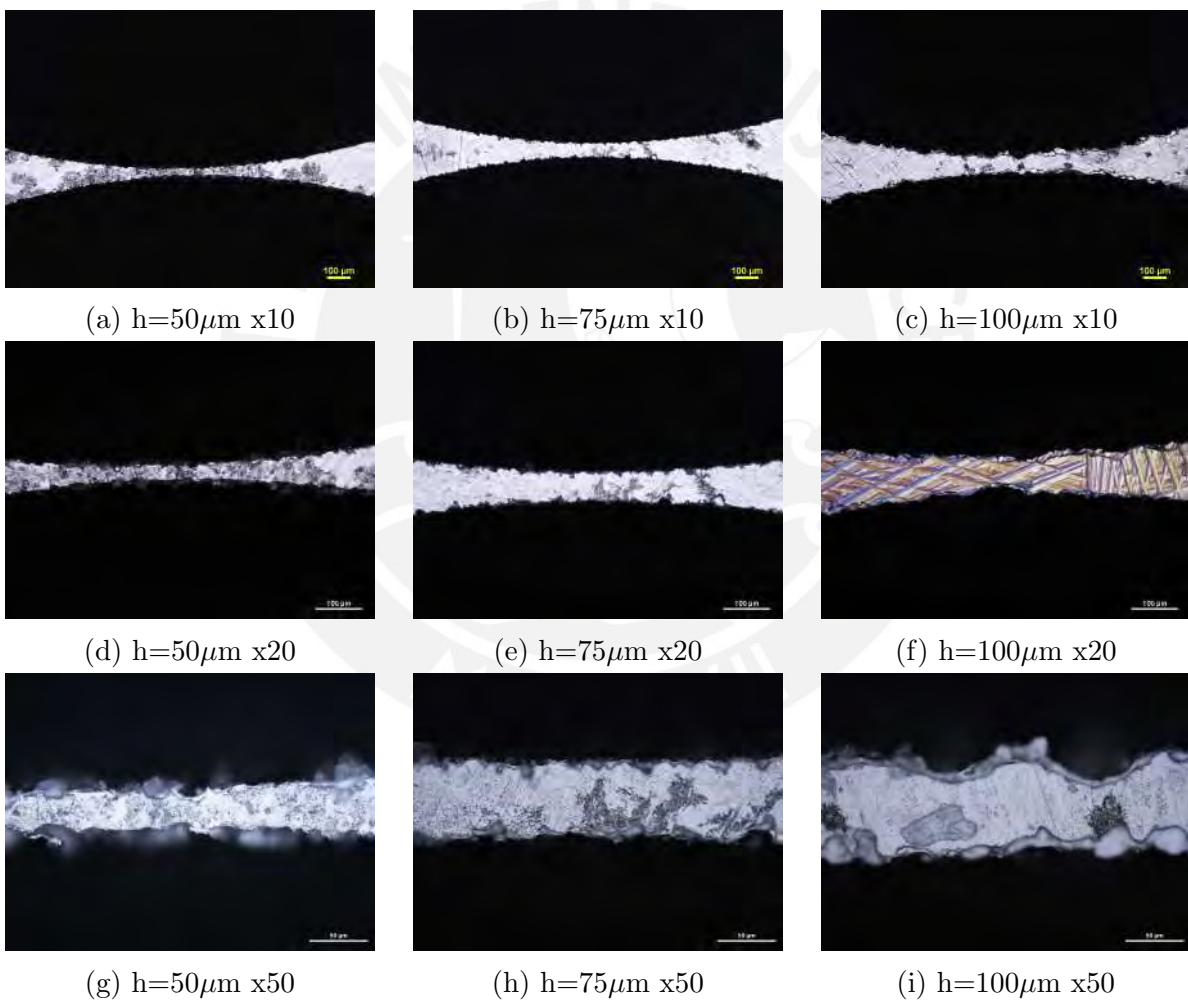


Figure 4.13.: Manufacturer A flexure hinges (magnifications of x10, x20 and x50)

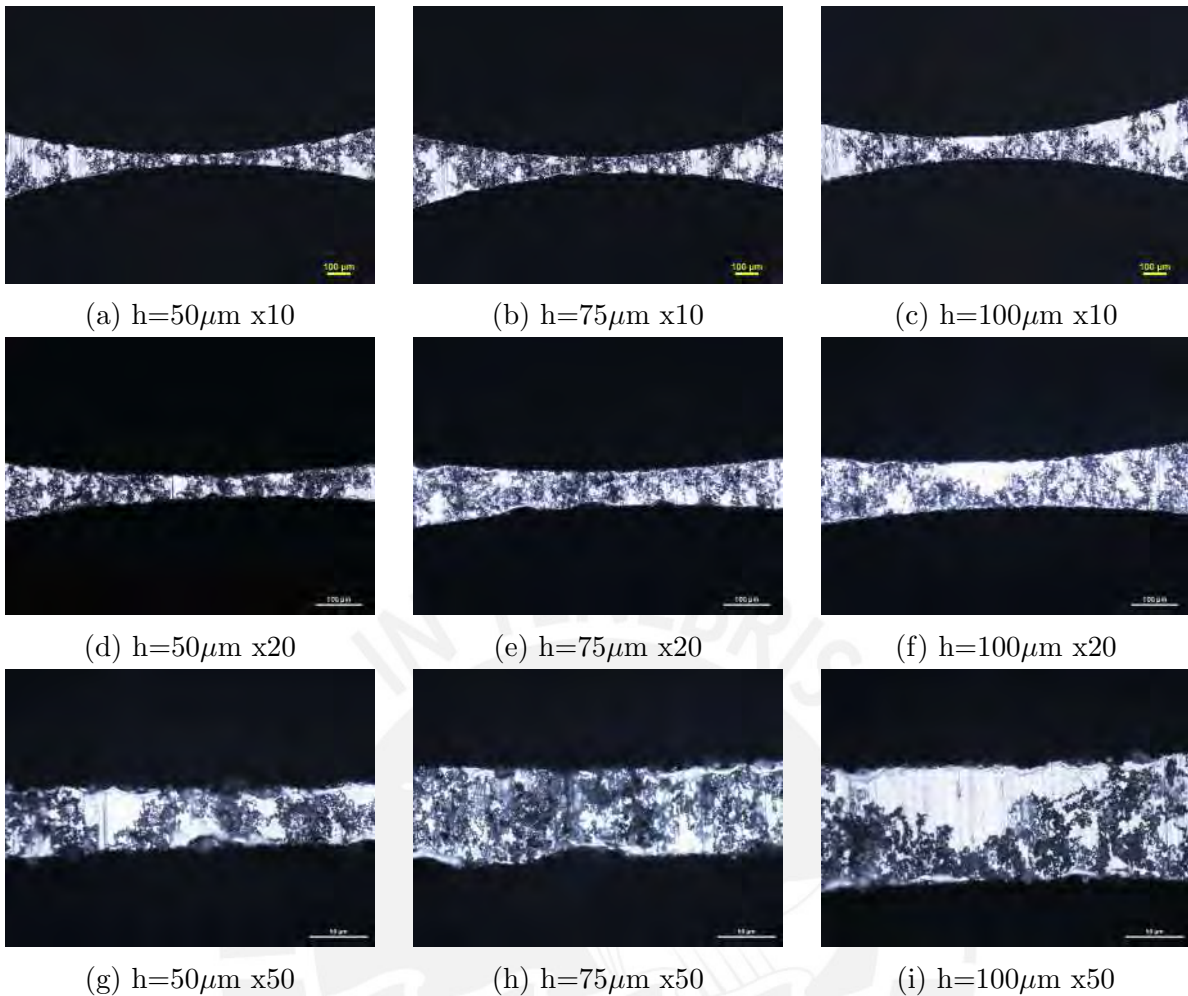


Figure 4.14.: Manufacturer B flexure hinges (magnifications of x10, x20 and x50)

The main observation that is achieved from the previous images is that there is a difference in the resulting surface provided by the manufacturing process of manufacturer A and manufacturer B. In the first case, cracks and eroded surfaces are observed in the most slender section of the joints from the magnification x10, which is even more evident for the magnification of x50. In other words, although it was expected to have circular flexure hinges, there are actually amorphous shapes flexure hinges. In the second case, the erosion in the surface and racks in its border are reduced with respect to the previous ones due to a better manufacturing process, so the flexure hinges approximate closer to being circular. Due to the difference between their shapes, when experimenting with the flexure hinges, considerably different rotational stiffness are obtained. These values allow us to realize that since they are not completely circular surfaces (for the case of manufacturer A), the analytical equations for determine their rotational stiffness are not being applied correctly. However, in the case of manufacturer B, the results obtained are closer to the analytical results because the shape of the manufactured parts are closer to the ideal shapes.

Then, thickness of each flexure is going to be visually estimated considering the images magnified 50 times. Fig. 4.15 highlights the size of the thickness that was considered to compare.

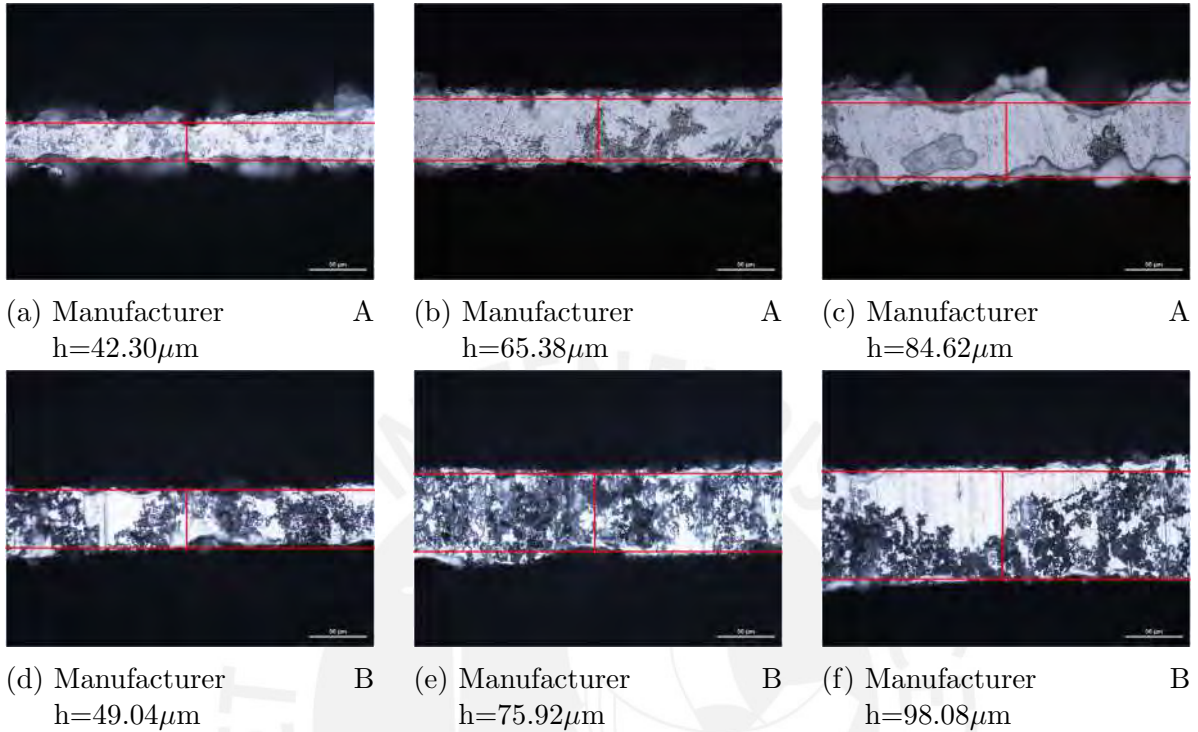


Figure 4.15.: Visual references considered to obtain the thickness of the flexure hinges

Experimental rotational stiffness ( $k_{\varphi_{exp}}$ ) is compared with those determined in three ways. First, the one obtained dividing torque produced by the setup with bending angle ( $k_{\varphi_{esti}}$ ). Second, the one calculated with the analytical formula of rotational stiffness for circular flexure hinges ( $k_{\varphi_{an}}$ ). Third, with rotational stiffness obtained by FEA<sup>1</sup> (without considering the weight of the materials below the center of mass of the flexure hinge ( $k_{FEA}$ ) and considering this weight ( $k_{FEA^*}$ )). The FEA results were obtained from a thesis work mentioned in the footnote. These results considered nominal values of thickness.

<sup>1</sup>Torres Melgarejo, Mario: Modeling of the elastic mechanical behavior of thin compliant joints under load for highest-precision applications (Ilmenau,2018)

Table 4.23.: Comparison of the different rotational stiffness evaluated in this research

$h_{nom}$ ( $\mu\text{m}$ )	$k_{\varphi_{esti}}$ (Nmm/rad)	Manufacturer A			Manufacturer B			$k_{FEA}$ (Nmm/rad)	$k_{FEA^*}$ (Nmm/rad)
		$h_{re}$ ( $\mu\text{m}$ )	$k_{\varphi_{an}}$ (Nmm/rad)	$k_{\varphi_{exp}}$ (Nmm/rad)	$h_{re}$ ( $\mu\text{m}$ )	$k_{\varphi_{an}}$ (Nmm/rad)	$k_{\varphi_{exp}}$ (Nmm/rad)		
<b>50</b>	17.73	<b>42.30</b>	10.67	10.74	<b>49.04</b>	15.44	19.09	18.03	17.89
<b>75</b>	48.54	<b>65.38</b>	31.69	33.86	<b>75.92</b>	46.04	50.52	49.51	49.34
<b>100</b>	98.98	<b>84.62</b>	63.88	60.64	<b>98.08</b>	87.35	99.81	101.3	101.1

Due to the difference in the manufacturing processes carried out by manufacturer A and manufacturer B, there are large differences between their experimental results. For practical purposes and due to its better behavior, only the results generated by the flexure hinges manufactured by manufacturer B are discussed.

In Table 4.23 it is clearly observed that the rotational stiffness obtained analytically differ of the experimental results and those obtained by FEA<sup>2</sup>. This is explained because the analytical formula only considers a flat state of stress for circular flexure hinges. Thus, the validity of this formula may be subject to revalidation. However, when comparing experimental results and results from the FEA, it can be seen certain approximation. It can verify that procedures taken into account (the choice of the mesh, the choice of number of finite elements, the boundary conditions, the loading application, the geometry, the material and the mathematical model) were well performed. There were considered two FEA, the first ( $k_{FEA}$ ) considered only a torque applied to the center of mass of the flexure hinges. The second ( $k_{FEA^*}$ ), besides this torque, it considered the weight of all parts that hung up from the center of the flexure hinge.

Results of the FEA that consider the extra weight differ from the first FEA results in different ways for each flexure hinge. On the one hand, it can explain the fact that the weight of the parts has greater influence for thinner flexure hinges than thicker ones. In consequence, the rotational stiffness is reduced because of this effect. On the other hand, it can demonstrate that probably the center of mass of the system is located above the geometrical center of the flexure hinge. It would be an error on the manufacturing protocols to manufactur the elements of the setup and mounting deviations.

To compare graphically all results of rotational stiffness, results were organized in Fig. 4.16. It displays more clearly the difference in the accuracy to obtain the rotational stiffness for the different methods considered in this work and for both sets of flexure hinges. The FEA results, the setup estimation results and the ones obtained experimentally with manufacturer B flexure hinges remain almost in the same range.

<sup>2</sup>Torres Melgarejo, Mario: Modeling of the elastic mechanical behavior of thin compliant joints under load for highest-precision applications (Ilmenau,2018)

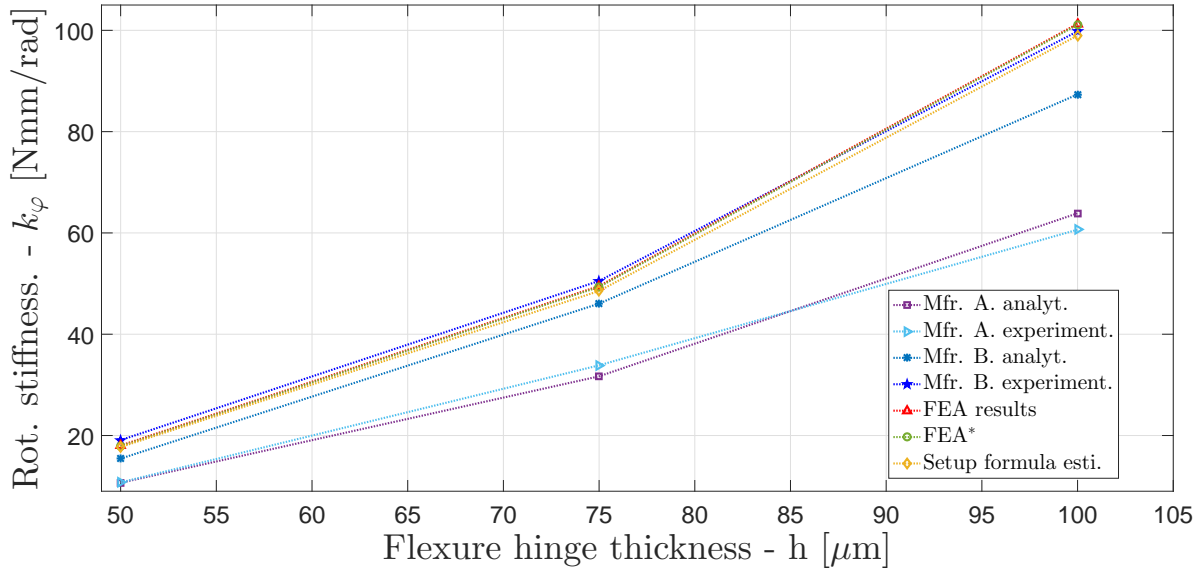


Figure 4.16.: Graphical comparison of the rotational stiffness results

Finally, with the purpose of contributing to the validation of mathematical models with experimental results, the approximate model that is given in the Eq. (3.1) for circular flexure hinges, is evaluated. In this equation, the exponent of the thickness ( $h$ ) was determined in [LSZ17] to be 2.5. With the experimental values obtained in this work, the exponent is going to be verified. The relation between the thickness ( $h$ ) and the rotational stiffness ( $k_\varphi$ ) is given in Eq. (4.1).

$$h^X = 1.0906 \cdot 10^{-12} \cdot k_\varphi \quad (4.1)$$

Where 'X' is the parameter to be determined.

Table 4.24.: Comparison of parameter 'X' obtained by the FEA and experimentally

$h$ ( $\mu\text{m}$ )	$X_{nom}$	$X_{FEA}$	$X_{FEA}/X_{nom}$ (%)	$X_{FEA^*}$	$X_{FEA^*}/X_{nom}$ (%)	$X_{exp}$	$X_{exp}/X_{nom}$ (%)
50		2.4892	<b>99.57</b>	2.490	<b>99.60</b>	2.4835	<b>99.34</b>
75	2.5	2.4892	<b>99.57</b>	2.4895	<b>99.58</b>	2.4870	<b>99.48</b>
100		2.4892	<b>99.57</b>	2.4894	<b>99.58</b>	2.4908	<b>99.63</b>

As is indicated in the analytical formula, 'X' must remain constant. With the results of FEA, due to the bending is directly applied to the center of mass of the flexure hinges, 'X' remains constant with a reduction of 0.43% respect to the nominal. When the weight of the setup is considered in the FEA, parameter 'X' remains still constant, but reduced by 0.42% with a little variation for the 50 microns hinge. However, when it is calculated

experimentally, it can be seen that there is a growing trend to achieve the value of 2.5 for thicker flexure hinges. In conclusion, the proposed model to calculate the rotational stiffness of circular flexure hinges is an approximate model that needs to be improved in order to get better approach in analytical results.





## 5. Conclusions and Future work

This thesis has presented a design of an experimental setup to obtain the rotational stiffness of thin circular flexure hinge experimentally. For the design, it was considered to reduce the effects of non-rotational loads in order to get the most approximate values of rotational stiffness. Also, it was considered to locate the center of mass of the setup in the same coordinates of the geometrical center of the flexure hinges. This is done to minimize the influence of an eccentric center of mass on the effective stiffness.

The proposed experimental setup has contributed to verify results of the FEA. There were good similarities between this and those that come from experimentation. Also, it helped to verify the elastic behavior of circular flexure hinges in a certain range of deflection. Graphs demonstrate the linear relation between torque applied and bending angle for circular flexure hinges. Tables give a numerical approach for each point on graphs and verify the minimal variations of its parameters. Further, it helped to prove that manufacturing techniques are important for the stiffness behavior of this kind of compliant joints. Two groups of flexure hinges manufactured by two different companies were compared. The manufacturing procedures of each one were tested evaluating the results of rotational stiffness. It could determine that the manufacturing process of one of them was better than the other because the final shape was closer to the nominal circular shape of the hinge and the deviation from the minimal notch height was smaller.

Some suggestions are provided in order to improve this work. First, to minimize the variations of measured parameters, it is proposed to implement the setup into a vacuum chamber with an anti-vibration table inside. Second, put the angle measuring device and the frame that support the motor and all the parts, on adjustable mounting rails for high precision applications. This to correct misalignments. Third, to improve the encoder positioning, set the most suitable control parameters of the motor driver (for example set the Corridor=1). Fourth, more precise cutting of the brass tape to the nominal width.

For future work, it is proposed to design another lever arm structure to reduce the weight held by the flexure hinge. The angle measuring device can be exchanged for another one of higher precision that can measure lower angles. Brass tape can be exchanged with another tape of different density in order to evaluate the stiffness of flexure hinges of different range of thickness.

# Bibliography

- [Cul04] Martin L Culpepper. “Design of quasi-kinematic couplings”. In: *Precision Engineering* 28.3 (2004), pp. 338–357.
- [DYD16] Zhijiang Du, Miao Yang, and Wei Dong. “Multi-objective optimization of a type of ellipse-parabola shaped superelastic flexure hinge”. In: *Mechanical Sciences* 7 (1 2016), pp. 127–134. DOI: 10.5194/ms-7-127-2016.
- [Du16] Zhijiang Du et al. “Static deformation modeling and analysis of flexure hinges made of a shape memory alloy”. In: *Smart Materials and Structures* 25 (11 2016), p. 115029. ISSN: 0964-1726. DOI: 10.1088/0964-1726/25/11/115029.
- [Fau] *Communication / Function Manual RS232*. FAULHABER. 2017, pp. 14–19. URL: [https://www.faulhaber.com/fileadmin/Import/Media/EN\\_7000\\_05029.pdf](https://www.faulhaber.com/fileadmin/Import/Media/EN_7000_05029.pdf).
- [GO04] Walter Gander and Urs Oswald. “The Catenary Curve”. In: *Solving problems in scientific computing using Maple and MATLAB*. Ed. by Walter Gander and Jiří Hřebíček. Berlin and New York: Springer, 2004, pp. 423–431. ISBN: 978-3-540-21127-3. DOI: 10.1007/978-3-642-18873-2{\textunderscore}29.
- [Gmb] SIOS Meßtechnik GmbH. *Triple-beam interferometer brochure*, p. 2. URL: [http://www.sios-de.com/wp-content/uploads/2015/09/SP-TR\\_engl\\_20141.pdf](http://www.sios-de.com/wp-content/uploads/2015/09/SP-TR_engl_20141.pdf).
- [HH10] Ifan Hughes and Thomas Hase. *Measurements and their Uncertainties: A practical guide to modern error analysis*. Oxford University Press, 2010. ISBN: 019956633X. URL: <https://www.amazon.com/Measurements-their-Uncertainties-practical-analysis/dp/019956633X?SubscriptionId=0JYN1NVW651KCA56C102&tag=techkie-20&linkCode=xm2&camp=2025&creative=165953&creativeASIN=019956633X>.
- [HP14] Yuhung Hsu and Chanping Pan. “The Static WKB Solution to Catenary Problems with Large Sag and Bending Stiffness”. In: *Mathematical Problems in Engineering* 2014.3 (2014), pp. 1–11. DOI: 10.1155/2014/231726.
- [HS01] Layton C. Hale and Alexander H. Slocum. “Optimal design techniques for kinematic couplings”. In: *Precision Engineering* 25.2 (2001), pp. 114–127. ISSN: 0141-6359. DOI: [https://doi.org/10.1016/S0141-6359\(00\)00066-0](https://doi.org/10.1016/S0141-6359(00)00066-0). URL: <http://www.sciencedirect.com/science/article/pii/S0141635900000660>.

- [Har68] M. Hart. “An aringngstromlm ruler”. In: *Journal of Physics D: Applied Physics* 1 (11 1968), pp. 1405–1408. ISSN: 00223727. DOI: 10.1088/0022-3727/1/11/303.
- [Has] *Special dimensions for precision gauge tape and reference sheets*. Hasberg-Schneider GmbH, p. 1. URL: <https://www.hasberg-schneider.de/en/precision-thickness-gauge-strip-custom-dimensions.html>.
- [IC14] Ivan Ivanov and Burkhard Corves. “Stiffness-Oriented Design of a Flexure Hinge-Based Parallel Manipulator”. In: *Mechanics Based Design of Structures and Machines* 42 (3 2014), pp. 326–342. ISSN: 1539-7734. DOI: 10.1080/15397734.2014.899913.
- [Jen14] Leif P. Jentoft et al. “Intrinsic embedded sensors for polymeric mechatronics. Flexure and force sensing”. In: *Sensors (Basel, Switzerland)* 14 (3 2014), pp. 3861–3870. ISSN: 1424-8220. DOI: 10.3390/s140303861.
- [LSZ17] Sebastian Linß, Philipp Schorr, and Lena Zentner. “General design equations for the rotational stiffness, maximal angular deflection and rotational precision of various notch flexure hinges”. In: *Mechanical Sciences* 8.1 (2017), pp. 29–49. DOI: 10.5194/ms-8-29-2017.
- [Lin11] Sebastian Linß et al. “The influence of asymmetric flexure hinges on the axis of rotation”. In: *Proceedings of the 56th International Scientific Colloquium*. 2011.
- [Lin15] S. Linß. “On polynomial flexure hinges”. In: (2015). DOI: 10.6567/IFTOMM.14TH.WC.PS10.008.
- [Lob01] Nicolae Lobontiu et al. “Corner-Filleted Flexure Hinges”. In: *Journal of Mechanical Design* 123 (3 2001), p. 346. ISSN: 10500472. DOI: 10.1115/1.1372190.
- [Lob03] Nicolae Lobontiu, ed. *Compliant mechanisms. Design of flexure hinges*. Boca Raton: CRC Press, 2003. ISBN: 978-0-8493-1367-7. DOI: 10.1201/9781420040272.
- [MW] Moller-Wedel. *Electronic autocollimators brochure*, p. 8. URL: [https://www.haag-streit.com/fileadmin/Moeller\\_wedel\\_optical/Brochures/Electronic\\_Autocollimators/ELCOMAT\\_\\_English.pdf](https://www.haag-streit.com/fileadmin/Moeller_wedel_optical/Brochures/Electronic_Autocollimators/ELCOMAT__English.pdf).
- [Men12] Qiaoling Meng. *A Design Method for Flexure-Based Compliant Mechanisms on the Basis of Stiffness and Stress Characteristics*. 2012. DOI: 10.6092/unibo/amsdottorato/4734.
- [PW65] J. M. Paros and L. Weisbord. “How to design flexure hinges”. In: *Machine design* 37 (1965), pp. 151–156.
- [Par14] F. Parvari. “Design and Characterization of Curved and Spherical Flexure Hinge for Planar and Spatial Compliant Mechanisms”. Università di Bologna, 2014.

- [Per16] Laurent Perdrieau. *How we make audio tapes*. 2016, pp. 2–3. URL: <http://www.recordingthemasters.com/wp-content/uploads/2016/07/HowWeMakeTapes.pdf>.
- [Sch05] Wouter O. Schotborgh et al. “Dimensionless design graphs for flexure elements and a comparison between three flexure elements”. In: *Precision Engineering* 29 (1 2005), pp. 41–47. ISSN: 01416359. DOI: 10.1016/j.precisioneng.2004.04.003.
- [Slo10] Alexander Slocum. “Kinematic couplings: A review of design principles and applications”. In: *International Journal of Machine Tools and Manufacture* 50.4 (2010). Design of Ultraprecision and Micro Machine Tools and their Key Enabling Technologies, pp. 310–327. ISSN: 0890-6955. DOI: <https://doi.org/10.1016/j.ijmachtools.2009.10.006>. URL: <http://www.sciencedirect.com/science/article/pii/S0890695509002090>.
- [Smi97] Stuart T. Smith et al. “Elliptical flexure hinges”. In: *Review of Scientific Instruments* 68 (3 1997), pp. 1474–1483. ISSN: 0034-6748. DOI: 10.1063/1.1147635.
- [Sta03] Sarah Stauderman. *Pictorial guide to sound recording media*. 2003, pp. 33–35.
- [Tia10] Y. Tian et al. “Three flexure hinges for compliant mechanism designs based on dimensionless graph analysis”. In: *Precision Engineering* 34 (1 2010), pp. 92–100. ISSN: 01416359. DOI: 10.1016/j.precisioneng.2009.03.004.
- [YL09] Yuen Kuan Yong and Tien-Fu Lu. “Comparison of circular flexure hinge design equations and the derivation of empirical stiffness formulations”. In: *Advanced Intelligent Mechatronics, 2009. AIM 2009. IEEE/ASME International Conference on*. IEEE, 2009, pp. 510–515.
- [ZH09] Zhaocheng Zhang and Hong Hu. “Comparison of Single-Notch Circular Flexure Hinge Rotational Stiffness Equations with FEA Results and Derivation of Empirical Formulations”. In: *2009 International Joint Conference on Computational Sciences and Optimization*. IEEE, 2009, pp. 286–288. ISBN: 978-0-7695-3605-7. DOI: 10.1109/CSO.2009.47.
- [Zhu15] Zhiwei Zhu et al. “A simple compliance modeling method for flexure hinges”. In: *Science China Technological Sciences* 58 (1 2015), pp. 56–63. ISSN: 1674-7321. DOI: 10.1007/s11431-014-5667-1.

## Appendix



# A. Tables

	<b>A</b>	<b>A<sub>eq</sub></b>	<b>B</b>	<b>B<sub>eq</sub></b>	<b>C</b>	<b>C<sub>eq</sub></b>	<b>D</b>	<b>D<sub>eq</sub></b>
<b>1</b>								
<b>2</b>								
<b>3</b>								
<b>4</b>								
<b>5</b>								
<b>6</b>								
<b>7</b>								
<b>8</b>								
<b>9</b>								
<b>10</b>								

Figure A.1.: General chart of loads application

## B. Flow Diagrams

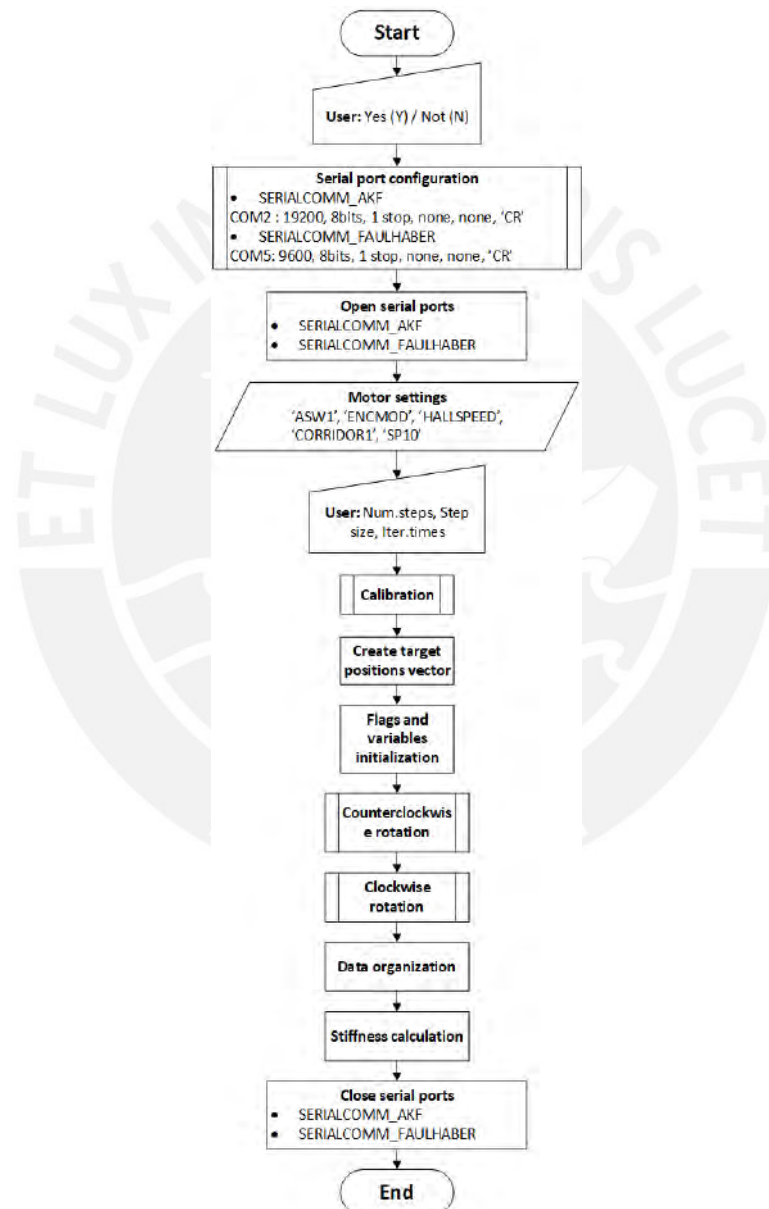


Figure B.1.: Flow chart - Main program